CONCEPTUAL ASSESSMENT OF AN OBLIQUE FLYING WING AIRCRAFT INCLUDING CONTROL AND TRIM CHARACTERISTICS

Ryan W. Plumley

Thesis submitted to the faculty of the Virginia Polytechnic Institute and State University
in partial fulfillment of the requirements for the degree of

Master of Science In
Aerospace Engineering

William H. Mason, Committee Chairman

Mayuresh J. Patil, Committee Member
Craig A. Woolsey, Committee Member

22 February 2008

Blacksburg, Virginia

Keywords: Wave Drag, Oblique Flying Wing, OFW, Vortex Lattice, Stability and Control

CONCEPTUAL ASSESSMENT OF AN OBLIQUE FLYING WING AIRCRAFT INCLUDING CONTROL AND TRIM CHARACTERISTICS

Ryan W. Plumley

ABSTRACT

A method was developed to assist with the understanding of a unique configuration and investigate some of its stability and control attributes. Oblique wing aircraft concepts are a design option that is well understood, but has yet to be used in a production aircraft. Risk involved in choosing such a design can be averted through additional knowledge early in the concept evaluation phase.

Analysis tools commonly used in early conceptual level analysis were evaluated for applicability to a non-standard aircraft design such as an oblique flying wing. Many tools used in early analyses make assumptions that are incompatible with the slewed wing configuration of the vehicle.

Using a simplified set of tools, an investigation of a unique configuration was done as well as showing that the aircraft could be trimmed at given conditions. Wave drag was investigated to determine benefits for an oblique flying wing. This form of drag was reduced by the distribution of volume afforded by the slewing of the aircraft's wing. Once a reasonable concept was developed, aerodynamic conditions were investigated for static stability of the aircraft. Longitudinal and lateral trim were established simultaneously due to its asymmetric nature.

Acknowledgements

I would like to thank my advisor, Dr. William H. Mason. I feel very fortunate to have been able to work with Dr. Mason because of his knowledge on the subjects I wished to explore. His experience helped mold my course of study and research into attainable goals. Fortunately, he had enough patience left to follow through to the conclusion.

This thesis was completed in course of a long term, full time training assignment through the Air Force Research Lab, Air Vehicle Directorate. I would like to thank all of those who afforded me the opportunity to complete my Master's degree. Nancy Benedict, Douglas Blake, Elaine Bryant, Thomas Cord, Denis Mrozinski, Dieter Multhopp, Chris Remillard, Tim Schumacher, Carl Tilmann, and others from AFRL/RB made it possible to do this within a slightly extended timeframe.

My parents, Robert and Shelia, instilled a love and excitement for learning and problem solving that led to engineering and eventually this work. For that, I am ever grateful. My wife, Lindsay has been beyond patient with me throughout, and I can't love her enough for it.

Table of Contents

List of Figures

List of Tables

List of Symbols

Symbol	Description	Units
a_{ell}	Ellipse semi minor axis	ft
AR	Wing aspect ratio, b^2/S	
b	Wing span at zero oblique sweep	ft
b_{ell}	Ellipse semi major axis	ft
c_r	Wing root chord	ft
c_t	Wing tip chord	ft
$\bar{c}$	Mean geometric chord	ft
h/b	Height above ground to wing span ratio	
q	Dynamic pressure	lbs/ft^2
C	Specific fuel consumption	lbs/hr/lb
C_A	Axial force coefficient, body axis F_A/qS	
C_D	Drag force coefficient, stability axis, D/qS	
C_L	Lift force coefficient, stability axis, L/qS	
C_l	Rolling moment coefficient, L_A/qSb	
C_m	Pitching moment coefficient, $M_A/qS\bar{c}$	
C_n	Yawing moment coefficient, N_A/qSb	
C_N	Normal force coefficient, body axis, F_N/qS	
C_Y	Side force coefficient, F_Y/qS	
D	Drag force, stability axis	lbs
F_A	Axial force, body axis	lbs
F_N	Normal force, body axis	lbs
F_Y	Side force	lbs
$\boldsymbol{I}$	Aircraft moment of inertia matrix	slugs*ft^2
L	Lift force, stability axis	lbs
L_A	Rolling moment	ft*lbs
M	Mach number	
M_A	Pitching moment	ft*lbs
N_A	Yawing moment	ft*lbs
R	Range	ft
$\boldsymbol{R}_{ij}$	Rotation tensor	
S	Wing reference area	ft^2
t/c	Maximum wing thickness to chord ratio	
X, Y, Z	Modeling coordinate system components	ft
X_b, Y_b, Z_b	Body coordinate system components	ft
X_s, Y_s, Z_s	Stability coordinate system components	ft

V	Velocity	ft/s
W/S	Wing Loading, W_0/S	lbs/ft^2
W_e	Weight empty	lbs
W_0	Take-off gross weight	lbs
α	Aircraft angle of attack	deg
β	Stability axis sideslip angle	deg
δ	Control deflection	deg
λ	Wing taper ratio, c_t/c_r	
Λ_{OS}	Oblique sweep angle	deg
Λ_n	Wing sweep angle, n fraction root chord	deg
μ	Half-angle of the Mach cone, $\sin\mu = 1/M$	deg

Subscripts

b	Body axis
s	Stability axis
w	Wind axis
flap	Due to combined elevon deflection
LL	Left-left elevon
LC	Left-center elevon
RC	Right-center elevon
RR	Right-right elevon
α	Due to aircraft angle of attack
β	Due to sideslip angle
δ	Deflection

1. Introduction

This report pursues a method of analyzing unique configurations at the conceptual level with attention to static stability and controllability of the concept. The case chosen was an oblique flying wing (OFW) vehicle. This topic was of interest due to the Defense Advanced Research Projects Agency (DARPA) demonstration vehicle in development[1]. This unmanned version of the OFW concept is a better role than previous attempts to develop a high-speed passenger or military transport. Its main attribute is a capability to perform in-flight asymmetric sweep of the wing as a whole. This is done to reduce drag at supersonic speeds. Making the vehicle unmanned relieves constraints established for manned vehicles that cause problems due to the asymmetric nature of an oblique flying wing. One example of difficulties for an oblique wing transport is from a Boeing study which showed that an FAA requirement limited sweep so that passengers could not face more than 18 degrees from the flight direction on take off and landing. For an oblique flying wing, passengers would possibly be facing up to 60° away from the front of the aircraft[2]. The hope of this study is that by looking at such an innovative concept, knowledge can be gained on weaknesses in processes used in the analysis for future investigations.

Examination of early aircraft design concepts is a difficult process due to a lack of detailed information and the broad scope of the problem at that stage. A range of possible concepts helps to create the best design space even though a number of the aircraft investigated may not meet requirements. If concepts are understood to the same precision on quantifiable criteria, the evaluation is clear-cut. But, some of these designs depart from well established aircraft configurations. Various fidelity for designs can create confusion. Such issues are related to analysis tool validation and knowledge base. In addition, it may be difficult to assess an innovative concept that doesn't meet some criteria which is written with a bias towards another approach. In particular, stability and controllability of a concept is a concern that can be difficult to assess in early aircraft evaluations.

Tools used at a conceptual level need to be understood and generic enough to handle many types of configurations. Ideally, modular design of tools adds flexibility for a well-informed analyst to investigate concepts.

An oblique flying wing aircraft was selected as an example of a common vehicle considered early in design evaluations due to desirable attributes for high-speed flight. Under the DARPA program, a conceptual design for an oblique flying wing is called for that can be used for long-range Intelligence, Surveillance and Reconnaissance, ISR, or a long-range bombing mission[1]. This concept taxes design tools and processes due to the asymmetric layout and lack of a fully realized supersonic vehicle with an oblique wing. Many simple, well-understood tools used to investigate concepts at the conceptual level make assumptions such as X-Z symmetry that cannot be used for an oblique wing vehicle due to the in-flight skewing of the wing relative to the direction of flight. Added to this is the need for both low-speed evaluation at take-off and landing and high-speed evaluation during flight.

Stability and controllability are important considerations in early design to reduce major design changes later on. For a specific concept, such an analysis can be the first time where geometric proportions are required. Prior to this, other analyses may only be using a point mass and non-dimensional variables relevant to the aircraft. The use of stability augmenting control systems that do not require static stability has increased the complexity of controls analyses. Requirements for such aircraft shift from stability to control requirements. Unlike most aircraft, the asymmetrical nature of this flying wing concept has not been exhaustively explored for the best control effectors to use. Evaluations should look at multiple oblique slew angles to investigate asymmetries. In addition, the advantage of the vehicle is efficient supersonic cruise as well as subsonic. This adds up to a complex set of conditions for analysis.

Investigating take-off and landing of a vehicle using an obliquely slewed wing has problems due to asymmetries. Sideslip and roll effects also need to be accounted for while taking off or landing in addition to normal considerations. If it is possible to slew to a symmetric orientation in these parts of flight it would simplify this operation to something more like a standard aircraft. Although, taking off at an oblique sweep angle

could simplify the pivoting system used. Additionally, problems can occur in-flight that may require landing at such a condition.

1.1 History

An oblique wing design was originally proposed by Edmond de Marcay and Emile Moonen in 1912. The idea was to vary sweep of oblique wings for landing in sideslip. It was further studied by Richard Vogt in Germany for increasing wing sweep as the speed of the aircraft increases. R. T. Jones (then at the NACA Langley Memorial Aeronautical Laboratory) was introduced to oblique wings soon after and remained the most notable advocate of the concept[2]. He initiated wind tunnel studies beginning in the late 1940's on the merits of such a wing and how it could be integrated into a high-speed civil transport. These studies can be divided into those concerned with an oblique wing mounted to a fuselage using a pivot and those pertaining to an oblique flying wing concept.

There have been many design studies of oblique wing aircraft for commercial and military applications. Because of the advantageous aerodynamic qualities at high speeds, an oblique wing design is considered in many cases, but normally rejected due to integration issues and control concerns. Two designs that were demonstrated are the NASA Dryden Oblique Wing Research Aircraft, OWRA RPV, and the Ames-Dryden AD-1. The OWRA RPV, shown in Figure 1, was developed in the early 1970's in order to investigate flying qualities of an oblique flying wing, although it did incorporate a tail and rudimentary fuselage. Several iterations of the design were completed based on wind tunnel data and flight testing. In flight, oblique sweep of the wing was explored up to 45°[1].

Burt Rutan designed the first manned oblique wing aircraft, the AD-1, which flew in 1979[3]. Figure 2 shows the demonstrator's range of sweep angles. The design was for a low cost, low-speed demonstrator for oblique wing sweep. Detailed wind tunnel testing and simulation were done in order to characterize the aircraft. The aircraft flew, without significant control augmentation, up to oblique wing sweep angles of 60°. The

asymmetry caused issues such as side force from the leading wing and an asymmetric stall that increased difficulty of piloting the vehicle at oblique wing sweeps of over 45°[4].

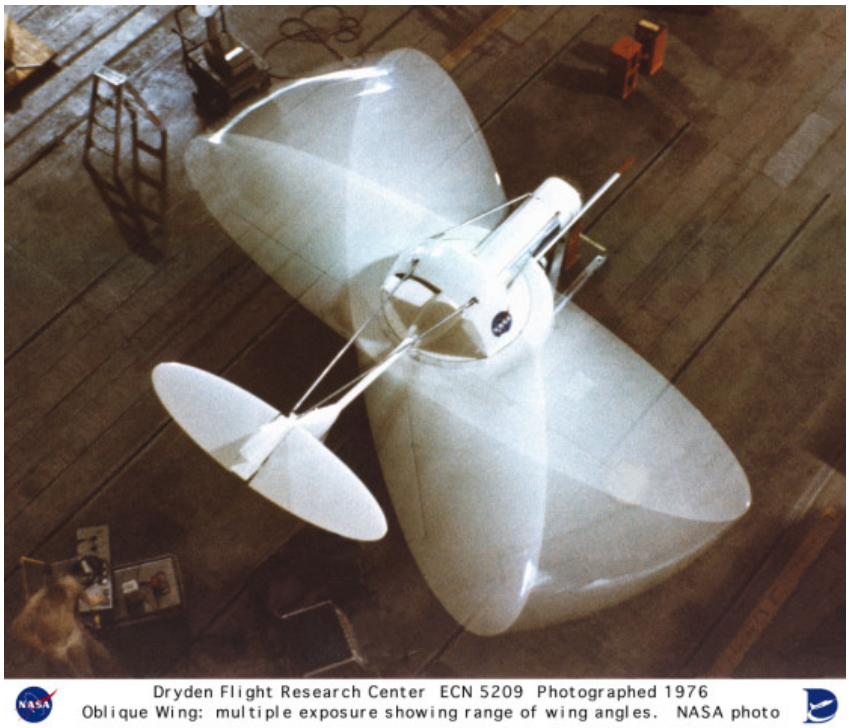

Figure 1: OWRA Oblique Wing Demonstrator[5]

In 1995, two small-scale oblique flying wing demonstrators, 10 ft and 20 ft span, were developed by Stephen Morris of Stanford University. The design was based on a NASA proposed, 400-passenger, OFW supersonic transport. The objective was to investigate control issues associated with asymmetric sweep that make unstable flight unavoidable. A smaller, stable radio controlled model was used to identify issues that were important to understand for the second, larger demonstrator. Vertical fins affected pitch on the 10-ft model such that they were re-designed. This vehicle used a control system to augment the pilot and allow the unstable vehicle to be flown successfully[6].

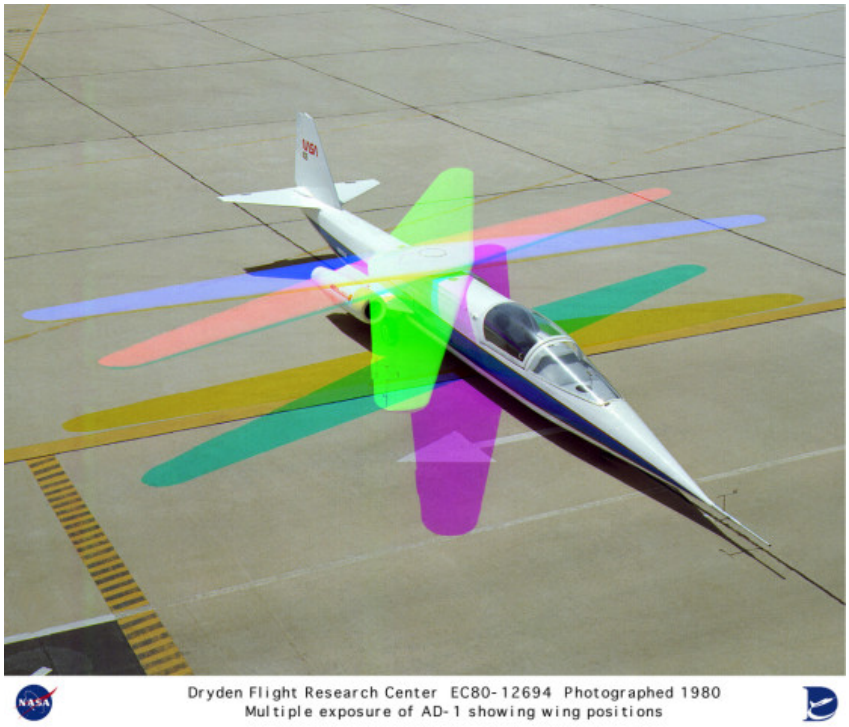

Figure 2: AD-1 Oblique Wing Demonstrator[5]

1.2 Objectives

It is the intention of this analysis to look at a unique configuration, in this case the oblique flying wing, and particularly its static stability and controllability at the conceptual level. The investigation includes an understanding of basic geometric parameters, the aerodynamics of the vehicle, mission synthesis, and static stability and control of the vehicle. Common conceptual analysis tools are used, evaluating how robust they may be in this case.

An investigation of an oblique flying wing offers an opportunity to look at inertial and force coefficient coupling not seen or assumed to be small on a normal, symmetric aircraft. Numerous effects normally can be ignored because symmetry cancels them out. For a wing that obliquely sweeps there is potential to see an entirely different concept which necessitates understanding of the relations between this motion and how it applies to the aircraft's absolute motion. Assessments are done using tools that do not require symmetry. Additional insight is necessary to combine this data in a reasonable fashion.

Conceptual stability and control assessment needs to be flexible to understand a flying wing, non-standard control surfaces, and oblique sweep of the vehicle.

1.3 Assumptions

Proponents of OFW designs have, at times, found that the use of one fixed body axis is beneficial while investigating an oblique swept wing. These results diverge from those in a stability axes that doesn't depend on the oblique sweep. Many analysis tools only present results in the stability axis. While information can be converted between the two, a model orientation around one axis may not be ideal when displaying results in another axis system. Results presented here are shown in both frames depending on the application of the data.

Also, aeroelastic effects are not investigated in this report. These effects are based on the interactions between the structure and the aerodynamic loading of the aircraft. While this effect is required in modern design, it is not included in this assessment in order to investigate a wider design space. A more confined study could include such effects using these results.

2. Conceptual assessment of an operational vehicle.

An operational vehicle is considered in lieu of a demonstration vehicle in order to investigate an oblique wing aircraft with realistic mission objectives. Understanding the geometry of the vehicle is important for an oblique flying wing due to the large changes in the configuration due to oblique sweep that invalidates assumptions like constant moments of inertia of the vehicle in the stability axis. Also, geometry parameters for a plausible vehicle are needed to limit variations to those most applicable for stability and controllability.

2.1 Problem Requirements

The idea of developing an oblique wing vehicle has been applied to multiple supersonic aircraft studies. To narrow the scope of this effort, the most recent DARPA program was used to understand desirable objectives for an operational vehicle. In order to look at this vehicle effectively, analysis tools were investigated to understand which ones were most appropriate to study such a vehicle.

2.1.1 Operational mission requirements

Requirements here are taken from the DARPA "Switchblade" program proposer pamphlet[1]. It was published in August 2005 and contains information pertaining to an operational oblique flying wing vehicle. The goal of that program is not a final operational aircraft, but to mature technologies and demonstrate them on an X-Plane. The objectives for the operational vehicle are to be capable of an information, surveillance, and reconnaissance (ISR) mission requiring long loiter, and a bombing mission that requires high-speed. Presumably, there may be further requirements for a possible hybrid mission type between the two. Another requirement is for "tailless" subsonic operation. This means operation without a vertical surface during some subsonic parts of the mission. The mission parameters are reproduced from the pamphlet below.

Table 1: Operational Oblique Wing Mission Parameters

	ISR Mission	Bombing Mission
Radius (unrefueled)	2,500 nm	2,500 nm
Loiter Capability	15 hrs	No Requirement
Altitude	60,000 ft	No Requirement
Cruise Speed	Subsonic	Mach 1.6
Maximum Speed	No Requirement	Mach 2.0
Payload	4,000 lbs	15,000 lbs

Further investigation of the requirements looked at possible sizes of the vehicle. The bombing mission appears to be the most strenuous with a high payload and long-range at high-speed. The oblique wing shows more benefit for larger-sized vehicles because of the needed integration inside a flying wing. The subsonic and supersonic requirements will also strain other sub-systems on the aircraft such as propulsion. In order to have optimal performance at the design points, engine technology that allows multiple optimum cycles may be necessary.

While not explicitly stated in the solicitation, the vehicle will very likely be unmanned. There are immediate benefits such as weight savings and reduced aircraft signature. This would also avert challenges such as proper pilot orientation at every oblique wing angle. An unmanned system can be autonomous to the point of concentrating on goals to achieve in flight and avoid focusing on a complex control scheme.

Based on the goals established, some assumptions of the vehicle can be made. The requirement for tailless operation suggests a minimization of signature for survivability. This will prevent the use of elliptical wings, as used in many OFW transport studies, to reduce radar cross section, RCS. Also, engine mounting will have to balance the need to change oblique sweep angle with the need to hide engine infrared (IR) signatures.

With these requirements and assumptions on what an oblique flying vehicle should resemble some estimates can be made of what the aircraft design space would look like and the feasibility of such a design. To give as fair an investigation as possible, many of the terms used are optimistic, reasonable values. An initial sizing was performed based on a standard empty weight curve fit based on existing vehicles, in equation 1 and the Breguet range equation, in equation 3. The Breguet range equation is based on a change in range, R, due to a change in weight, W, with fuel usage, shown in equations 2 and 3.

$$W_e / W_0 = A W_0^C \tag{1}$$

$$\frac{dR}{dW} = \frac{V}{-CD} = \frac{V(L/D)}{-CW} \tag{2}$$

$$\frac{W_i}{W_{i-1}} = \exp\left(\frac{-RC}{V(L/D)}\right) \tag{3}$$

Using these two equations the fuel fraction can be determined based on the mission and converge on an empty weight. Curve fits of empty weight fractions are used as a guide, but these are approximate and don't completely represent the case presented here. A look at both missions shows that the bombing mission has slightly more strenuous requirements than the ISR mission. This could change if the vehicle is unable to achieve low drag during the 15 hour loiter. Also, it would be easier to achieve the ISR mission if the offset payload weight from the bombing mission can be used for fuel. Some assumptions about aerodynamics and fuel efficiency of the aircraft in this mission are shown in Table 2. This is based on an oblique wing vehicle with supersonic cruise capabilities.

Table 2: Oblique Flying Wing Performance Assumptions

Mission Segment	SFC	L/D
Cruise (High Vel.)	1.2 lb/hr/lb	10
Cruise (Low Vel.)	0.5 lb/hr/lb	17

Figure 3 shows the results of the regression on weight based on the estimated bombing mission performance. Also, example vehicles are plotted alongside for reference. The problem is bounded by using two jet aircraft curve fits, available as examples in the design book written by Raymer[7]. The Jet Fighter curve represents an upper bound and the Jet Transport curve, a lower bound. Due to the inaccuracy of the regression to this case, a 10% margin is added to the weight estimate plotted on each curve to show the scope for designs. This forms a box which represents possible designs of such a vehicle. This also leaves a significant range of values for the gross weight. One issue is the assumption that the empty weight fraction will be reduced as the take off gross weight increases. Van der Velden's design[8] is plotted as well for an oblique flying wing transport that doesn't match the regressions shown, but is within the range of empty weight ratios estimated for an oblique flying wing aircraft. This is due to expansion of the curves outside of the applicable range of the regression. The range established for the oblique flying wing aircraft, however, is appropriate.

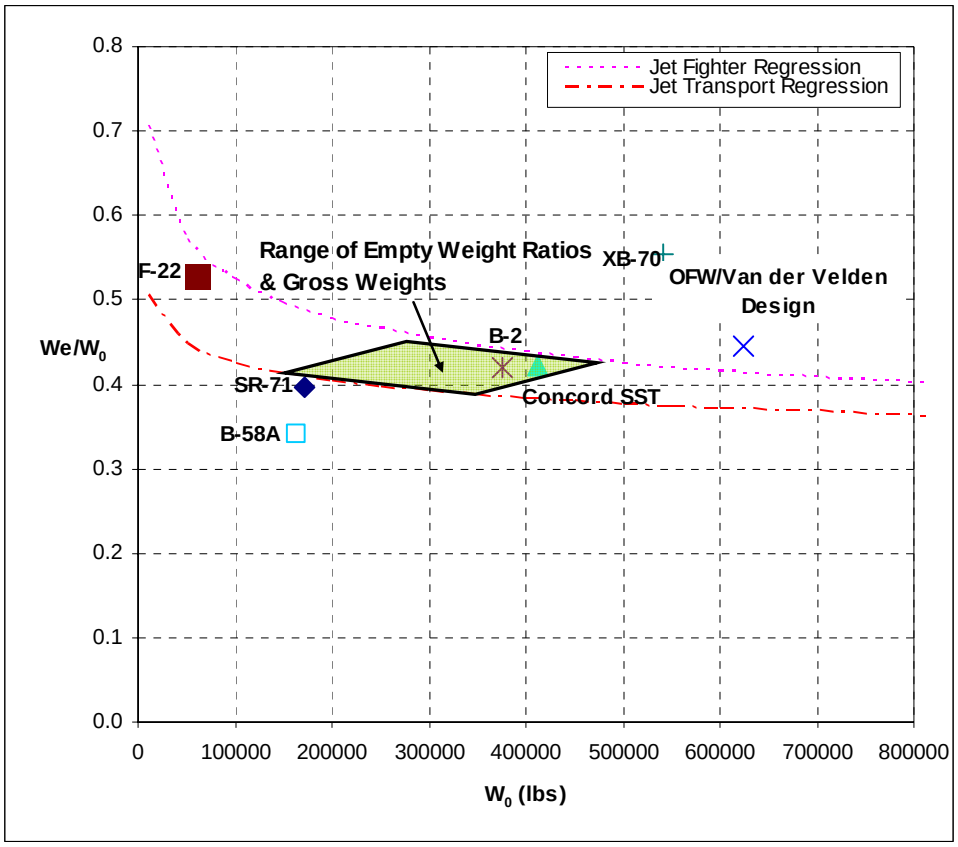

Figure 3: Bounding Take-Off Gross Weight Based on Mission

Looking back at the mission, this analysis shows that the vehicle will be fairly large but it should be possible to produce such a vehicle under a half-million pounds. Requirements such as the need for additional range can drive the design such that it has less capability in other areas such as take-off performance. Multiple assumptions go into this as far as weight gained due to the oblique sweeping mechanism and efficient operation in several significantly different flight cases. Technologies such as those for structural weight reduction and engine efficiency can change the outcome of the design greatly.

2.1.2 Tool selection

There is an array of analysis tools available for evaluation of conceptual aircraft. Tejtel, et al. presents a compelling implementation of some of those tools, with an eye toward developing future capability[9]. In that case, it was important to use standard tools, but the need was there to increase assessments of quantifiable impacts of technologies. There are numerous criteria on which a tool could be evaluated, but confidence and timeliness are two of the most important. Confidence comes from tool verification and validation as well as user experience. The time allowed for a given effort is often not in an analyst's control. Increasing detail for an investigation may make it difficult to accomplish under this limitation and some flexibility in the methods used is called for.

When assessing what tools to use there are several factors to keep in mind other than use of the tools themselves. These factors require more information on the tools as they affect the specific analysis. Increased fidelity in the analysis is only useful when benefits can be shown for conceptual evaluation goals. Level of confidence in solutions also needs to be gauged based on what went into the analysis. In the case of ModelCenter, which is software that allows analysis program integration, output of one code that is compatible with the input of another such that interfaces are possible that can run outside of direct interaction. A low-fidelity design fed into a high-fidelity analysis will give solutions that need to be evaluated for lost accuracy and possible divergent behavior due to inconsistent levels of approximation.

Multiple design concepts under analysis should have the same consideration to have an accurate evaluation. Many low-level tools based on a standard three-surface

aircraft are not able to accurately represent a non-standard vehicle, such as with the oblique flying wing. Oblique skewing of the wing violates the assumption of symmetry. Other examples of possible problems are analysis of a joined-wing aircraft with tools that do not allow lifting surfaces to overlap and cranked flying wing concepts that are difficult to split into fuselage and wing parts.

Tool Attributes

User input is the means to control a program's execution. Complexity can vary for tools used in vehicle analysis. Classically, the input card format is used by many of these codes. Increasingly, graphical user interfaces (GUI) are used as a way to give logical input controls, instantaneous feedback, and assist with post-processing of an analysis.

A useful feedback to the user is accurately representing a model as the analysis "sees" it. Figure 4 shows an example of vortex lattice program geometry displayed in the user interface based on input parameters that can be used to determine if the tool will accurately represent the modeled geometry.

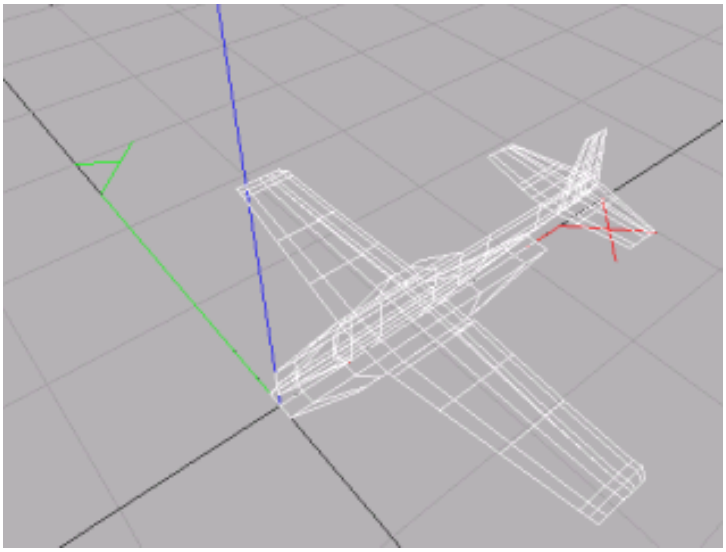

Figure 4: Aircraft Perspective View in Bihrle Applied Research's SimGen Tool [10]

Determining the worth of the program's output is helpful in selection. Information as to the quality of the analysis should be given such as the residual in CFD analysis codes. The goal is to have a measure of how close it comes to properly representing truth.

While an absolute certainty can never be achieved a range of possible answers can be used. The issue then becomes effectively communicating this type of solution.

Many times lower-order codes are used in assessing vehicle designs not only for computational efficiency, but to exercise multiple designs and understand effects at a basic level. Tools of higher fidelity can also require a more detailed geometry or other information that increases complexity of executing the analysis. Adding parametric analysis models into the processes improves capabilities while retaining the ability to assess variations on a concept as in lower-order codes.

Table 3 below shows some of the tools in use in conceptual aerodynamics and assessment of vehicles. Table 4 is an extension of this table. The table includes the list of tools considered for use in this analysis. Mostly aerodynamic tools, some of which have been used to evaluate aircraft stability attributes, are shown. Gray highlights identify tools that were selected and data presented.

Table 3: Tool Information and Compatibility Assessment

	Program	Distribution	Use	OS	Fidelity	Compatibility
	Aerodynamics/ Stability Information Tools					
1	AVL	MIT Web	Vorlax, Auto Aircraft Trim	Unix, Windows	Medium	Yes
2	Awave	NASA/PDAS	Wave Drag	Fortran	Medium	No
3	Cart3D	NASA Ames/ ANSYS	Euler Inviscid Aero	Linux, Mac	High	Yes
4	Digital DATCOM	AFRL/Unlimited	Empirical Analysis	Windows	Low	No
5	FLOPS	NASA Langley	Mission Analysis, CG	Windows	Low	Mission Only
6	Friction	VT AOE	Skin Friction Method	Windows	Low	Yes
7	HASC/ SIMGEN	AFRL Unlimited/ BAR	Vorlax, Ground Effect	Windows	Medium	Yes
8	NASCART-GT	Georgia Tech	Euler Inviscid Aero/Viscous	Windows	High	Yes
9	PANAIR	PDAS	Panel Code	Windows	Medium	Unknown
10	X-Foil	GNU	e^n Airfoil code	Unix, Windows	High	Yes
11	Zero Lift Wave Drag	COSMIC/Abandoned	Arbitrary Body Wave Drag	Windows	Medium	Yes
12	Zonair	Zona	Panel Code	Windows	Medium	Unknown
	Geometry Tools					
13	Rhino 3D	McNeel	Geometry Dev & Manipulation	Windows	N/A	N/A
14	Solidworks	Solidworks	CAD/CAM Tool	Windows	N/A	N/A
15	Vehicle Sketch Pad	NASA Langley	Conceptual Aircraft Geometry	Windows	Medium	No

Table 4: Tool Information and Comments

	Website	Comments
	Aerodynamics/ Stability Information Tools	
1	http://web.mit.edu/drela/Public/web/avl/	Vorlax, thin body, console UI, and auto trim
2	http://www.pdas.com/wavedrag.htm	Harris Wave Drag, incompatible – symmetric assumption
3	http://people.nas.nasa.gov/~aftosmis/cart3d/	Used in Desktop Aero OFW white paper
4	http://www.rb.afrl.af.mil/org/RBC/RBCA/vaca_index.html	Incompatible symmetric assumption
5	Not Available	Imported Aerodynamic tables/ issues for multiple possible polars
6	http://www.aoe.vt.edu/~mason/Mason_f/MRsoft.html#SkinFriction	Simple compared to high level codes, Transition information needed
7	http://www.bihrle.com/site/products_simgen.html	High Angle Stability and Control, GUI developed by Bihrle A. R.
8	http://www.ae.gatech.edu/people/sruffin/nascart/	Found to be much slower than Cart3D, but some different features
9	http://www.pdas.com/panair.htm	High Level of difficulty
10	http://web.mit.edu/drela/Public/web/xfoil/	Accurate airfoil analysis. Well used. 2-D transition prediction
11	Not Available	Useful for complex aircraft. No users. Source updated.
12	http://www.zonatech.com/ZONAIR.htm	Commercial Software, Stress Analysis Compatibility
	Geometry Tools	
13	http://www.rhino3d.com/	Used in many environments, Good support for formats
14	http://www.solidworks.com/	Good compromise between part building capability and ease of use
15	Not Available	Parametric Tool Dev by NASA, new RAM, Useful output formats

In-depth investigations of several analysis codes were performed. Criteria for evaluation were based on verification, user base, code execution time, and ease of use. Many tools are commercially available, but none of the tools were evaluated without prior experience to reduce time spent on each.

High-Angle-of-Attack Stability and Control—HASC prediction code[11]

This is a subsonic aerodynamic prediction code developed for NASA Langley Research Center in 1995. The code was updated in 2002 and publicly released without the vortex chine evaluation module. This is a well-exercised code with a substantial user base. Code input is moderately complex, but it has been automated through the use of scripts. The rudimentary inputs for each panel are the leading edge locations, chords, and incidence angles. It is also used as a module in the SimGen tool which allows for GUI input. An output of the tool is the lattice.out file that is readable by Tecplot and shows the user what geometry was used.

The module in HASC implemented here (VORLAX) is a generalized vortex lattice program. The method uses a thin panel lattice method developed by Miranda Elliott and Baker[12]. Panels are modeled from the wing and surfaces and represented by horseshoe vortices, superimposed onto the panels. The induced velocities are summed for

each panel at a control point. The boundary condition assumes no flow through. Wing circulation pressures are computed from the panel velocities. These are integrated to find forces. Compensation for leading edge suction (LES) is also allowed through the use of a parameter between 0.0 and 1.0. A value of 0.0 represents 0% LES, and a value of 1.0 represents 100% LES.

Figure 5 shows the output geometry from the HASC program. This shows two-dimensional panels based on geometry input and also shows density of sub-panels on each panel. This compares well with OAW panel, the one model created by Downen, et al. of Kansas University[13]. It is possible to input panels asymmetrically, but the definition of the moment reference center is entered in Z-coordinates and X-coordinates. An unsymmetrical design must be input such that required Y-coordinate location for the reference center is on the Y-axis.

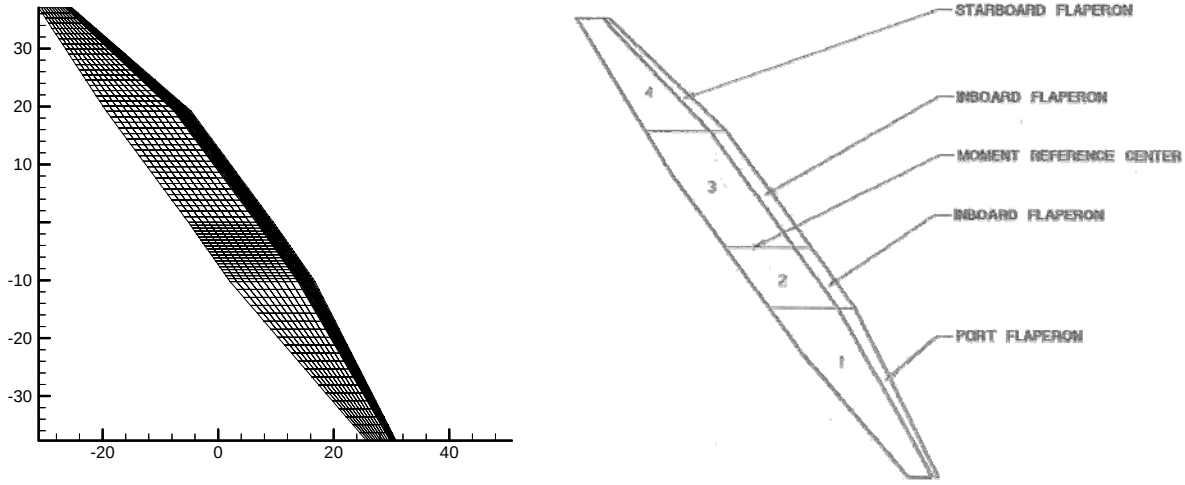

Figure 5: Comparison OAW HASC Model to KU Model[13]

The Revised Wave Drag Analysis – AWAVE Program[14]

Also known as the Harris wave drag program, AWAVE determines wave drag based on geometric definitions. It is currently distributed by NASA Langley and last maintained by L. A. McCullers in 1992. Simple shapes such as fuselages can be defined by radii or sets of points can be entered for each surface. Geometry is assumed to be symmetrical over the X-Z plane. This tool is reasonably maintained and there are some

geometry interfaces for tools such as NASA's Rapid Aircraft Modeler[15] to develop this type of input file.

Issues with the tool are typical for this type of program. The geometry input is difficult to work with when compared to some other analysis codes. Data must be aligned in columns as specified in the documentation. For an oblique flying wing vehicle, this program is not practical due to the assumption of symmetry.

Zero-Lift Wave Drag Program for Complex Configuration[16]

This program is a supersonic wave drag program similar to AWAVE, but geometries are input as sets of curves defined by points where symmetry is not necessary. The tool was developed by Craidon in 1983. Figure 6 shows the sample geometry used as a baseline for this tool and included in the user's guide. The program is able to interpret the points used and extrapolate curves based on a minimum wave drag case.

It is unknown when it was last in use. Considerable effort was made to compile the source code and change input to point to files. The sample input hard copy was converted to an electronic version and used as a baseline to confirm that the analysis tool was working. While this was the case, it has not been updated in a significant amount of time, there were no other users to consult, and efforts to match theoretical and experimental data was not successful.

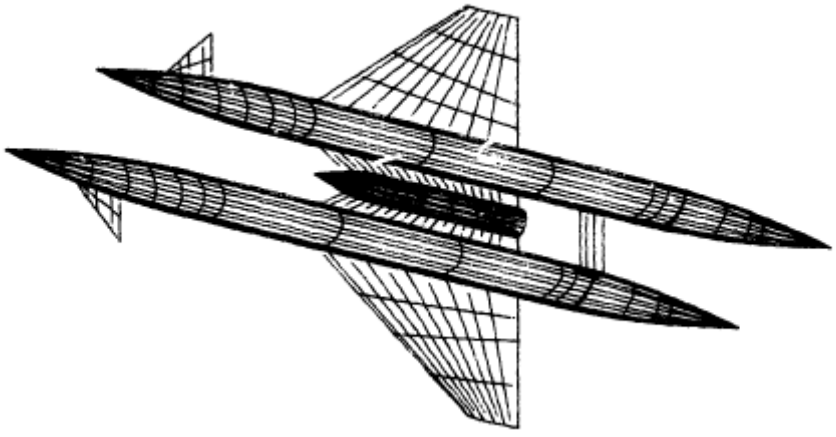

Figure 6: Staggered Multi-Body Sample Input[16]

Cart3D[17]

Cart3D is an inviscid Euler CFD code with simplified input compared to most. It was developed at NASA Ames and has been integrated into ANSYS ICEM CFD for commercial use. The NASA releases can be used with IRIX, Linux, SOLARIS, and Apple OS-X. The Linux installation requires a program available from the Portland Group called PGI portability package. Basic geometry imported to the automated mesh generator is a triangulated mesh. Automation in order to perform drag polar creation is fairly simple to implement with command line scripting. Aerodynamic coefficients are available through a post-processor that integrates pressure data. Other outputs include pressure and Mach Tecplot formatted plots.

This tool has been used for oblique wing studies by Desktop Aeronautics in a white paper "Oblique Flying Wings: An Introduction and White Paper" published on their website[21] and an AIAA paper "Conceptual Design of Conventional and Oblique Wing Configurations for Small Supersonic Aircraft[22]." Figure 7 shows an example oblique wing pressure plot created using Cart3D as a trial.

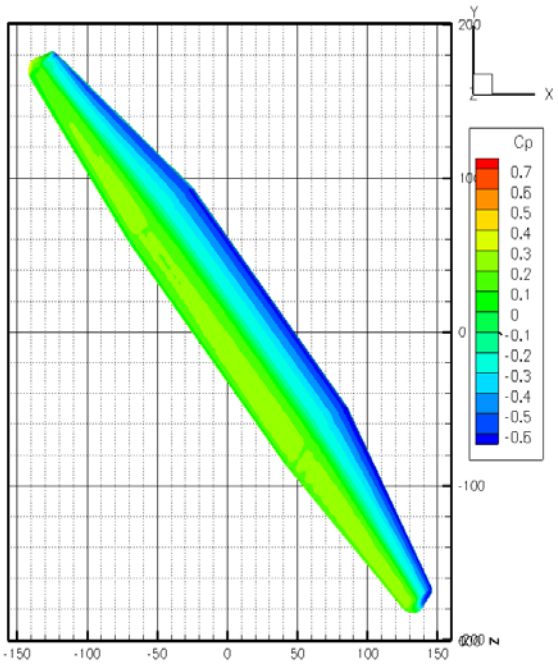

Figure 7: Oblique All Wing Model Pressure Coefficients M=1.4, α = 5 degrees

Several of these tools were selected from here for use in an oblique flying wing analysis. HASC was used for linear-subsonic analysis including ground effects. The Zero Lift Wave Drag code has the highest probability of finding realistic volumetric wave drag for an oblique wing, but it is difficult to have higher confidence in the tool without a current user base that has experience. MATLAB is capable of post-processing much of the analysis used, as well as implementing various simplified methods. Geometry is important for higher-fidelity analysis. Many decisions on tool usage depend on specific user experience. HASC, FRICTION, and MATLAB were used in the analysis.

2.2 Geometry parameters

Coordinate System

The coordinate systems used in determining the geometry for analysis are based on a standard Cartesian system. It is usually chosen for convenience in performing an analysis. One constant is that the Y-axis goes out the right side when facing the front of the aircraft, although in the wind axis the Y-axis can be affected by sideslip. Different types of analysis, such as aerodynamics, structures, and controls simulation, can have varying coordinate systems for the same vehicle. Figure 8 shows a normally accepted axis system for design and aerodynamic modeling. This is not based on a fixed location on the aircraft. If that were the case a slight change in the model could shift all parts, requiring more effort than necessary.

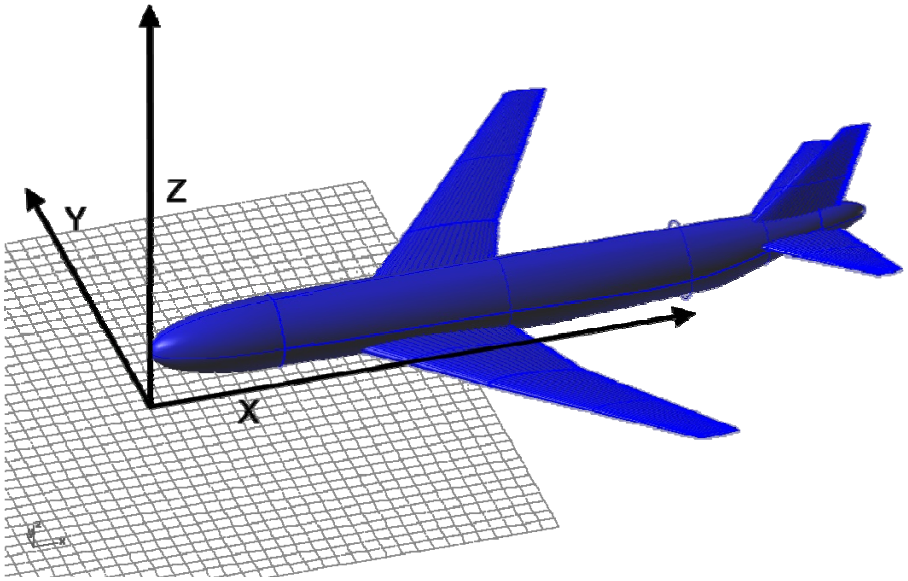

Figure 8: Design Axis Coordinate System

The body axis frame is typically used when discussing the actual motion of the aircraft. Figure 9 shows the body axis frame. The origin reference is usually at the center of gravity. Although designs are based on a nominal location, the center of gravity will be related to the location of weights not part of the empty weight of the aircraft. The Z-axis is through the bottom of the aircraft, yaw represents a rotation around this axis. Normal force is defined in opposition to this direction. The Y-axis is through the wing of the aircraft, pitch represents a rotation around this axis. The X-axis is through the nose of the aircraft, roll represents a rotation around this axis. Axial force is along this direction.

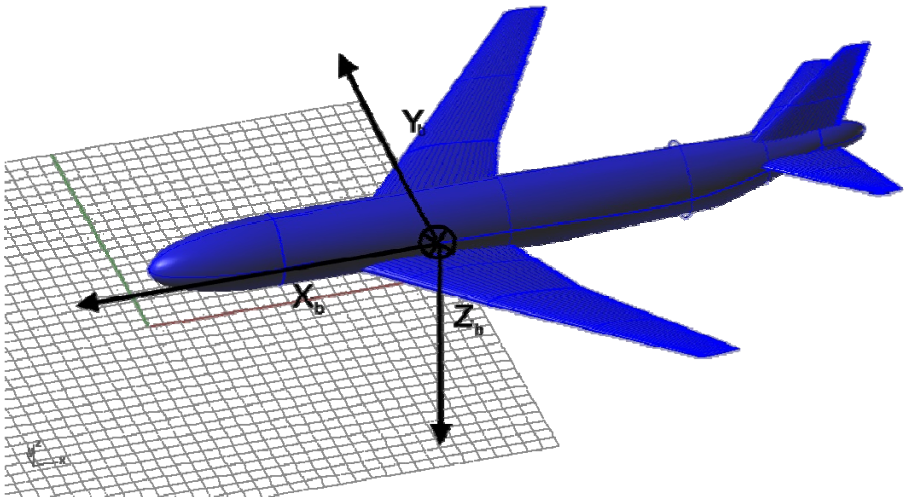

Figure 9: Body Axis Coordinate System

The stability axis of the aircraft is relative to the velocity vector at which the aircraft is traveling and the aircraft body axis. Figure 10 shows the stability axis frame. The aircraft is reversed to correctly show the velocity vector. Like the body axis, it is also usually referenced to the center of gravity of the aircraft. Lift is considered positive up such that it is opposed to the Z-axis. Drag is in the same direction as the X-axis. The angle of attack is the angle between the projection of velocity vector onto the body X-Z plane and the body X-axis. Both the X and Z axes are affected by this angle. It will change relative to the flight conditions of the aircraft.

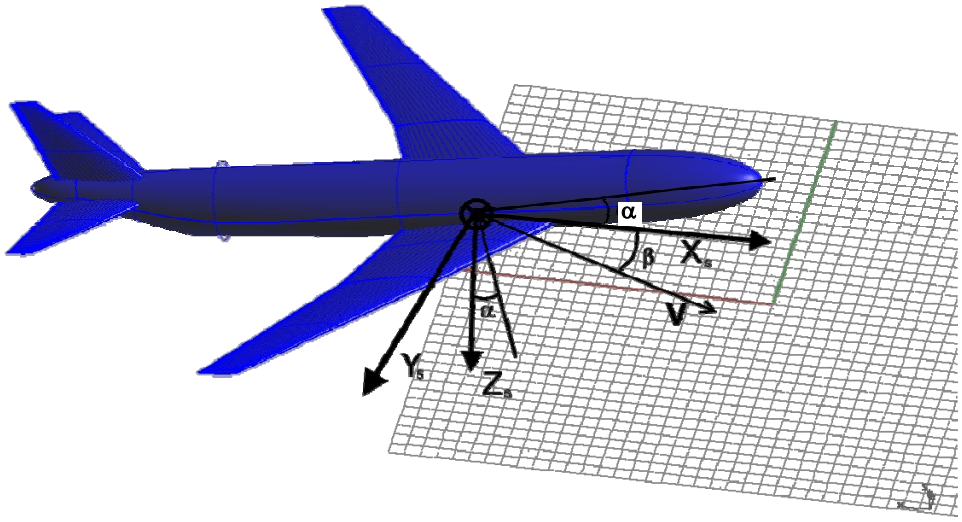

Figure 10: Stability Axis Coordinate System

The wind axis of the aircraft is completely based on the velocity vector at which it is flying. At zero sideslip the stability and wind axes are equivalent. Figure 11 shows the wind axis frame. This velocity vector is equivalent in orientation to the X-axis. The Z-axis is placed perpendicular to the X-axis in the plane formed by the velocity vector and the Z-axis from the body. Since the wind axis is not fixed, moments of inertia in the wind axis would be a function of the transformation between the wind and body axes.

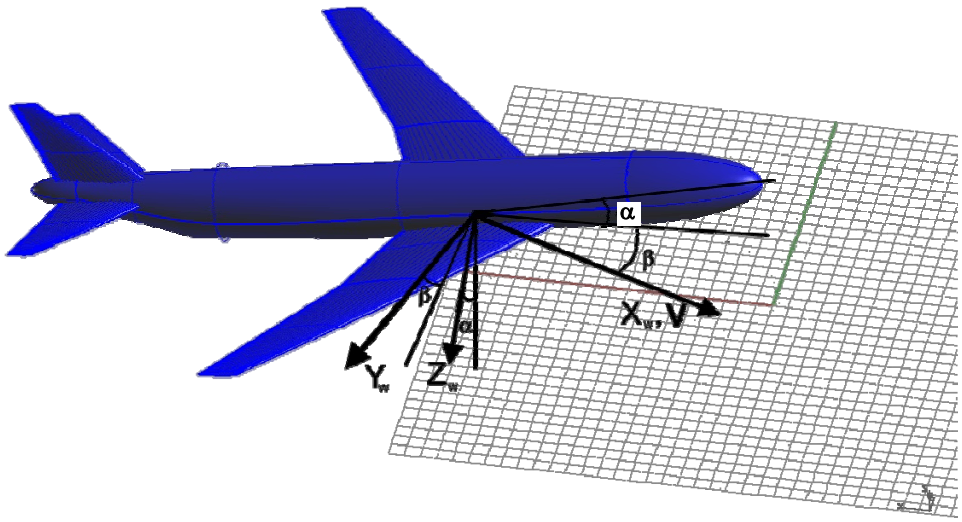

Figure 11: Wind Axis Coordinate System

2.2.1 DARPA oblique flying wing

The geometry used in this report is based on the oblique flying wing concept. Oblique wings represent a special case because the oblique sweep (Λ_{OS}) is active during flight. This angle is positive counter-clockwise looking down at the top view of the aircraft. The right tip looking toward the front of the aircraft goes forward as it is swept. The sweep changes lead to the need to understand how the vehicle operates at multiple sweep angles. In addition, the literature contains notation in multiple axis systems for this concept. There is merit to choosing an axis system that stays with the body axis of the flying wing, but an axis more consistent with the velocity vector at each slew angle can be advantageous in some cases.

The planform for an operational vehicle would be based on the demonstration vehicle design. This makes it similar to those used by DARPA and Northrop Grumman in their oblique flying wing program. Figure 12 through Figure 14 show a mock-up of the demonstration oblique wing vehicle[23]. Note that the vehicle is asymmetric even at zero slew angles. This makes for an interesting design as most vehicles have symmetry in the X-Z plane. The demonstration vehicle has no axis of symmetry at any of the oblique slew angles. Furthermore, the trailing edge is perpendicular to the vehicle direction at zero slew, and the tips are parallel to each other at 45° oblique slew. The vehicle also appears to be capable of at least an oblique angle of 65°, but likely limited there due to integration of a rotating propulsion system.

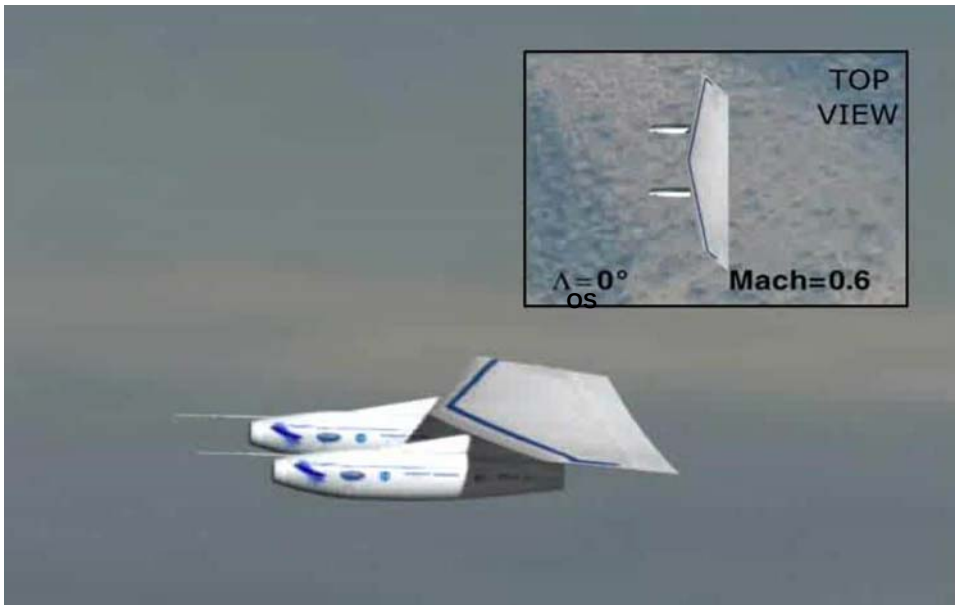

Figure 12: DARPA Oblique Flying Wing, 0° Slew[23]

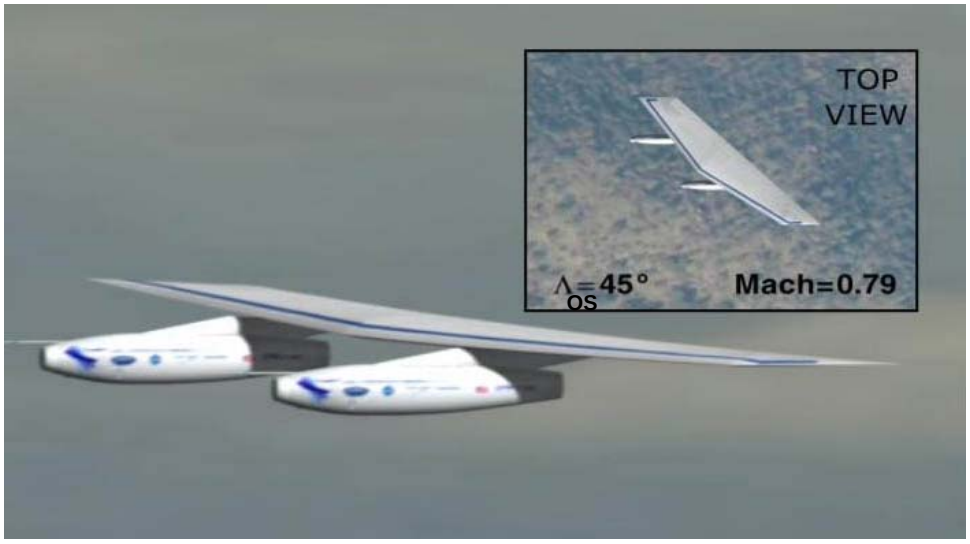

Figure 13: DARPA Oblique Flying Wing, 45° Slew[23]

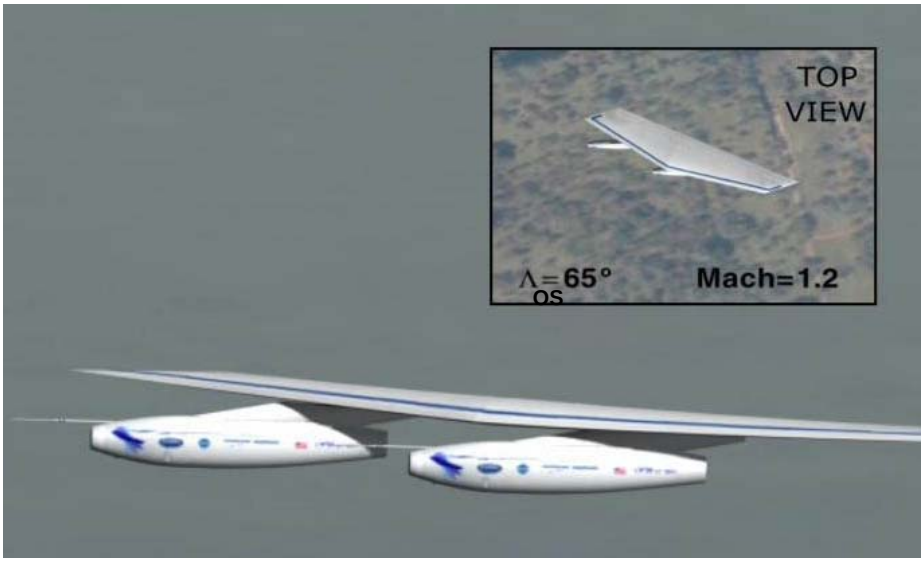

Figure 14: DARPA Oblique Flying Wing, 65° Slew[23]

2.2.2 Oblique sweep parameters

Based on these top views of the vehicle, a simple geometry was implemented that closely matches, but does not precisely duplicate the wing geometry. The type of wing chosen for a baseline is a trapezoidal wing, which was modified to resemble the demonstration vehicle. Figure 15 shows a representation of this wing. The taper ratio here is estimated at 0.6 and the aspect ratio as shown is 9. A sweep is selected based on the trailing edge of the wing being unswept. From that assumption, sweep at other chord-wise locations the simplified wing can be found.

Equation 4 is used to determine quarter chord sweep based on a straight trailing edge for a trapezoidal wing as shown in Figure 15. The equation was found for sweep at the trailing edge, then reversing the equation based on a trailing edge angle of 0°.

$$\tan \Lambda_{.25} = \frac{3(1-\lambda)}{AR(1+\lambda)} \qquad (4)$$

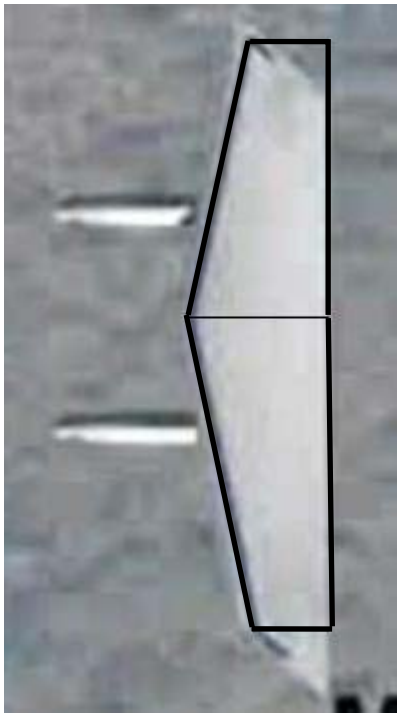

Figure 15: Enlarged Top View with Trapezoidal Wing Overlaid

The wing is modified from this geometry such that, at a 45° oblique sweep, the tips of the vehicle are parallel to the flow. The new top view is shown in Figure 16. Part of the tip on the right side is removed and then added to the left side of the wing. This does not change the top view area of the wing and closely resembles the demonstration vehicle design. This will have an effect on symmetry of the vehicle so that there will no longer symmetry at the unswept case. This likely creates additional rolling and yawing moments that would have to be trimmed even with no sideslip.

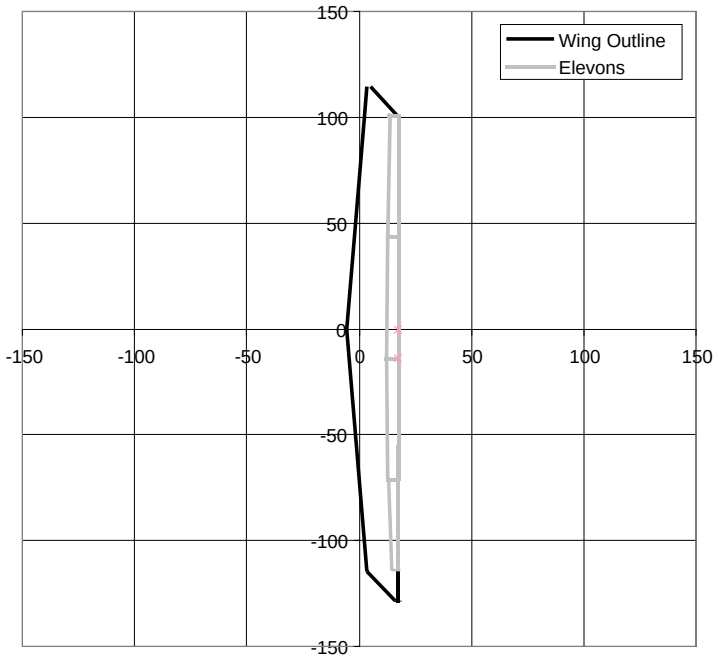

Figure 16: Top View of Vehicle Planform, 45° Parallel Tips

Oblique Slew Rotation

Determination of vehicle sweep is not difficult. A 2-D rotation can be used based on a counter-clockwise rotation—Λ_{OS} about the Z-axis. In order to correctly define moments, the vehicle should be positioned at a reference center before rotation. Equation 5 defines this rotation.

$$\boldsymbol{x}_i^{'} = \boldsymbol{R}^{'}_{ij}\,\boldsymbol{x}_{s\_i}$$

$$\begin{bmatrix} x' \\ y' \\ z' \end{bmatrix} = \begin{bmatrix} \cos\Lambda_{OS} & \sin\Lambda_{OS} & 0 \\ -\sin\Lambda_{OS} & \cos\Lambda_{OS} & 0 \\ 0 & 0 & 1 \end{bmatrix} \begin{bmatrix} x_s \\ y_s \\ z_s \end{bmatrix} \tag{5}$$

It is of interest to look at the vehicle both from body and stability axes orientations. Data can be re-interpreted from stability axis to body axis using a rotation matrix based on the current oblique slew rotation from equation 5 and alpha rotation based on equation 6.

$$\boldsymbol{x}_{bi} = \boldsymbol{R}^{''}_{ij}\boldsymbol{x}^{'}_{i}$$

$$\begin{bmatrix} x_b \\ y_b \\ z_b \end{bmatrix} = \begin{bmatrix} \cos\alpha & 0 & \sin\alpha \\ 0 & 1 & 0 \\ -\sin\alpha & 0 & \cos\alpha \end{bmatrix} \begin{bmatrix} x' \\ y' \\ z' \end{bmatrix} \tag{6}$$

The resultant rotation from body to stabilities axes is shown in equation 7.

$$\boldsymbol{R}_{ij} = \boldsymbol{R}_{ij}^{'}\boldsymbol{R}_{ij}^{''}$$

$$\boldsymbol{R}_{ij} = \begin{bmatrix} \cos\Lambda_{OS} & \sin\Lambda_{OS} & 0 \\ -\sin\Lambda_{OS} & \cos\Lambda_{OS} & 0 \\ 0 & 0 & 1 \end{bmatrix} \begin{bmatrix} \cos\alpha & 0 & \sin\alpha \\ 0 & 1 & 0 \\ -\sin\alpha & 0 & \cos\alpha \end{bmatrix} =$$

$$\begin{bmatrix} \cos\alpha\cos\Lambda_{OS} & \sin\Lambda_{OS} & \sin\alpha\cos\Lambda_{OS} \\ -\cos\alpha\sin\Lambda_{OS} & \cos\Lambda_{OS} & -\sin\alpha\sin\Lambda_{OS} \\ -\sin\alpha & 0 & \cos\alpha \end{bmatrix}$$

$$\boldsymbol{x}_{bi} = \boldsymbol{R}_{ij}\boldsymbol{x}_{i} \tag{7}$$

Due to the asymmetric sweep of an oblique wing, inertias, shown in equation 8, change in the stability axis based on each swept position. For the oblique body axis the values are always constant. In simple analyses of aircraft, these inertias are considered constant for small angle changes, but in this case there are large changes in the values considered in the stability axis. Note that the matrix of inertias is always symmetric such that six terms need to be found without assuming any symmetry. New inertias can be found using the combined rotation matrix from equation 9 for inertia.

$$\boldsymbol{I}_{ij} = \begin{bmatrix} I_{xx} & I_{xy} & I_{xz} \\ I_{yx} & I_{yy} & I_{yz} \\ I_{zx} & I_{zy} & I_{zz} \end{bmatrix} \tag{8}$$

$$\boldsymbol{I}_{ij_s} = \boldsymbol{R}_{ij}\boldsymbol{I}_{ij_b}\boldsymbol{R}_{ij}^{-1} \tag{9}$$

Aerodynamic forces and moments can be converted from one axis system to another by using this rotation matrix as well. Equations 10 and 11 express the conversion from the stability to body axis, but this can also be reversed. Orienting the vehicle in the stability axis, the angle of attack is expressed between the planes of the X-Y axes and the vertical component of the velocity vector. For an oblique wing body axis perspective, this angle is seen as a pitch and roll.

$$C_{F_b} = \begin{bmatrix} C_{A_b} \\ C_{Y_b} \\ -C_{N_b} \end{bmatrix} = R_{ij} C_{F_s} = R_{ij} \begin{bmatrix} C_{D_s} \\ C_{Y_s} \\ -C_{L_s} \end{bmatrix} \tag{10}$$

$$C_{M_b} = \begin{bmatrix} C_{l_b} \\ C_{m_b} \\ C_{n_b} \end{bmatrix} = R_{ij} C_{M_s} = R_{ij} \begin{bmatrix} C_{l_s} \\ C_{m_s} \\ C_{n_s} \end{bmatrix} \tag{11}$$

Example Case

Rotations between the body axis and the stability axis were examined using the example geometry from Figure 16. Inertias are estimated below based on a simple trapezoidal wing estimation in Lanham[23]. The resulting moments of inertia are based on an oblique slew of 35° and an alpha of 10 degrees.

$$I_{ij_b} = \begin{bmatrix} 2.0\text{e}+7 & 0 & 1.5\text{e}+5 \\ 0 & 1.9\text{e}+5 & 0 \\ 1.5e+005 & 0 & 2.1e+7 \end{bmatrix} \text{slugs*ft}^2$$

$$I_{ij_{s,\Lambda=35,\alpha=10}} = \begin{bmatrix} 1.4e+7 & \text{-}9.67\text{e}+6 & 1.4\text{e}+5 \\ \text{-}9.67\text{e}+6 & 6.955e+6 & -9.92e+4 \\ 1.5e+005 & -9.92e+4 & 2.1e+7 \end{bmatrix} \text{slugs*ft}^2$$

Aerodynamic force coefficients for this case can be found in the stability axis of the slewed wing and then converted back into the unswept oblique body axis using equation 6. Moment results shown can be used to trim out the vehicle based on the selected axis system

$$C_{F_b} = \begin{bmatrix} C_{A\_obli\_b} \\ C_{Y\_obli\_b} \\ -C_{N\_obli\_b} \end{bmatrix} = R_{ij} \begin{bmatrix} 0.1099 \\ 0.01 \\ -0.6234 \end{bmatrix} = \begin{bmatrix} 0.0057 \\ 0.0082 \\ -0.6330 \end{bmatrix}$$

$$C_{M_b} = \begin{bmatrix} C_{l\_obli\_b} \\ C_{m\_obli\_b} \\ C_{n\_obli\_b} \end{bmatrix} = R_{ij} \begin{bmatrix} 0.0105 \\ -0.206 \\ -0.0018 \end{bmatrix} = \begin{bmatrix} -0.1099 \\ -0.175 \\ -0.0036 \end{bmatrix}$$

2.3 Aerodynamic analysis

Wave and viscous drag are investigated for potentially useful methods for initial investigations. Higher-level analyses are useful for more detailed studies, but complexity in setup keep them from being as useful for this case. While not in the aerodynamic analysis section, HASC vortex lattice method is explored in the stability and trim analysis section for finding coefficients used in a trim analysis.

2.3.1 Wave drag

Wave drag is caused by shock waves forming around an aircraft in supersonic flight. Two types of such drag are discussed. Volumetric wave drag results from traveling at supersonic speeds. Lift-induced wave drag is a part of the drag due to lift at supersonic speeds. For a wing, volumetric wave drag accounts for thickness and is independent of lift, and lift-induced wave drag is independent of thickness. Purely supersonic flow is investigated here.

This form of drag is the main reason behind oblique wing designs. These designs have been found to reduce wave drag for a supersonic-lift-generating wing, and can be thought of as an aerodynamic evolution to swept wings on symmetric aircraft configurations. The oblique wing is not symmetric in supersonic flight, but rotates about a central pivot, which allows the maximum cross sectional area perpendicular to the flow to be half that of a similar symmetric design. By skewing the wing in flight to minimize inviscid drag; it can be efficient at supersonic and subsonic speeds. In subsonic flight, the wing can have a high aspect ratio and associated lift. In supersonic flight, the wing can effectively have a lower aspect ratio when slewed, and with a sufficient angle, the flow normal to the leading edge of the wing can be subsonic.

Figure 17 shows a simplified example of the influence that a shock wave on the forward leading edge has on a highly swept elliptical wing. The half-angle of the Mach cone, μ, is represented for a free stream Mach number of 1.414. Properly aligned behind the shock wave, drag due to the disturbances on the wing can be reduced due to subsonic flow normal to the leading edge. Outside of the half angle of the Mach cone is the zone of silence where the shock has no effect such that further shock waves will occur creating more drag on the vehicle.

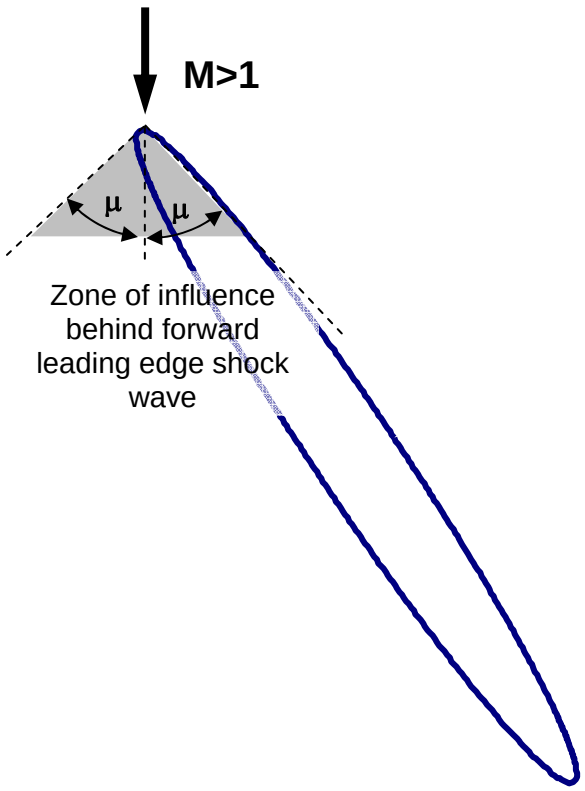

Figure 17: Elliptical Wing at 60° Oblique Sweep in Supersonic Flow

A sample case was selected based on that explored in Oblique Flying Wing Studies by A. R. Seebass[1]. Figure 18 shows the representation of an elliptical wing case. Elliptic wings are a simplified geometry that allow for a theoretical solution. Here, the ratio of the semi major axis (b_{ell}) to the semi minor axis (a_{ell}) is 10. Note that in this case the semi major axis of an elliptical wing is half of the wing's span (b). Aspect ratio can be determined based on the area of an ellipse given in equation 12. Equation 13 develops this into aspect ratio for the ellipse. In the example case, the aspect ratio is $40/\pi=12.73$.

$$S = \pi a_{ell} b_{ell} \tag{12}$$

$$AR = 4b_{ell} / \pi a_{ell} \tag{13}$$

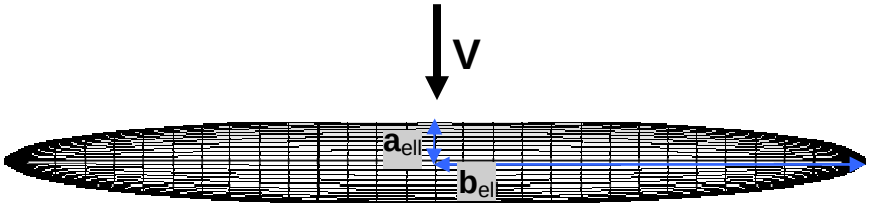

Figure 18: Oblique Wing Flying Wing Elliptical Model, Λ_{OS}=0°

Volumetric

Volumetric wave drag is additional drag occurring at supersonic speeds due only to the volume of the vehicle. To minimize this type of drag for supersonic vehicles, area ruling is used to smoothly distribute the cross sectional area perpendicular to the flow.

J. H. B. Smith derived equations that can be used to show the effect of asymmetric slewing of elliptic wings, and published his results in 1961[25]. Minimum drag for a given lift can be achieved with an elliptic wing slewed to the appropriate angle. Results of the study revealed that it was theoretically possible to find a high-speed oblique wing aircraft capable of a lift-to-drag of 12 or higher. Equations 14 through 18 reproduce the equations from that paper with nomenclature used here.

$$\beta^2 = M^2 - 1 \tag{14}$$

The actual semi-span from the ellipse's center when yawed is shown in equation 15. Equation 16 calculates the distance from the center of the ellipse its edge in the direction of the velocity. Another geometric parameter, m', is shown in equation 17.

$$b_{ell}' = (a_{ell}^{\ 2} \sin^2(\Lambda_{OS}) + b_{ell}^{\ 2} \cos^2(\Lambda_{OS}))^{1/2} \tag{15}$$

$$a_{ell}' = a_{ell} b_{ell} / b_{ell}' \tag{16}$$

$$m' = (b_{ell}^{\ 2} - a_{ell}^{\ 2}) \cos(\Lambda_{OS}) \sin(\Lambda_{OS}) / b_{ell}'^2 \tag{17}$$

Zero-lift wave drag is found using equation 18. Only the real part of the right hand quantity is used.

$$C_{D_{0w}} = \frac{t^2}{a'^2} R.P.\left\{ \frac{\beta - \left(m' + i\frac{a_{ell}'}{b_{ell}'} \right)\left(m' + 2i\frac{a_{ell}'}{b_{ell}'} \right)}{\left[\beta^2 - \left(m' + i\frac{a_{ell}'}{b_{ell}'} \right)^2 \right]^{3/2}} \right\} \qquad (18)$$

Figure 19 shows a comparison of oblique wings of different thicknesses using Smith's equations. The oblique sweep used in all the plots is 60°. Similar plots were made by Jones[26]. Thickness-to-chord ratio is based on the thickest part of the airfoil for the unswept chord of the wing.

Wave drag decreases for thin wings. Thin wings also delay the drag rise. As Mach number increases the difference in drag becomes more dramatic. A wing design for higher supersonic speeds is increasingly constrained in wing thickness due to the rapidly increasing drag penalty.

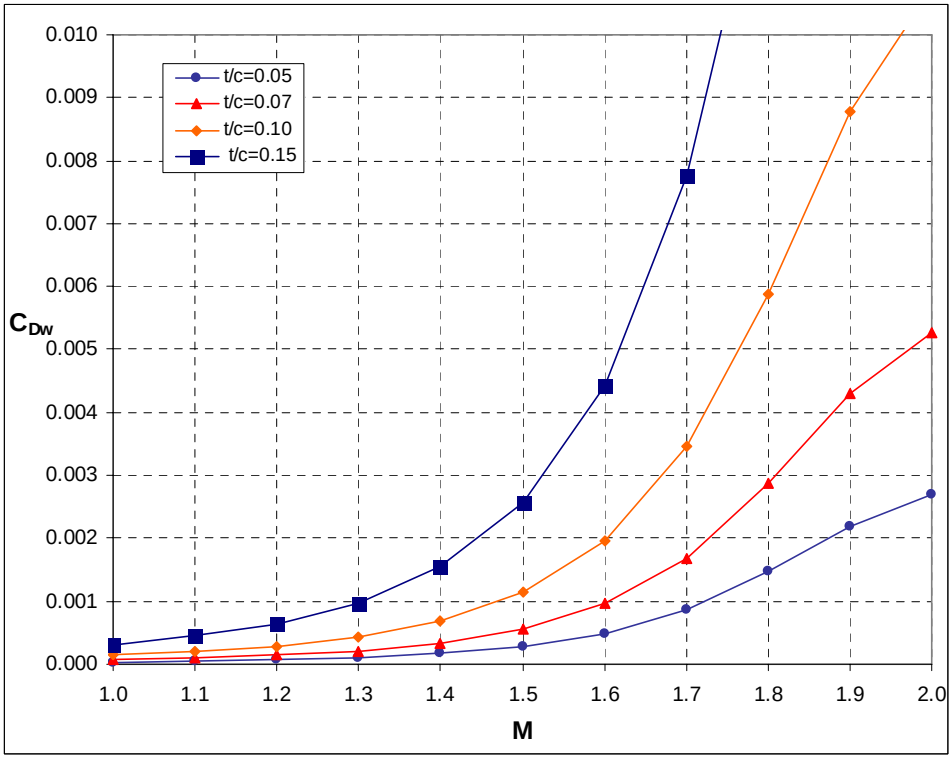

Figure 19: Theoretical Volumetric Wave Drag for Differing Thicknesses of 60° Swept Oblique Wings

Figure 20 shows a comparison of an oblique wing with a fixed thickness, swept to different oblique angles. The thickness is kept at 10% t/c for all of the plots in the figure. In order to keep from experiencing drag rise, the wing must be swept such that the areas of the cutting planes tangent to each instance of the Mach cone are minimized. As Mach increases this effect decreases suggesting a greater oblique angle of the wing. If this doesn't happen, the drag follows a similar trend to the 0° sweep case which is a magnitude higher, but slowly decreases as speed increases. This compares with other supersonic vehicle's behavior. The cross sectional area perpendicular to the flow along the wing is significant, shown by oblique sweep angles 15° through 55° which have an incremental decrease in drag from the 0° case at Mach 2 and above. Mach 1.4 - 1.6 would be the best speed to design to because the most benefit for an oblique wing can be had.

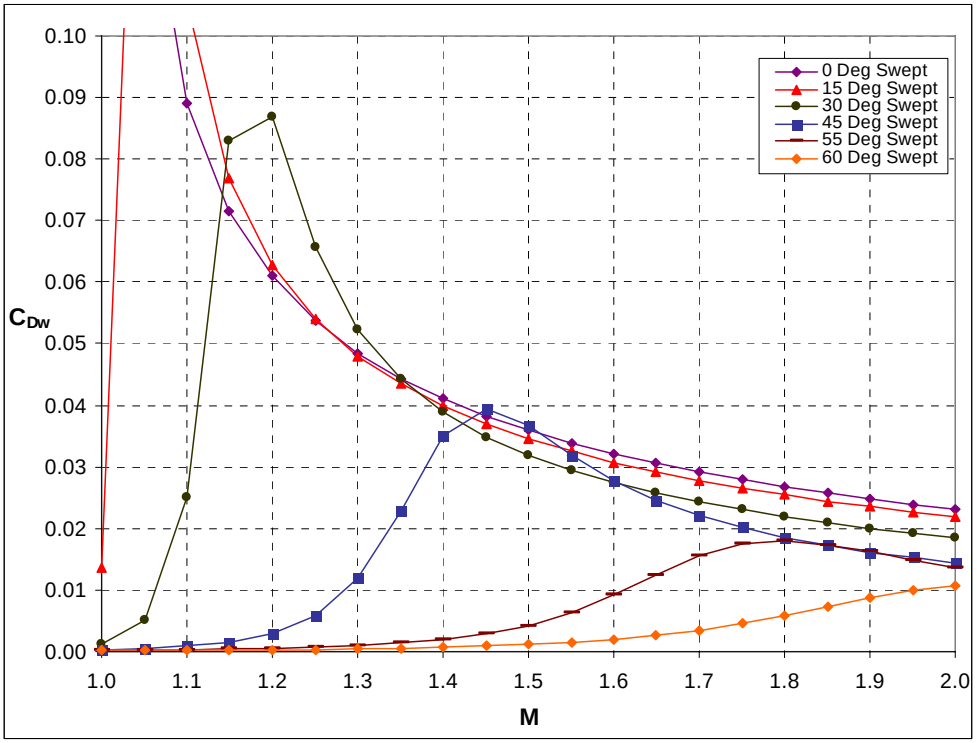

Figure 20: Theoretical Volumetric Wave Drag for Different Sweeps of an Oblique Wing (t/c=10%), (AR=40/π)

Wave drag can be determined more precisely than the theoretical case using analytical tools such as the Zero-Lift Wave Drag Program[16]. This process uses Mach

planes that cut the wing into sections that can be analyzed together to determine volumetric drag. This can be done for an arbitrary input geometry.

Biconvex airfoils were selected for the wing in the program to minimize wave drag for a given thickness to chord. While this is not an optimal overall airfoil design, it should capture the trends for any given oblique sweep. Figure 21 shows this airfoil.

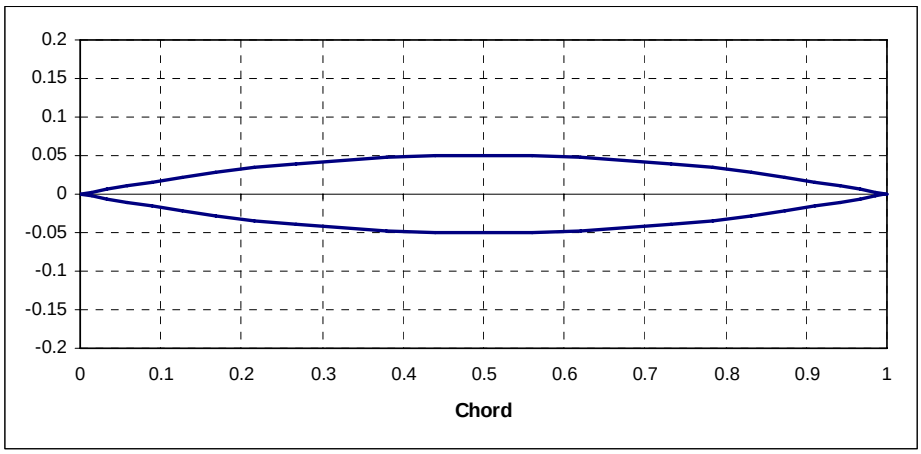

Figure 21: 10% t/c Biconvex Airfoil

Figure 22 shows the wave drag program output for changes in thickness at 60° oblique sweep. The thin wing displays similar drag to the theoretical case, but thicker wings have a higher drag than the theoretical solution. Drag is still below the rise experienced by a less swept wing.

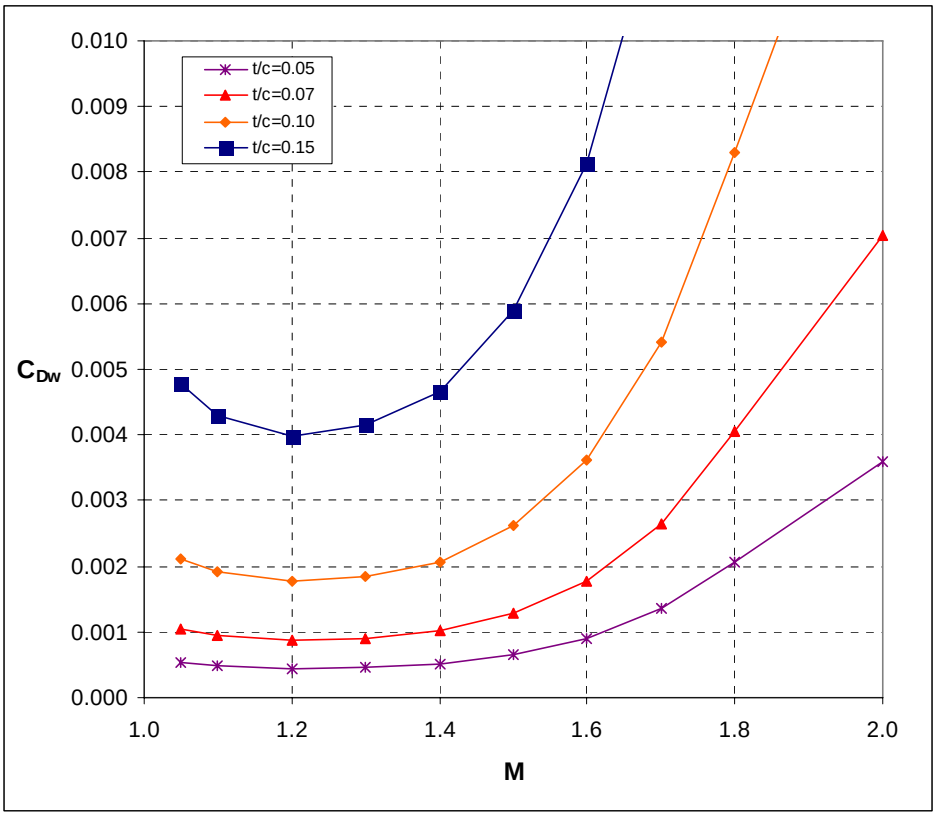

Figure 22: Volumetric Wave Drag Program Results for Differing Thicknesses of 60° Swept Oblique Wings

Figure 23 shows the results of the wave drag program for various oblique sweeps of the same 10% t/c wing. Unfortunately this plot isn't entirely consistent with Figure 22. Drag is higher in all cases. The 30° oblique sweep case has a high peak drag that does not follow the trends and exceeds the 0° case. At higher Mach numbers, the plots do not converge, with the unswept wing maintaining a higher drag and if the 30° case is discounted, the lower sweep wings actually have lower drag at Mach 2.0. One possibility is the function of the program to interpolate to the least drag case is creating slight changes to the geometry input that is affecting the drag output differently in each case.

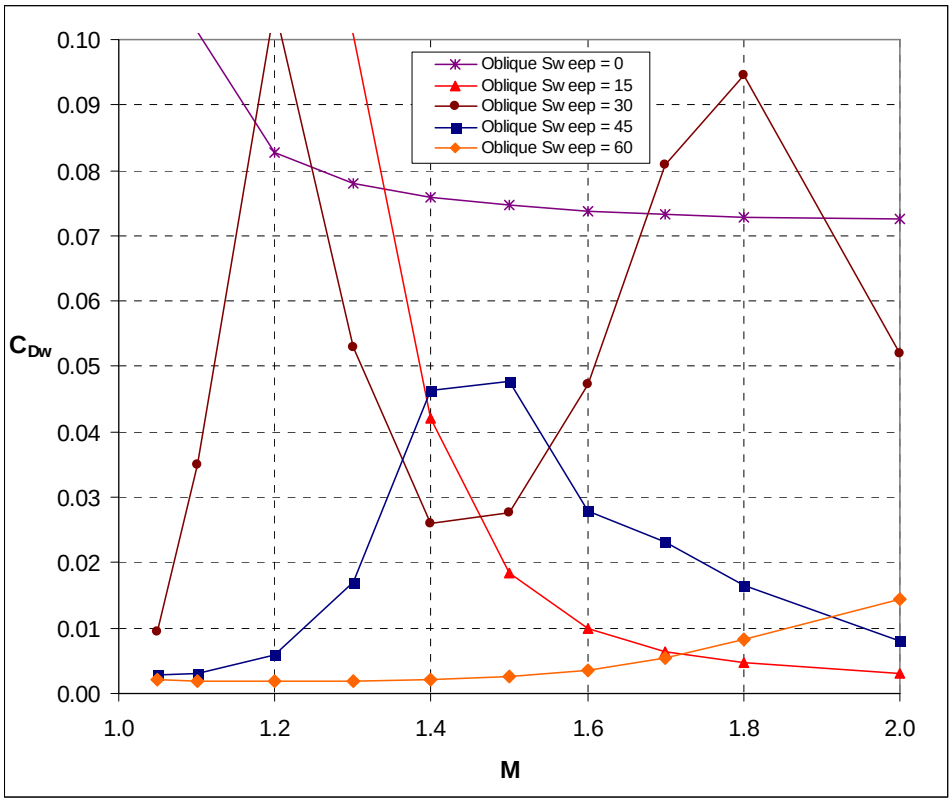

Figure 23: Volumetric Wave Drag Program Results for Different Sweeps of an Oblique Wing (t/c=10%), (AR=40/π)

Lift-Induced

Wave drag due to lift, proportional to the square of lift and independent of the thickness of the wing, is normally lower than that of volumetric wave drag and skin friction to the point that it can, in some cases, be ignored at low supersonic speeds. This is partially due to the lift capacity of the wing, which is much greater than necessary at these speeds, due to being optimized for subsonic flight. In the case of the oblique flying wing, at subsonic speeds, less drag due to lift can be achieved with a higher aspect ratio. As speed increases the lift coefficient requirement is reduced and the wing can be obliquely swept to minimize volumetric drag at reduced lifting capability.

2.3.2 Viscous drag

Viscous drag can be obtained through approximations of skin friction and pressure drag. The program FRICTION[17] provides a template for a simple solution for viscous drag based on Eckert Reference Temperature Method for a laminar flow over a

flat plate[19] or the van Driest II Method for turbulent flow over a flat plate[20] depending on the conditions. The latter method assumes a temperature recovery factor of 0.89 based on flat-plate skin friction data that improves predictions.

This method is simple to implement in any software code based on the original program. It can be used directly for aerodynamic analysis of the vehicle in a mission analysis.

2.4 Vehicle sizing and mission analysis

An initial sizing was performed for an oblique flying wing aircraft to the DARPA requirements as outlined. This is not a detailed design, but a starting point in order to understand some of the sizing issues and have a basis for further integration.

Figure 24 shows linear design constraints for wing loading and thrust to weight based on takeoff, landing, and optimal cruise at subsonic and supersonic speeds. The area between the optimal points for subsonic and supersonic speeds and the thrust to weight are great enough to take off within a given balanced field length. A range of possible takeoff field lengths are shown. Depending on the wing loading requirement, more thrust may be required for supersonic flight than for takeoff. The selected wing loading, 60 lb/ft^2, and thrust to weight ratio, 0.6, used in this sizing is marked with a star in the figure.

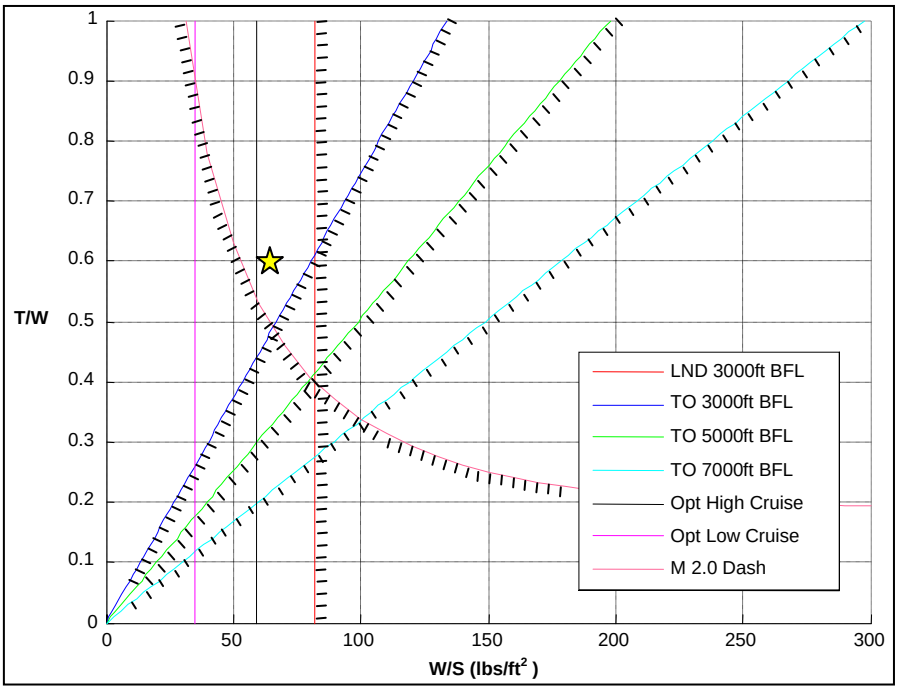

Figure 24: Initial Wing Loading and Thrust to Weight

Initial sizing equations are taken from Raymer[7]. These equations were coded in MATLAB to include initial fuel sizing of the vehicle and weight group calculations for an attack vehicle attributable to a flying wing aircraft, but with 50% increase in wing structural weight due to not having a fuselage. Figure 25 shows the bombing mission profile selected for sizing. The supersonic cruise and dash use most of the fuel for the mission. The analytical volumetric wave drag from Smith[25] and viscous drag calculations from the FRICTION[18] were coded in MATLAB and used in the loop during these segments.

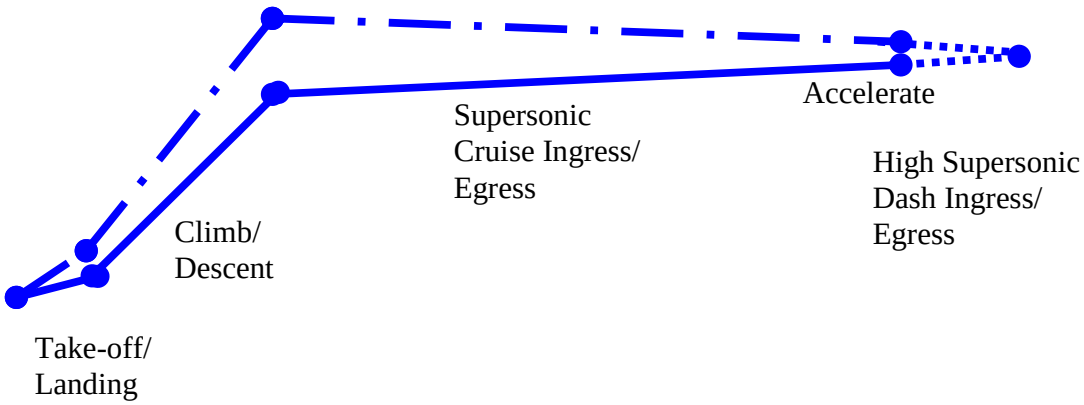

Figure 25: OFW Bomber Mission Profile

Figure 26 shows the results of the sizing routine as a carpet plot of gross weight for various wing loadings and aspect ratios of the wing. Assumptions in the sizing are that an engine is sized based on the Appendix E afterburning turbofan from Raymer[7]. A thrust to weight of 0.6 was found based on cruise thrust requirement estimates. Also some geometry constraints were applied such as a taper ratio of 0.6 based on the DARPA geometry and a wing maximum thickness to chord of 0.15 at the unswept wing case in order to achieve the necessary volume. The resulting design wing aspect ratio decreases the weight as the vehicle size increases. This is opposed to normal supersonic vehicles which have low aspect ratio. The oblique wing at high speeds will be swept back causing wing loading to have a dramatic effect on weight such that at the two lowest wing loadings, the sizing does not converge.

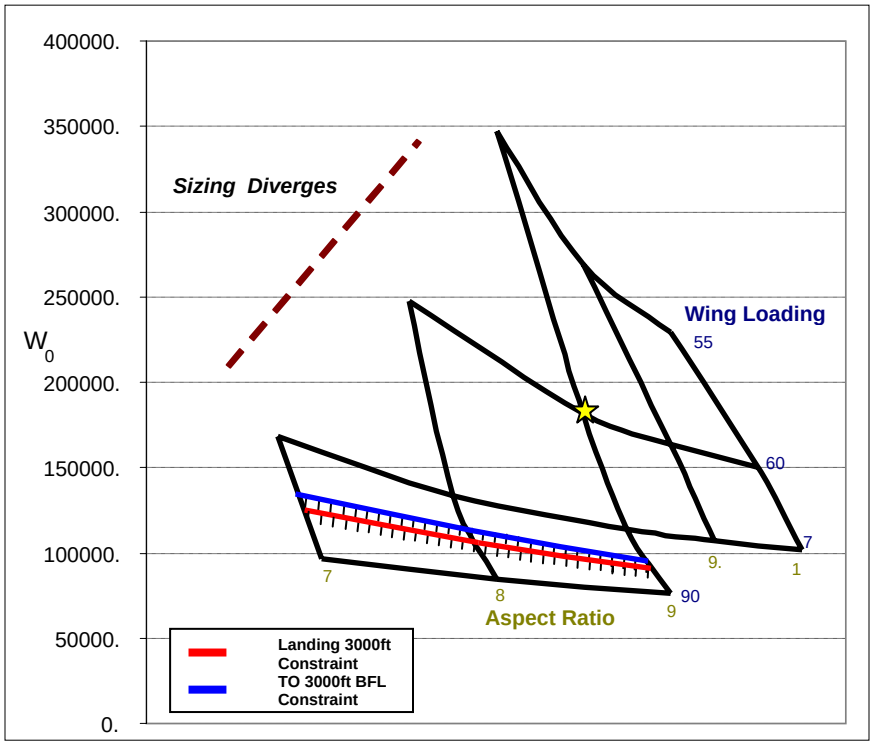

Figure 26: Wing Geometry and Sizing Effect on Gross Weight

A point was chosen in the design space with a wing aspect ratio of 9 and a wing loading of 60 lbs/ft^2. After sizing, the gross weight comes to 182,000 lbs. This includes 94,000 lbs of fuel. Figure 27 shows a break down of the weights based on the estimates for each group in the structural weight.

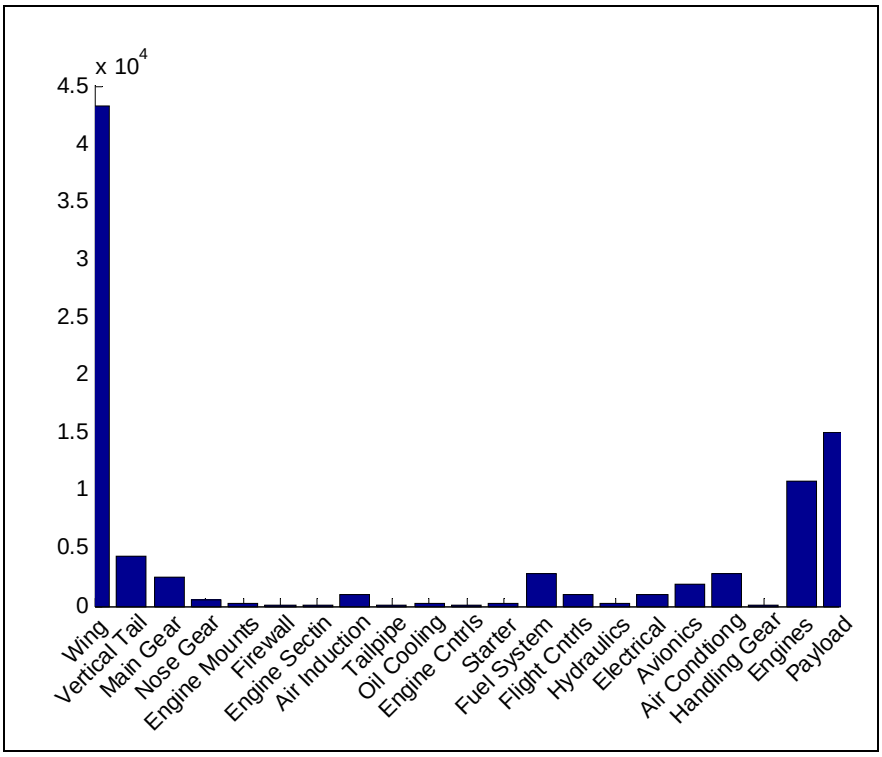

Figure 27: Initial Sizing Weights Breakdown

3. Static Stability and Trim Analysis

An area important to look at early for a vehicle is stability and control. A major requirement of such an investigation is the ability to trim the vehicle. Problems that are not caught early in the design process can be costly or degrade performance later on. Stability and control issues were part of the reason that an OFW concept was not practical for many years. With modern control systems this may no longer be the case, but there is still remaining anxiety about introducing the complexity of such a vehicle and having adequate control.

3.1 Takeoff-analysis

Takeoff and landing for an oblique flying wing are interesting cases due to the arrangement of such a vehicle. Some takeoff metrics are better defined for vehicles with fuselages. Distance constraints for takeoff and landing are not as much of a concern as this vehicle will likely have specialized basing.

3.1.1 Landing gear positioning

Positioning of landing gear is important to maintain balance and gust tolerance of the aircraft while in contact with the ground. For an oblique flying wing, a quadricycle landing gear, or a four landing gear configuration, is suggested due to the unswept nature of the wing and lack of a fuselage that would make a tricycle or conventional landing gear more practical. Also, the center of the vehicle will be mostly used for payload storage in the bombing mission. While the following considerations are for setting bounds on landing gear location, packaging of the volume of the vehicle is also a consideration.

Longitudinal positioning of landing gear at the ground is suggested by Torenbeek, in a discussion of a tailwheel undercarriage. The position should be at least 14° to 17° in front of the center of gravity location. This is to ensure stability when braking during landing. This should also be applicable for this vehicle. Assuming a forward and rear spar to attach to, the gear would be toward the front and rear of the vehicle[27].

Lateral tip over due to steady gusts was used in investigating gear positioning for the vehicle. The placement is determined such that wind gusts will not roll the aircraft while on the ground because other options for finding lateral gear positions do not seem to fit this case. [13] This is based on the rolling moment at various gust angles around the aircraft, which can be related to sideslip. The method of calculating the rolling moment is taken from Roskam's aircraft design book[28]. The case investigated here is the same configuration from the subsonic analysis section. The HASC vortex-lattice is used for higher beta values. Figure 28 shows that the spacing of the landing gear must be at least greater than 10 feet from the center of the vehicle to avoid tip over due to gusts of 100 knots. The critical moment arm maximum of less than 10 feet means that there will likely not be an issue for this aircraft designed to have over 75 feet half-span.

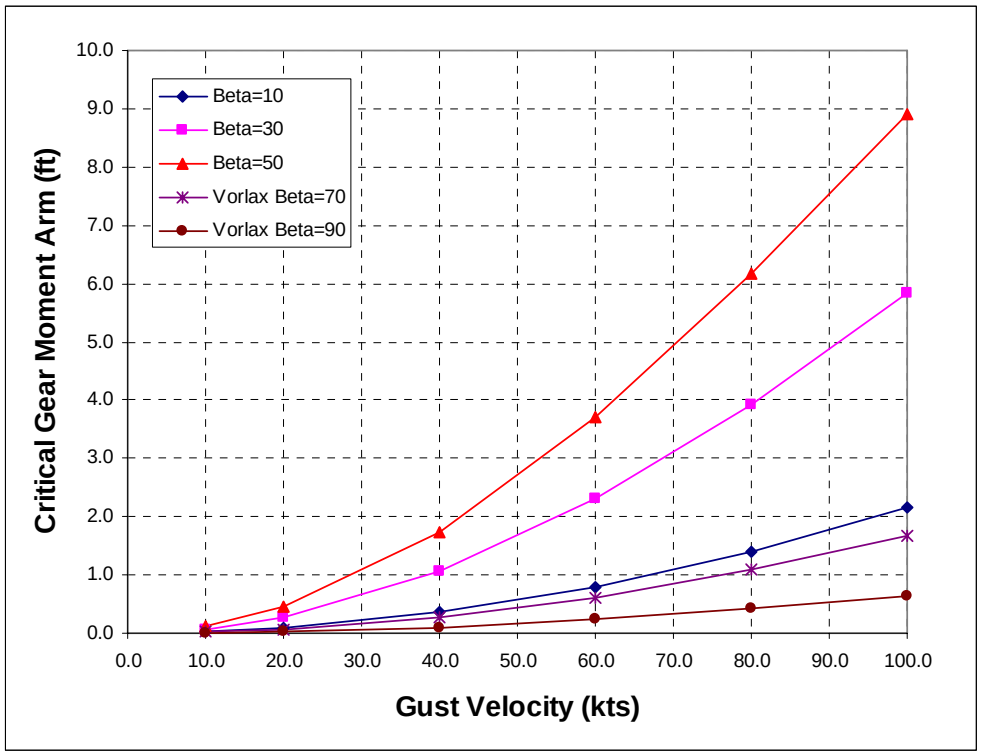

Figure 28: Lateral Landing Gear Critical Distance to Prevent Tip Over

3.1.2 Ground effect

Porpoising Issues

Porpoising can be defined by a condition where an aircraft can not maintain a constant attitude and is associated with an uncommanded pitching of the aircraft. Unmanned aircraft are particularly vulnerable to this condition at take-off and landing[29]. This behavior is due to a change in operating conditions from which the unmanned vehicle was designed. The control system applied to the aircraft may be based on insufficient data to compensate such a situation. While compensation for such deficits is possible, it will be less effective with less data available in the model.

Ground effect is caused by an aircraft's close proximity to the ground which can affect an aircraft's flying dynamics. A pilot has enough situational awareness that this is usually not an issue. If an incomplete aerodynamic model is used for the control system of an unmanned vehicle, this can cause the aircraft's characteristics to change and has been the cause of some crashes at takeoff, such as DarkStar AV1[30,31].

A flying wing aircraft like DarkStar or an oblique flying wing aircraft are designed with relaxed static stability for volume to be more equally distributed in the wing as well as the aerodynamic and observability benefits. Ground effect issues need to be explored because the stability of such vehicles can change rapidly in ground effect. For an unmanned vehicle, this problem is exacerbated because human controllers tend to be better at correcting such departures than control systems based on an incomplete aerodynamic database. This can change based on more advanced control algorithms, but those are still based on some modeling.

Oblique Flying Wing in Ground Effect

Inviscid analysis was done using the HASC program which uses a Vortex-Lattice (Vorlax) method[11]. The ground was represented using a mirroring technique. Here the model was represented by a reflection across the defined ground level such that any vortices will also be reflected in contact with the mirrored version. Height above ground was input as a fraction of span. No ground effect was found above a height equal to half-span. Analytically, the vehicle can be pitched about the reference point such that it goes below the ground plane creating an error in the analysis code.

The oblique wing being demonstrated in the DARPA program does not have an oblique sweep during take-off and landing. Figure 29 shows the vortex lattice models at different oblique sweep angles. The unswept wing has fairly straight-forward aerodynamic changes due to ground effect shown in Figure 30 through Figure 33. Figure 30 shows a modest increase in inviscid only lift to drag at higher angles of attack. Pitching moment is increasingly negative due to ground effect in Figure 31. Oblique sweep in ground effect is an interesting issue related to asymmetries.

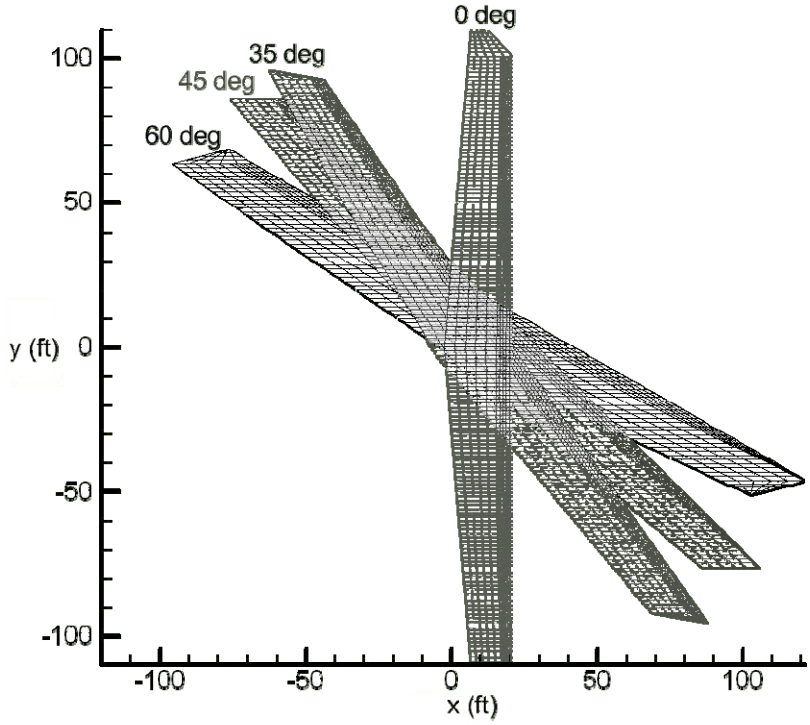

Figure 29: Vortex Lattice Model at Oblique Swept Positions

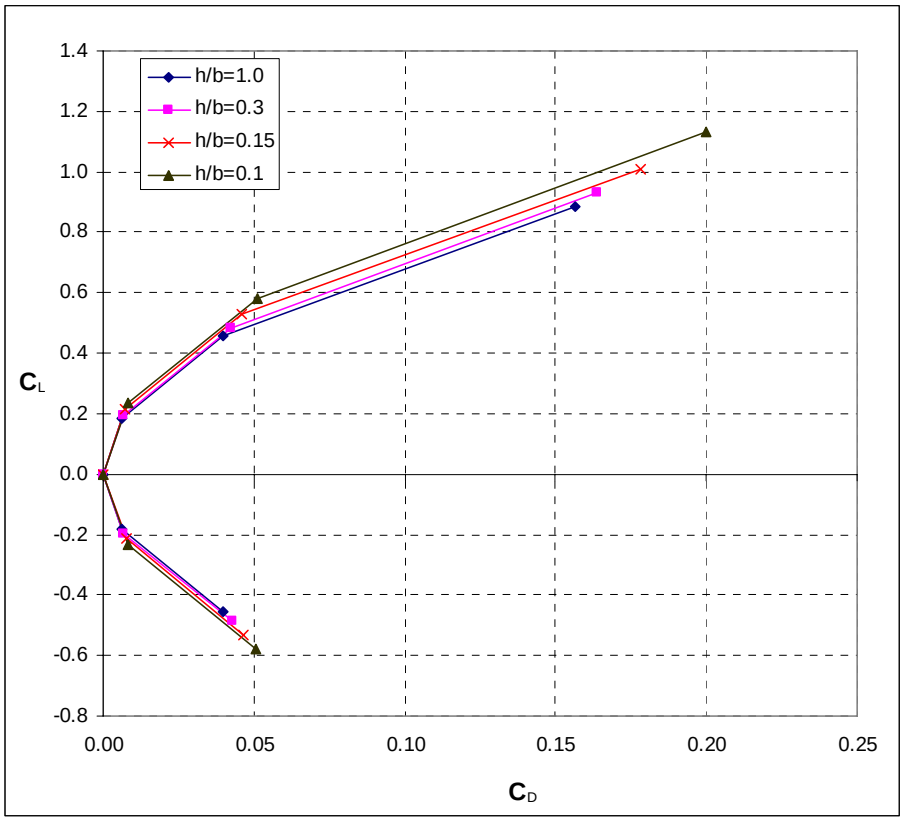

Figure 30: Drag Polar in Ground Effect for Unswept Wing

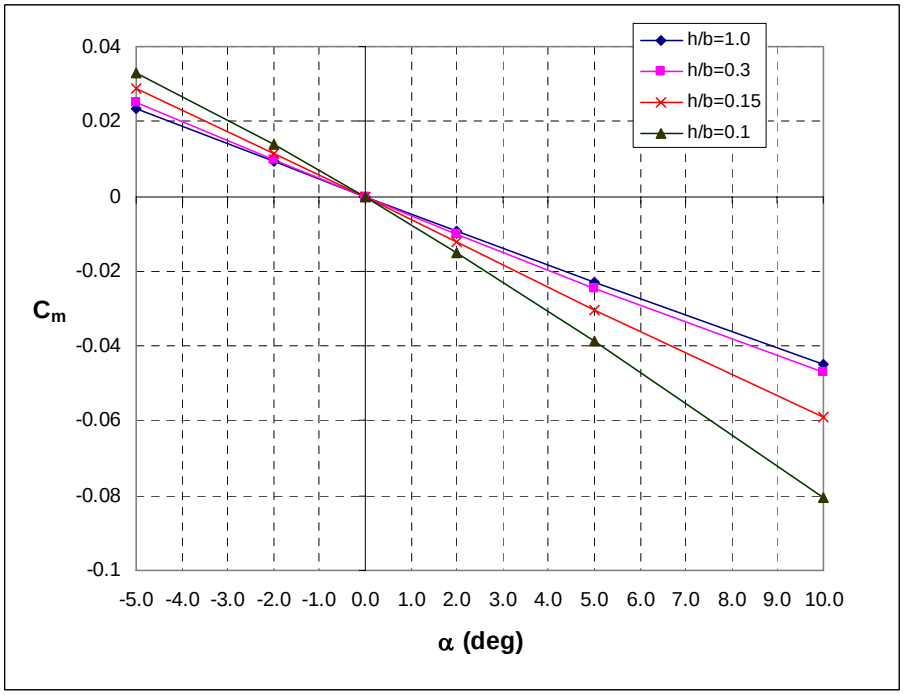

Figure 31: Pitching Moment in Ground Effect for Unswept Wing

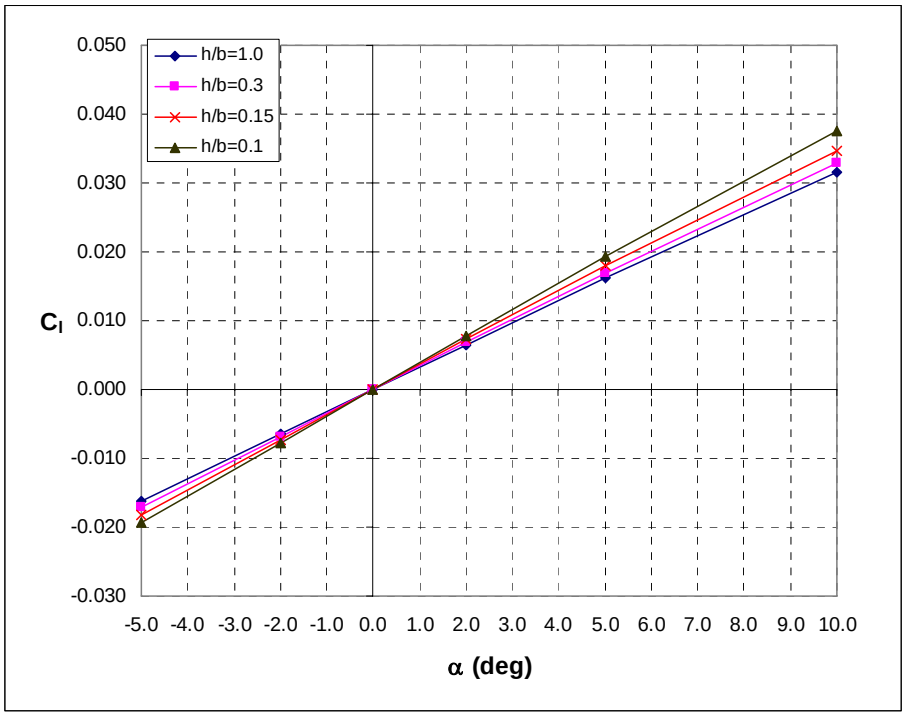

Figure 32: Rolling Moment in Ground Effect for Unswept Wing

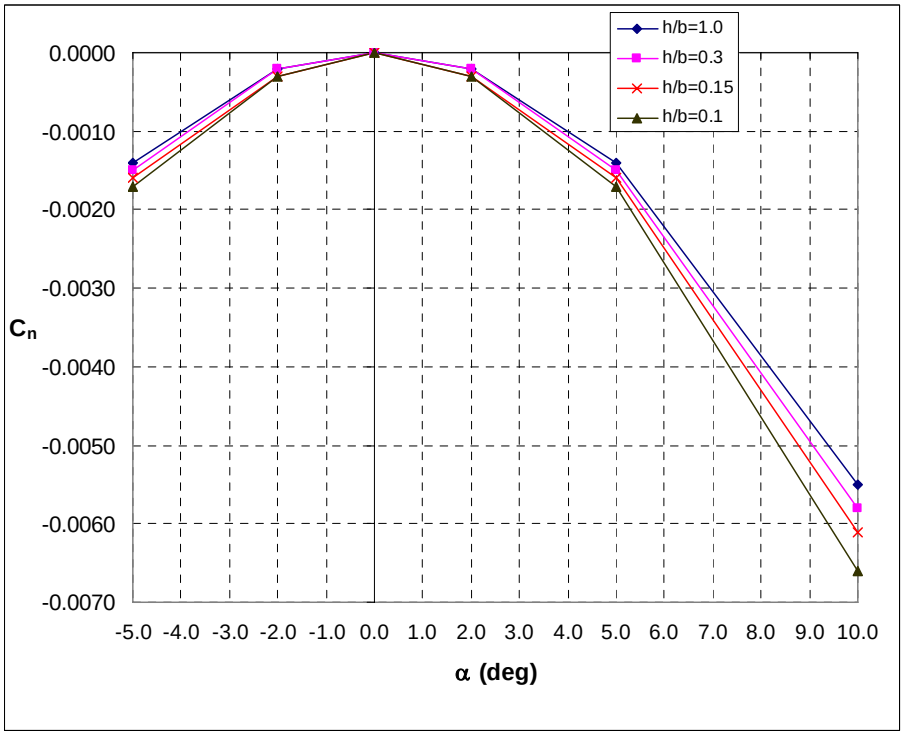

Figure 33: Yawing Moment in Ground Effect for Unswept Wing

Figure 34 through Figure 37 show the in ground effect results for the same model at an oblique sweep of 35°. There is a larger increase in lift than the unswept case. The moments in pitch, roll, and yaw begin to diverge at 5° angles of attack for height above ground of 0.15 and below.

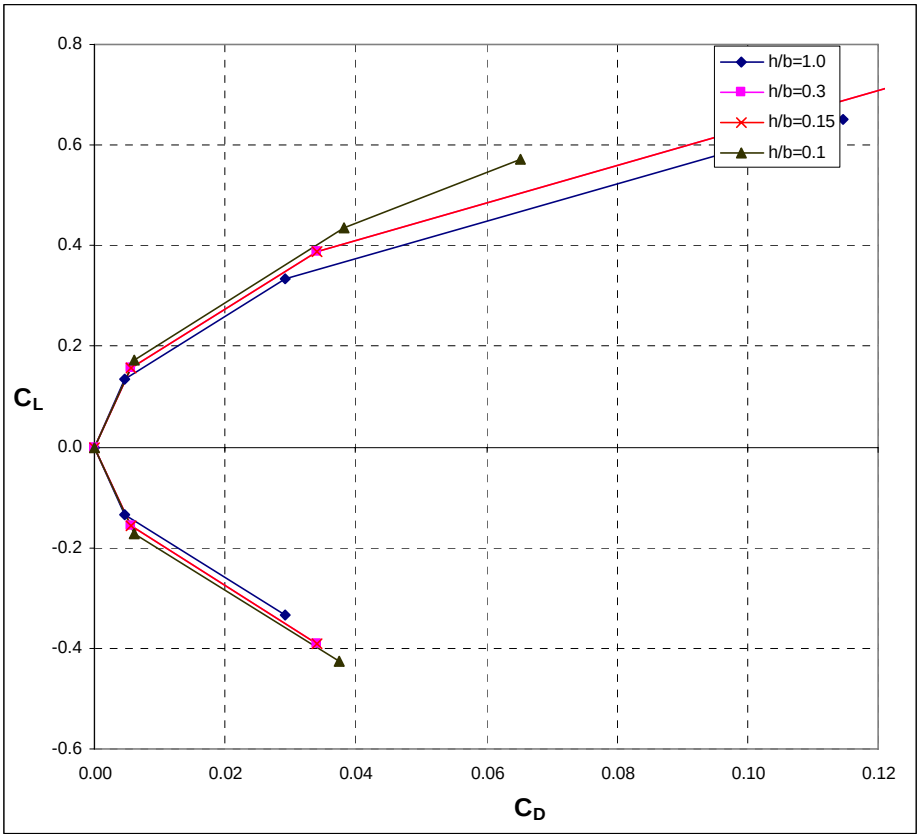

Figure 34: Drag Polar in Ground Effect for 35° Oblique Swept Wing

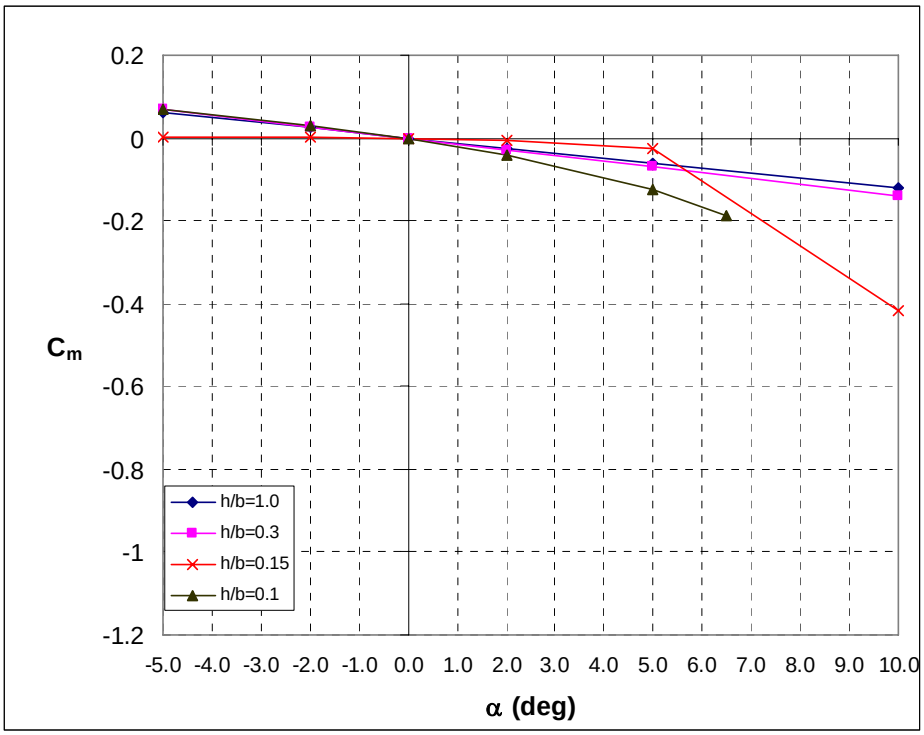

Figure 35: Pitching Moment in Ground Effect for 35° Oblique Swept Wing

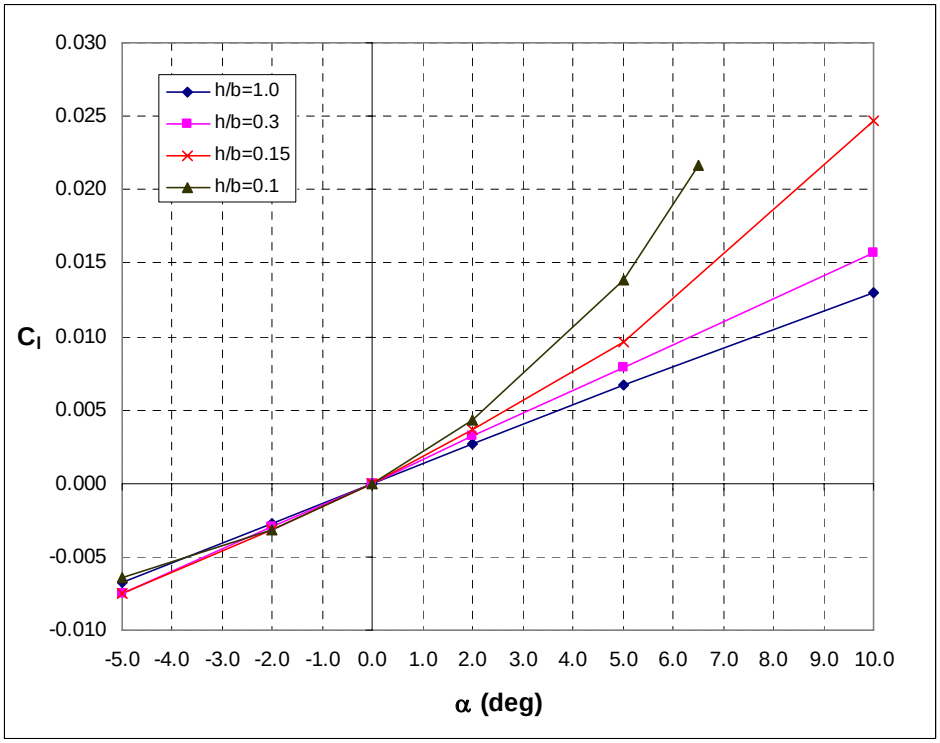

Figure 36: Rolling Moment in Ground Effect for 35° Oblique Swept Wing

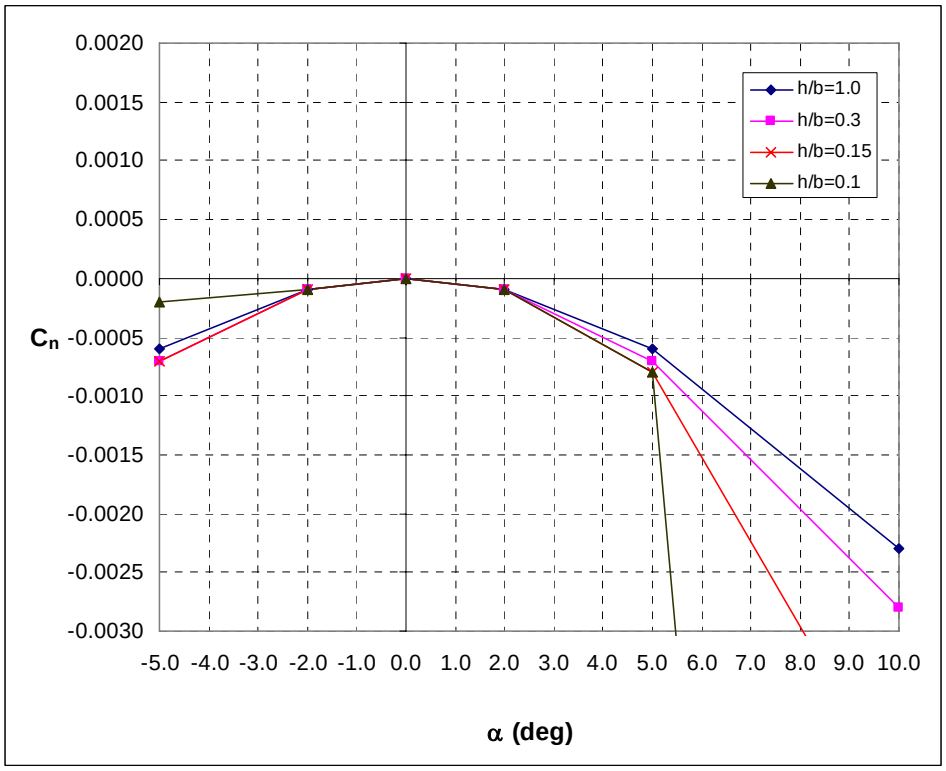

Figure 37: Yawing Moment in Ground Effect for 35° Oblique Swept Wing

Figure 38 through Figure 41 show the in ground effect results at an oblique sweep of 45°. Lift increases and drag decreases as height above ground is below 0.15 wing span. The pitching moment begins to diverge at 5° angles of attack for height above ground of 0.15 and below. However, rolling and yawing moments become reversed due to the asymmetries that are occurring coupled with ground effect. This could be an issue for an oblique wing vehicle attempting to maneuver in ground effect.

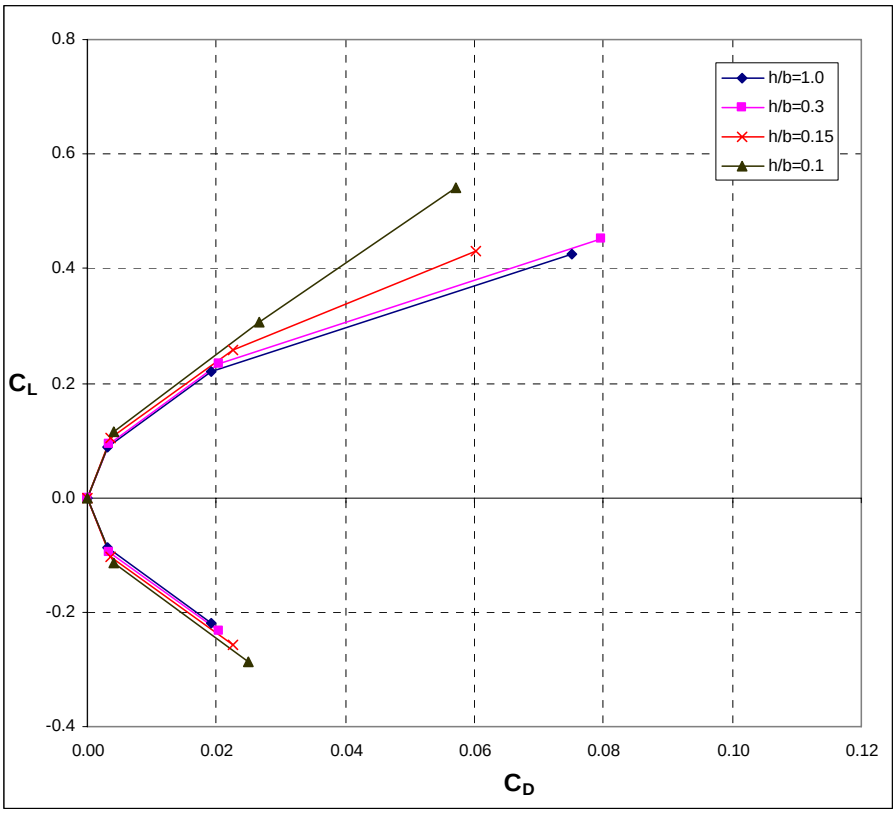

Figure 38: Drag Polar in Ground Effect for 45° Oblique Swept Wing

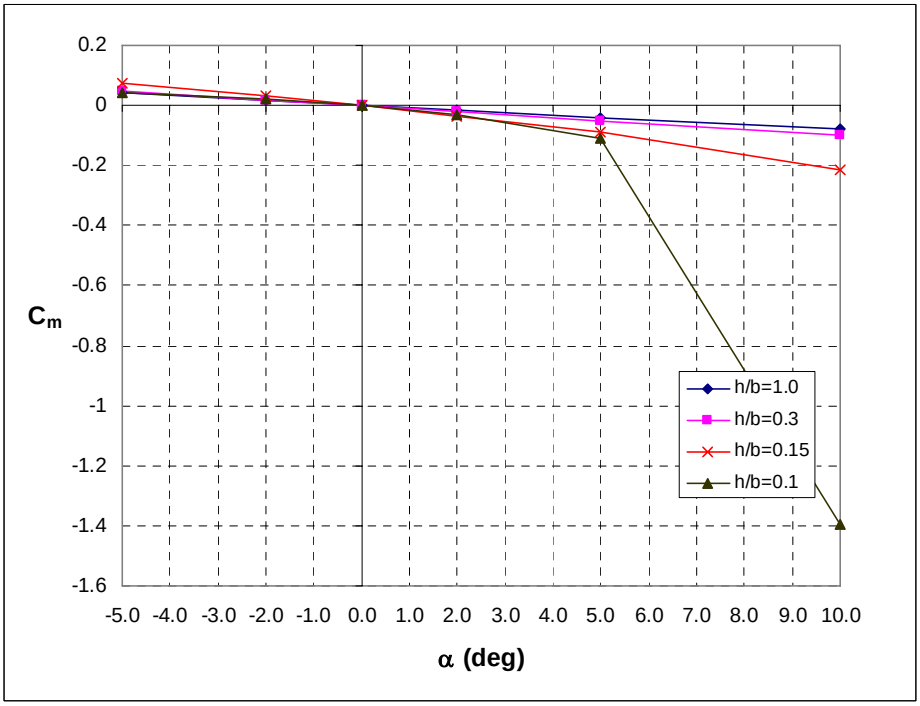

Figure 39: Pitching Moment in Ground Effect for 45° Oblique Swept Wing

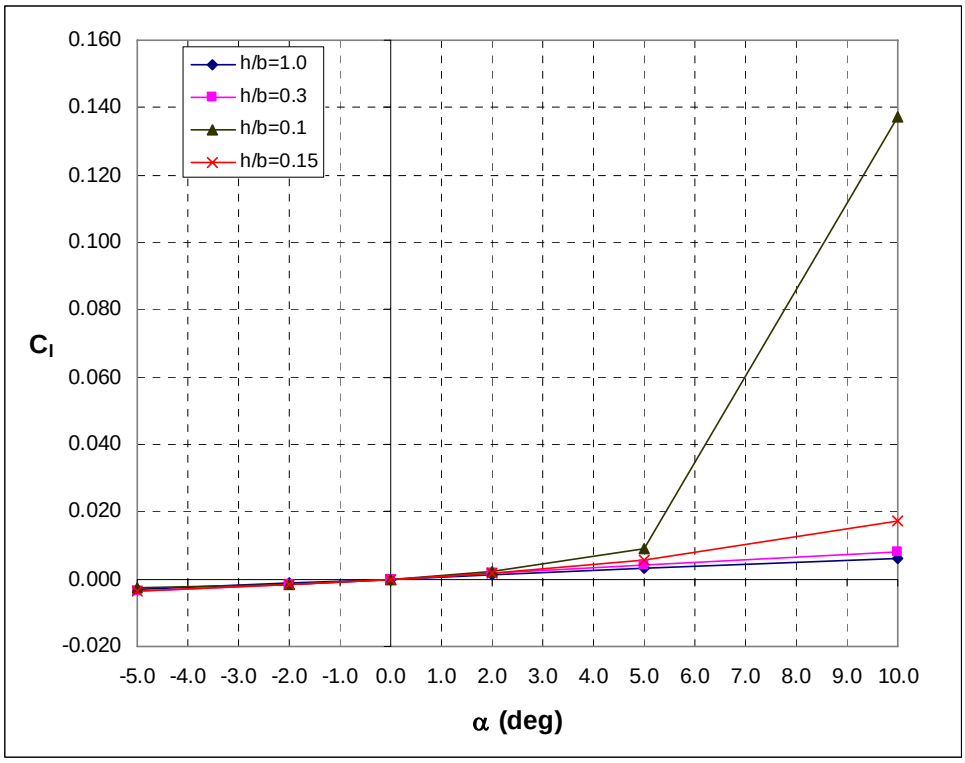

Figure 40: Rolling Moment in Ground Effect for 45° Oblique Swept Wing

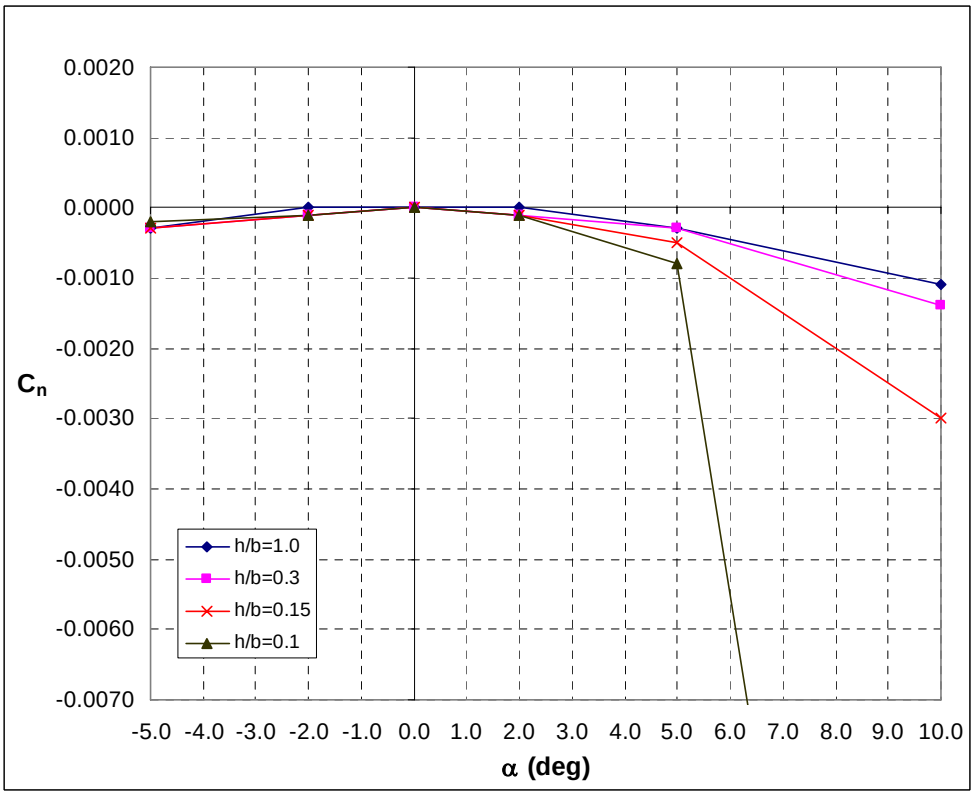

Figure 41: Yawing Moment in Ground Effect for 45° Oblique Swept Wing

Figure 42 through Figure 45 show the ground effect resulting from an oblique sweep of 60°. Lift increases and drag decreases as height above ground is below 15% of the span. The pitching moment begins to exponentially increase at 5° angles of attack for height above ground of 0.15 and below. Again, rolling and yawing moments become reversed and it is much more apparent. This suggests that if an oblique wing is to be at an angle while in ground effect it would be best to keep that angle low to prevent reversal of roll and yawing moments that are being encountered.

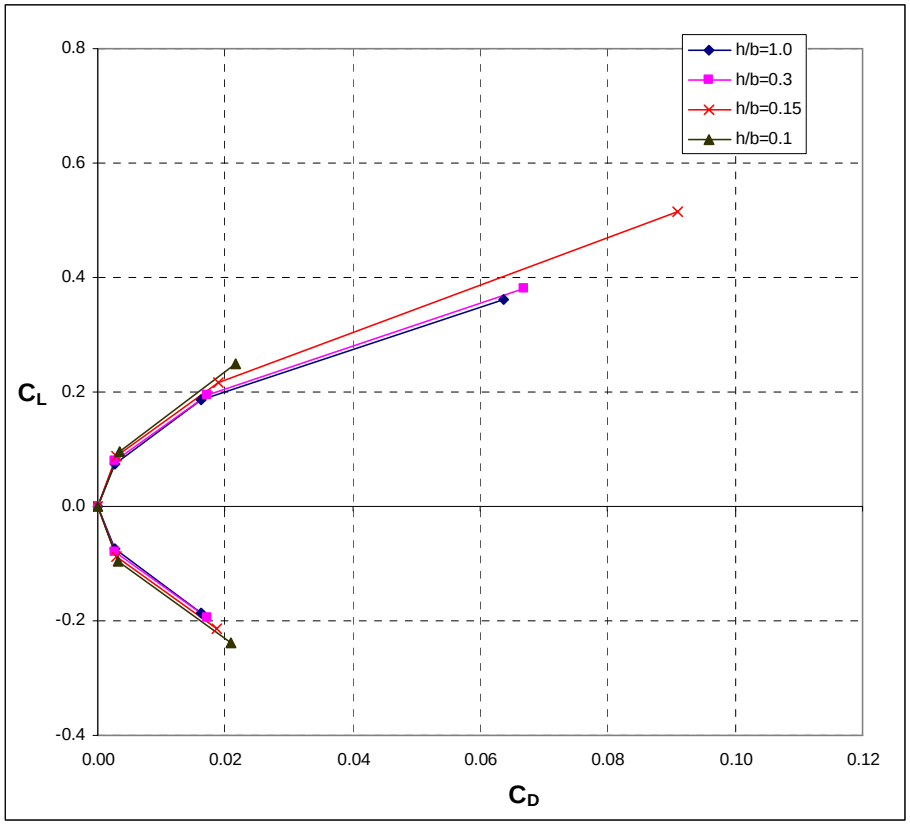

Figure 42: Drag Polar in Ground Effect for a 60° Oblique Swept Wing

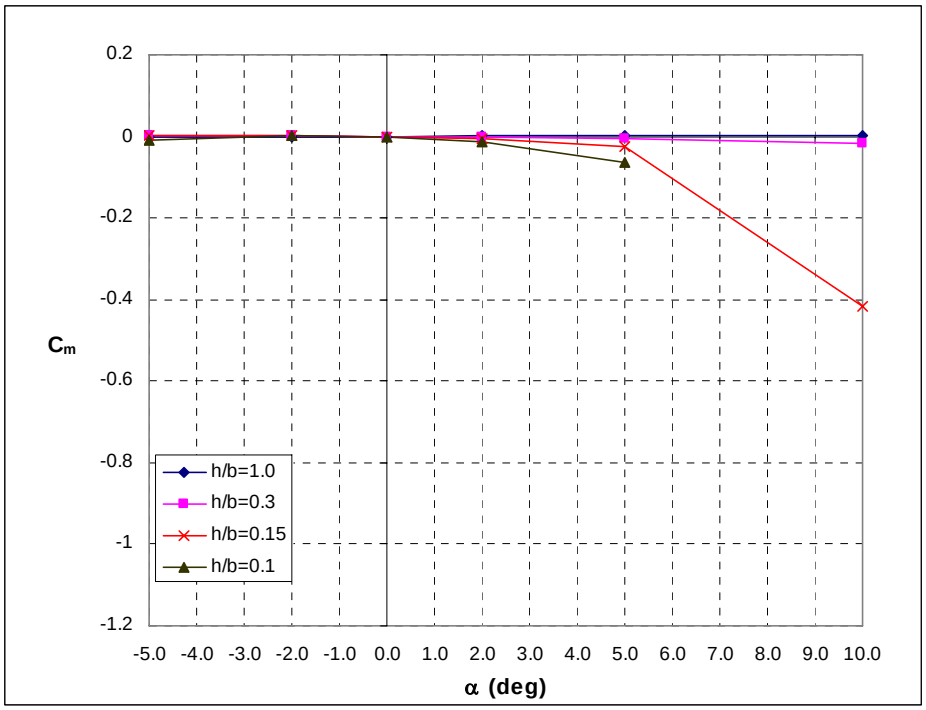

Figure 43: Pitching Moment in Ground Effect for a 60° Oblique Swept Wing

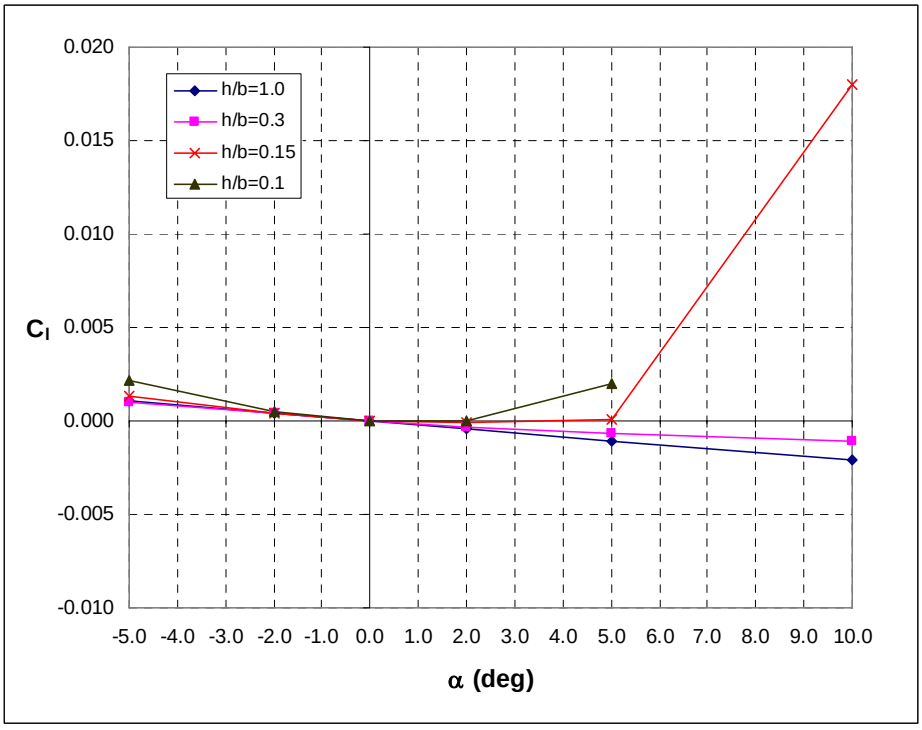

Figure 44: Rolling Moment in Ground Effect for a 60° Oblique Swept Wing

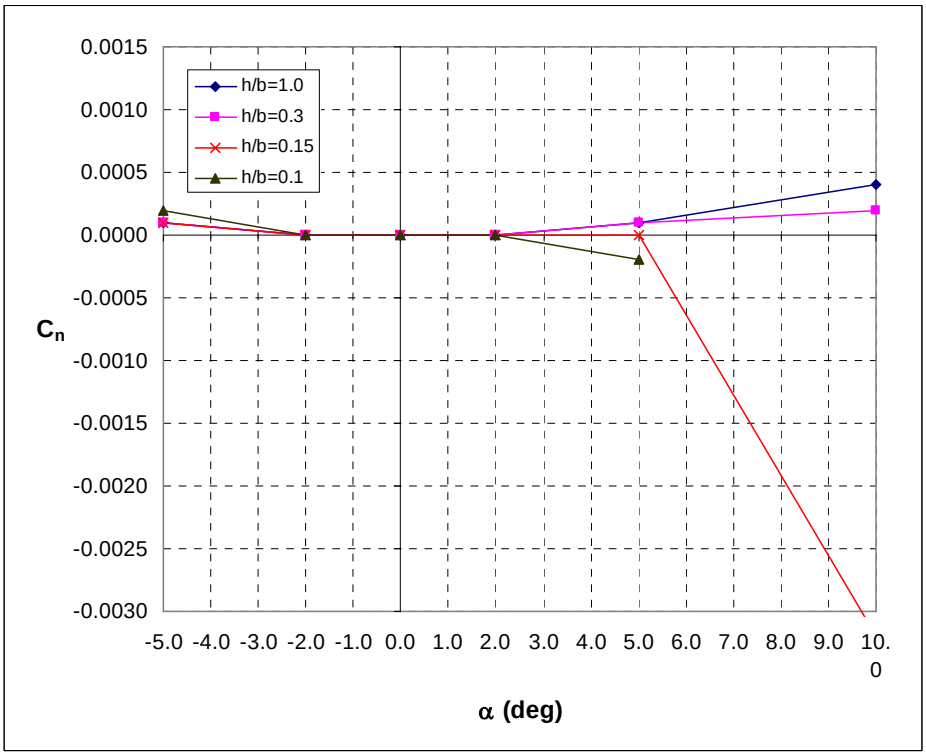

Figure 45: Yawing Moment in Ground Effect for a 60° Oblique Swept Wing

3.3. In-Flight analysis

Specific flight conditions for the aircraft were examined as they applied to an oblique flying wing. Inertias were estimated for further usage in a simulation that integrates such an aerodynamic model. A subsonic cruise condition was used to investigate some configurations and conditions that an OFW is capable of operating at.

3.3.1 Controllability parameters

Inertia Calculation

Inertias for the example oblique wing vehicle were calculated based on Inertia Calculation Procedure for Preliminary Design[28]. Table 5 shows the inputs and resulting inertias. This is based on an unswept trapezoidal wing. Translation of the inertia in the stability axis for an obliquely swept wing can be found based on the method described in the geometry section.

Table 5: Unswept Inertia Estimate Results

Inputs	Value	Units
Weight	182000	lbs
Root thickness	22.9	in
Tip thickness	4.5	in
Span (half)	1980	in
LE Sweep	7	deg
TE Sweep	0	deg
Root chord	381.6	in
Dihedral	0	deg
Generated		
Volume	7.79E+06	in^3
I_{xx}	1.20E+11	$lb\text{-}in^2$
I_{yy}	1.17E+11	$lb\text{-}in^2$
I_{zz}	2.36E+11	$lb\text{-}in^2$
I_{xz}	-2.42E+09	$lb\text{-}in^2$

The center of gravity is approximated at 35% root chord. The geometry has an estimated center of volume estimate at 40% root chord. Based on the distribution of weight the center of gravity can be shifted forward (as well as managed in flight using the fuel transferred), but likely no more than this amount without thickening the flying wing.

3.3.2 Subsonic

An analysis was done on an oblique flying wing model using elevon control effectors across the trailing edge. This was accomplished using the HASC tool which uses for a Vortex-Lattice (Vorlax) analysis. Figure 46 shows an example of the model used. The model has four elevons labeled Right-Right (RR), Right-Center (RC), Left-Center (LC), Left-Left (LL). The elevon deflection angle is positive trailing edge down. The reference coordinate is marked in the figure at 35% of the root of the wing. This remains constant for all conditions. The analysis is capable of using airfoil coordinates, but it only uses the camber and since this vehicle will likely have minimal camber, it was not included such that the results have no moment at zero angle of attack.

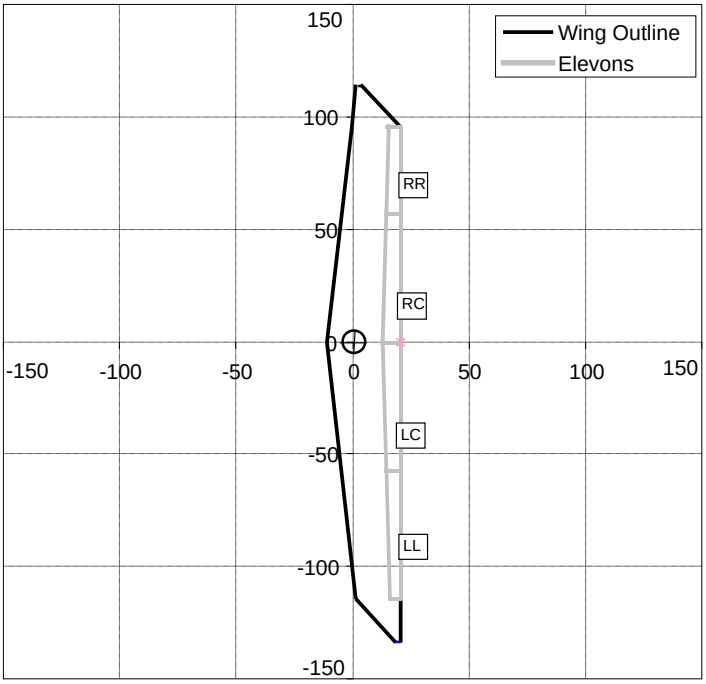

Figure 46: Oblique Flying Wing Elevon Model

In developing the input to the code, an Excel sheet was utilized in order to control the model based on common wing parameters that are translated to a proper input to the code. It also has the capability to rotate the input model such that wing is skewed for different conditions. Wing parameters used in this analysis are included in Table 6. Any changes to the input parameters are reflected in the input to the code allowing for simple updates to the model.

Table 6: Vorlax Model Controls, Wing Parameters

Input	Value	Units		
W/S	60	lb/ft^2		
W_0	182,000	lb		
AR	9			
TR	0.6			
%Ref	35			
Sweep	35			
Flap Ratio	0.25			
M	0.8			
V	829.6	ft/s		
Alt	20000	ft		
Re	6.00E+7			
FLAP RR	FLAP RC	FLAP LC	FLAP LL	
0	0	0	0	deg
Generated				
S	3,033.0	ft^2		
b	165.2			
c_r	22.9			
c_t	13.8			
$\bar{c}$	18.74			

Figure 47 shows the resulting model built in Excel at a 30° oblique sweep. Note that panels are defined parallel to the flow for each oblique sweep condition. This requires regenerating all points for the input which, would be tedious if it were not automated.

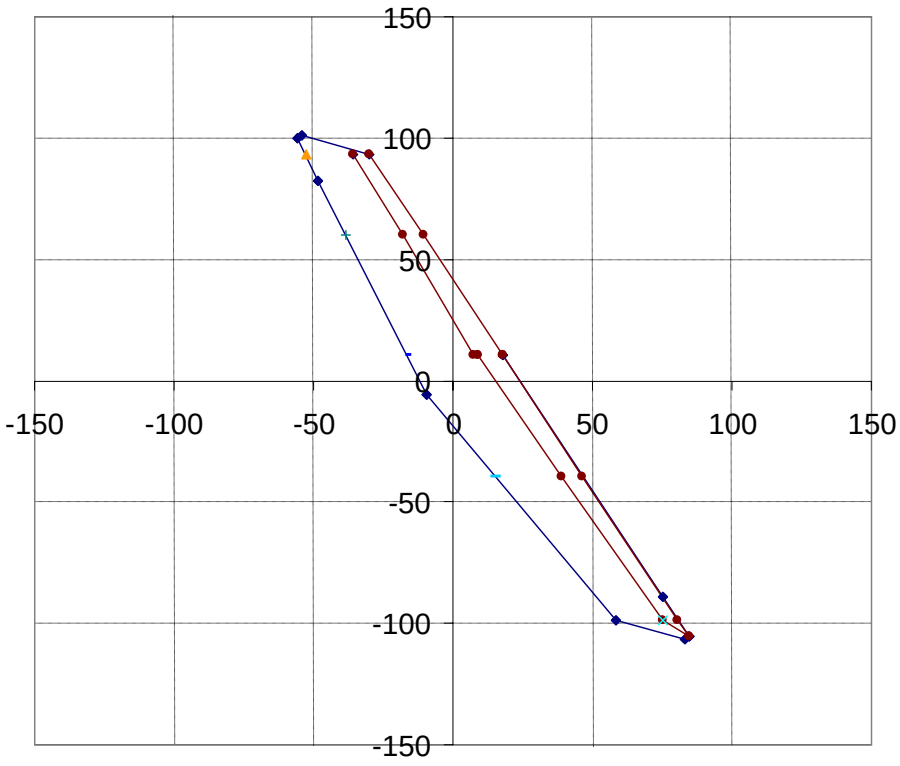

Figure 47: Model Produced by Excel Sheet

Figure 48 through Figure 53 show the case at 20,000 ft, Mach 0.8, and no oblique slew. Figure 48 is the model output from the HASC program. This output compares favorably with the input geometry verifying that is was properly interpreted.

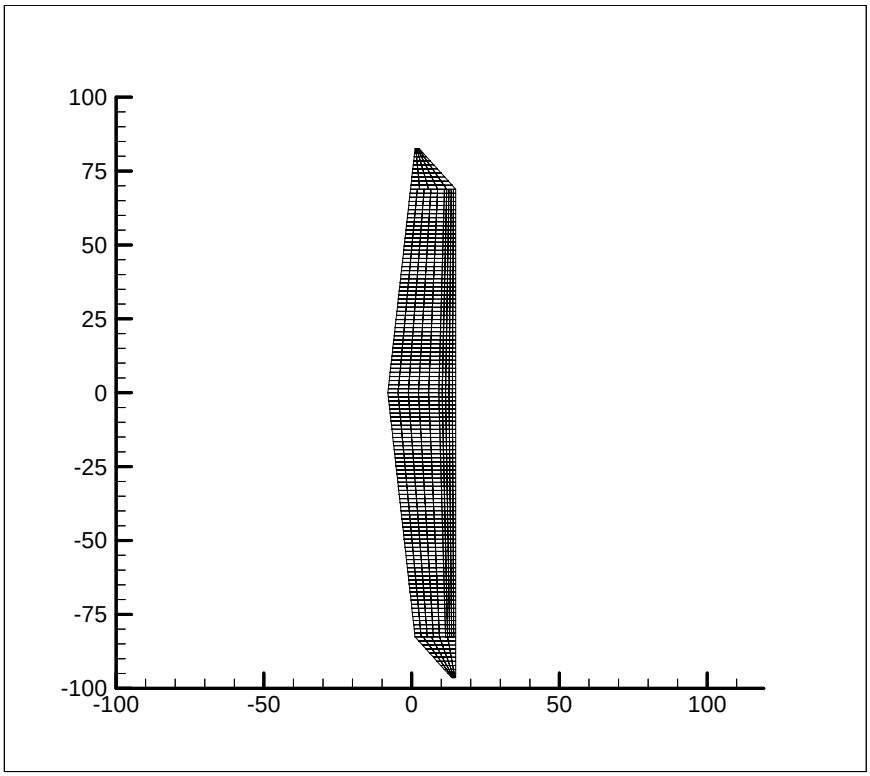

Figure 48: Unswept HASC Vorlax Model Output

The pitching moment was evaluated at different elevon defection angles. In the case of Figure 49, the aerodynamic center is 5% of $\bar{c}$ behind the reference coordinates, giving a negative, stable pitching moment as alpha increases for the clean configuration. This doesn't necessary lead to a stable vehicle due to asymmetries in X-Z plane. Elevons increase negative pitching moment with the trailing edge deflected down and create positive pitching moment when deflected up.

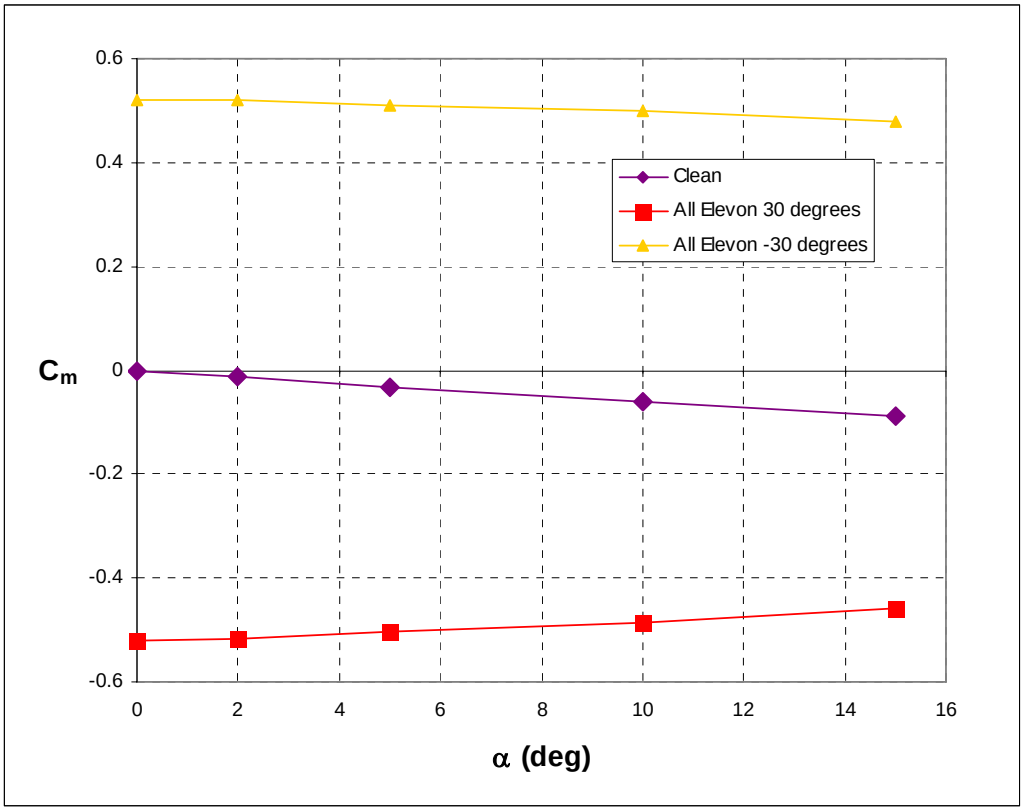

Figure 49: Unswept C_m Due to Combined T.E. Elevons, Stability Axis

Figure 50 shows the deflection of each individual elevon and its effect on pitching moment. All elevons create a negative pitching moment similar to the combined effect. However, there is a small non-linearity around 3° angle of attack. This could be due to a shifting aerodynamic center when only one surface is used.

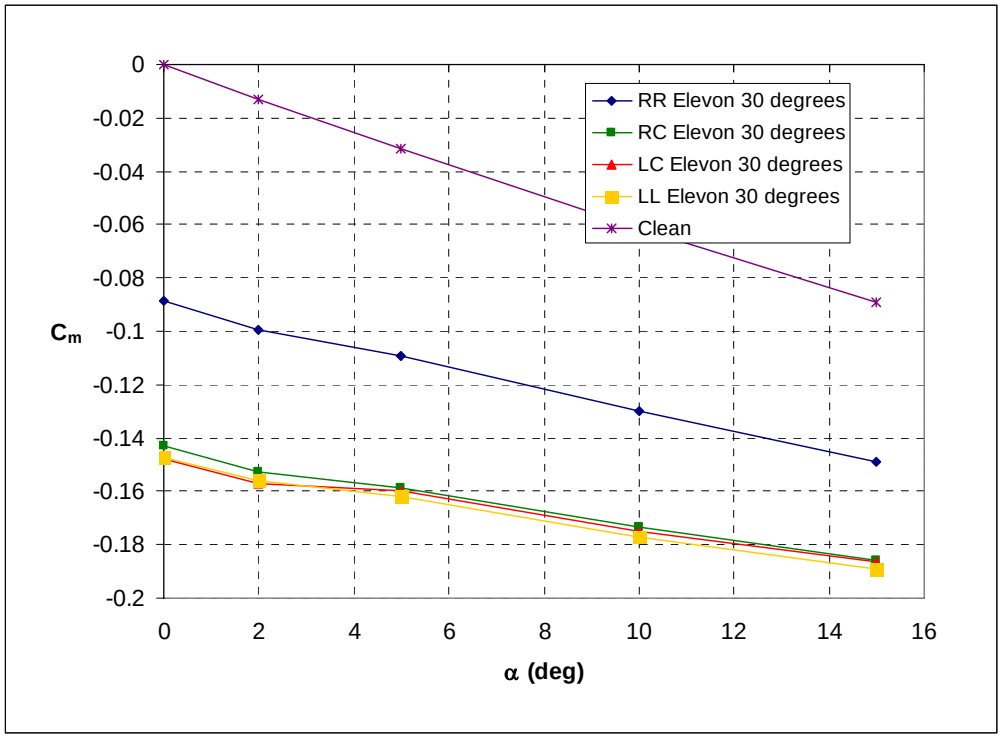

Figure 50: Unswept C_m Due to Individual T.E. Elevons, Stability Axis

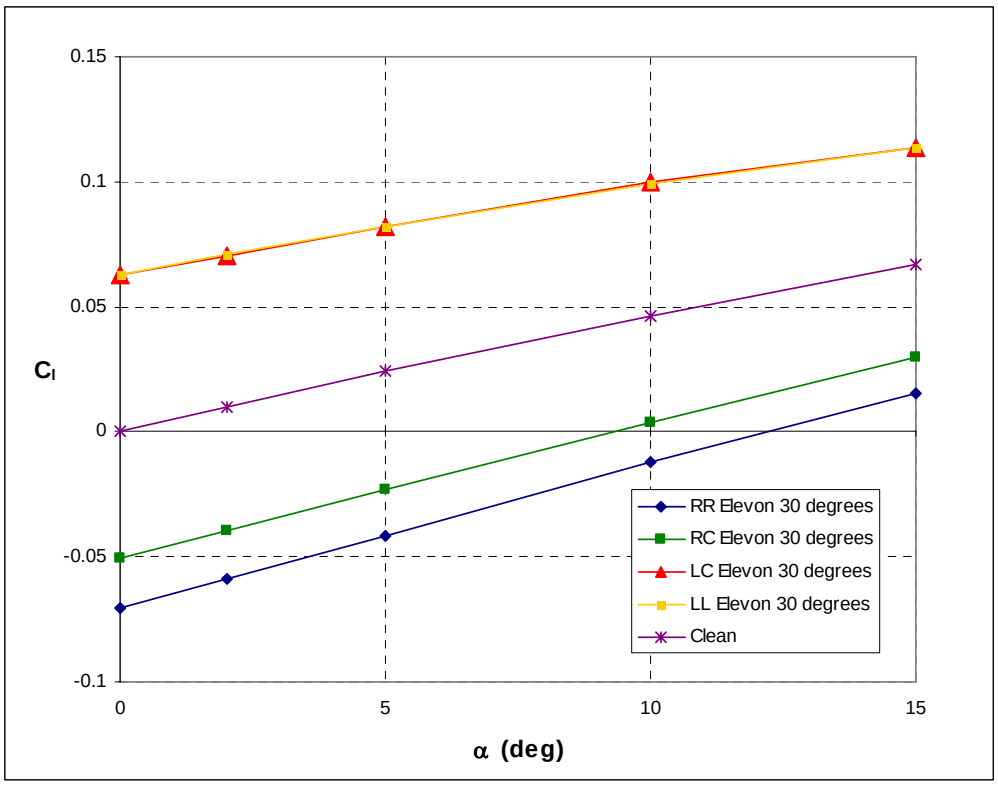

Figure 51: Unswept Total C_l Due to Individual T.E. Elevons, Stability Axis

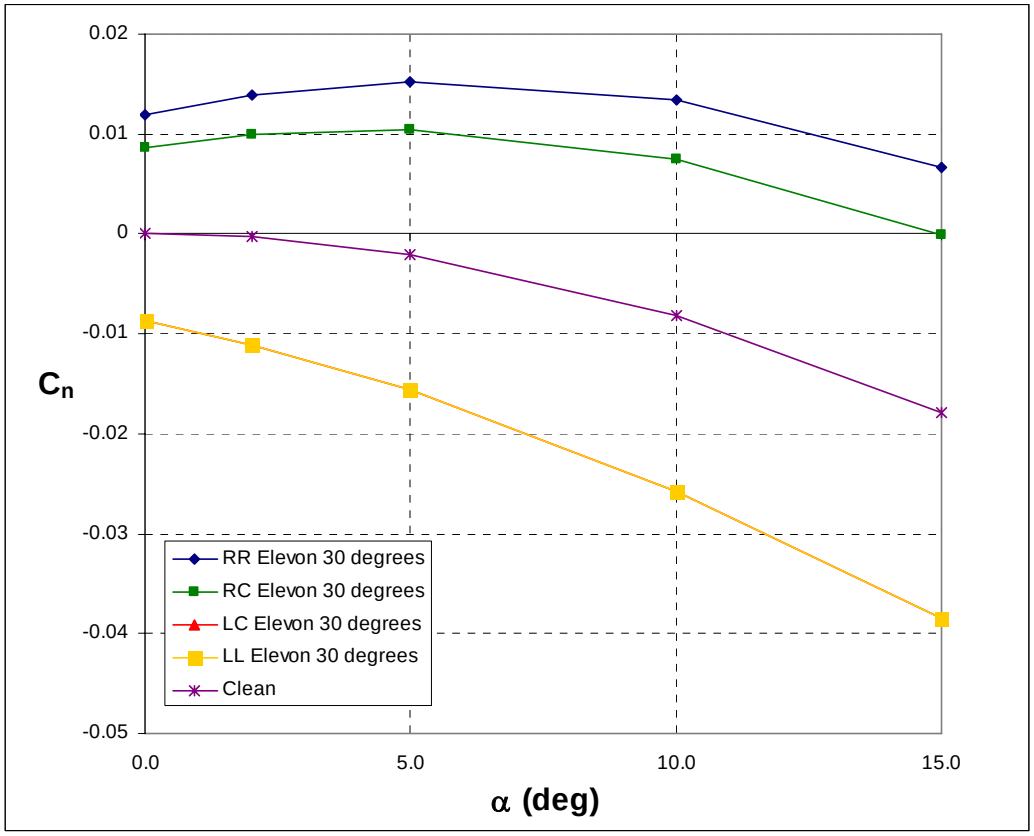

Figure 52: Unswept Total C_n Due to Individual T.E. Elevons, Stability Axis

Table 7: Unswept Coefficient Variations

Case	C_{L_α}	C_{m_α}	C_{l_α}
Due to Alpha	0.1259	-0.0062	0.0047
	$C_{L_{\delta\_selected}}$	$C_{m_{\delta\_selected}}$	$C_{l_{\delta\_selected}}$
Due to Combined Elevon	0.058	-0.017	0.0025
Due to LL Elevon	0.0041	-0.0042	0.0029
Due to LC Elevon	0.0039	-0.0042	0.0029
Due to RC Elevon	0.0039	-0.0041	-0.0015
Due to RR Elevon	0.0039	-0.0025	-0.0021

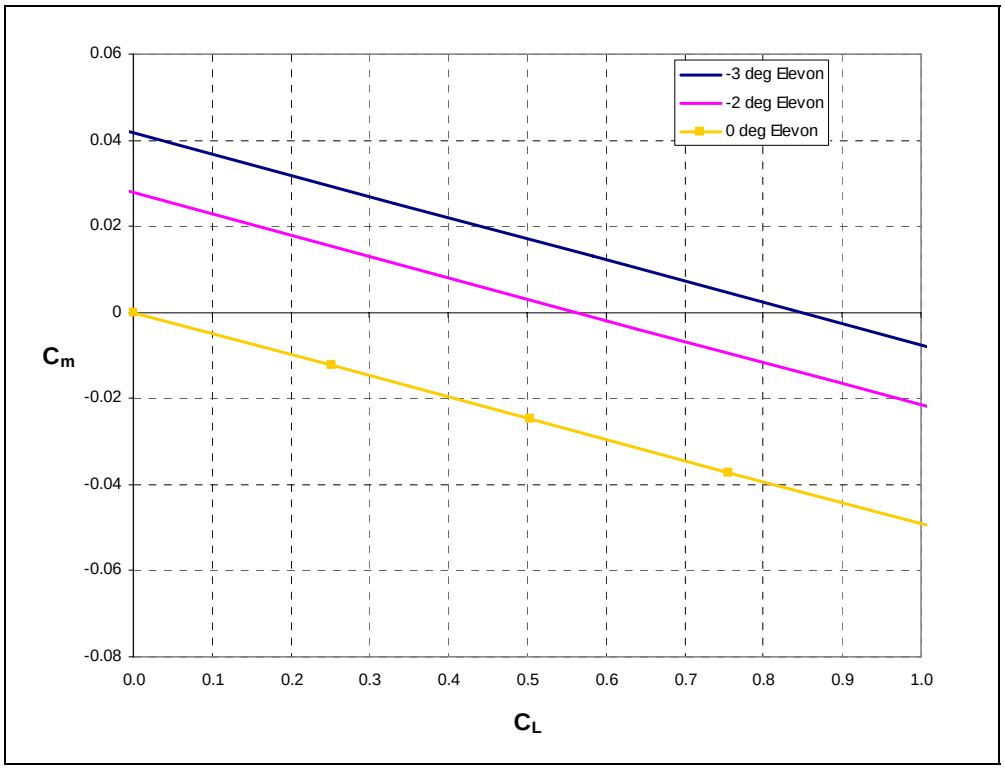

Figure 53: Unswept Trim Cross Plot for C_m

Figure 54 through Figure 56 show the case at 40,000 ft, Mach 0.8, and a 25° oblique slew.

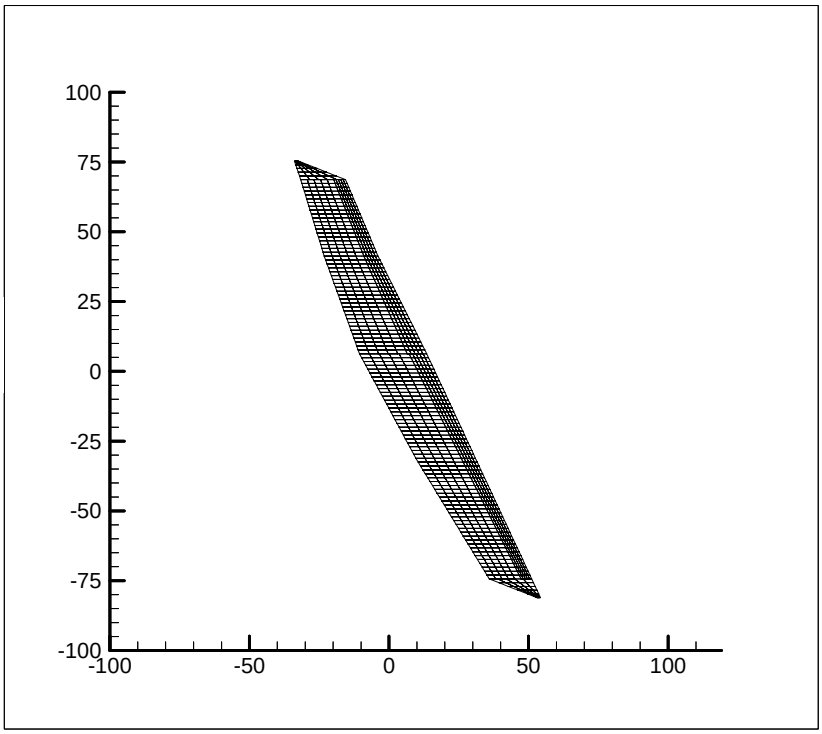

Figure 54: 25° HASC Vorlax Model Output

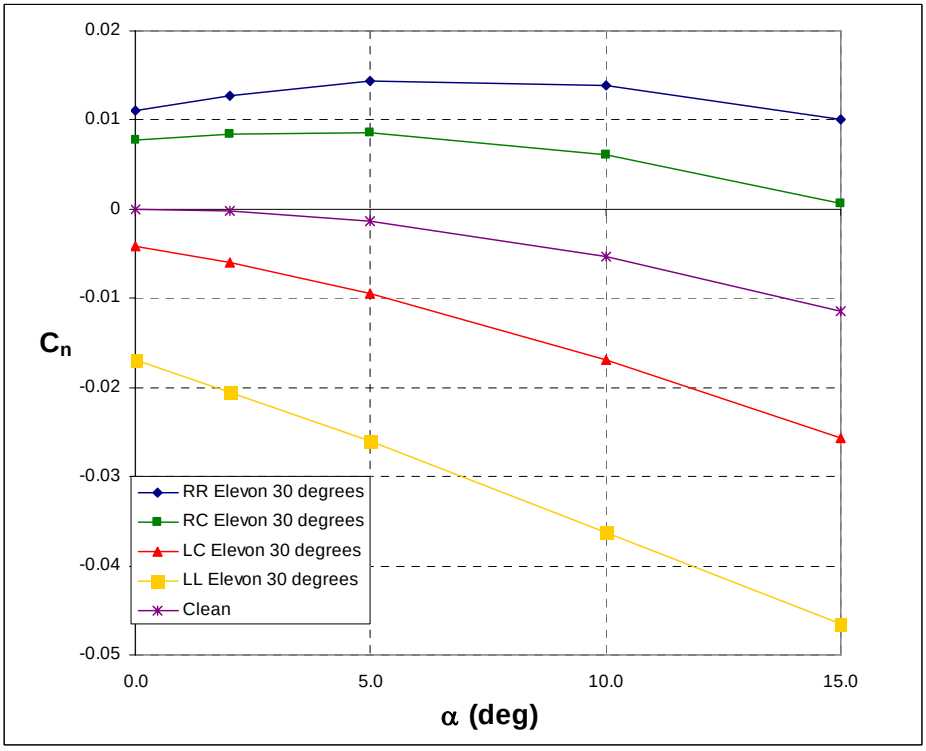

Figure 55: 25° Sweep Total C_n Due to Individual T.E. Elevons, Stability Axis

Table 8: 25° Sweep Coefficient Variations

Case	C_{L_α}	C_{m_α}	C_{l_α}
Due to Alpha	0.096	-0.017	0.0030
	$C_{L_{\delta\_selected}}$	$C_{m_{\delta\_selected}}$	$C_{l_{\delta\_selected}}$
Due to Combined Elevon	0.046	-0.025	0.0021
Due to LL Elevon	0.0085	-0.018	0.0030
Due to LC Elevon	0.017	-0.010	0.0022
Due to RC Elevon	0.017	0.0004	-0.0008
Due to RR Elevon	0.017	0.0048	-0.0018

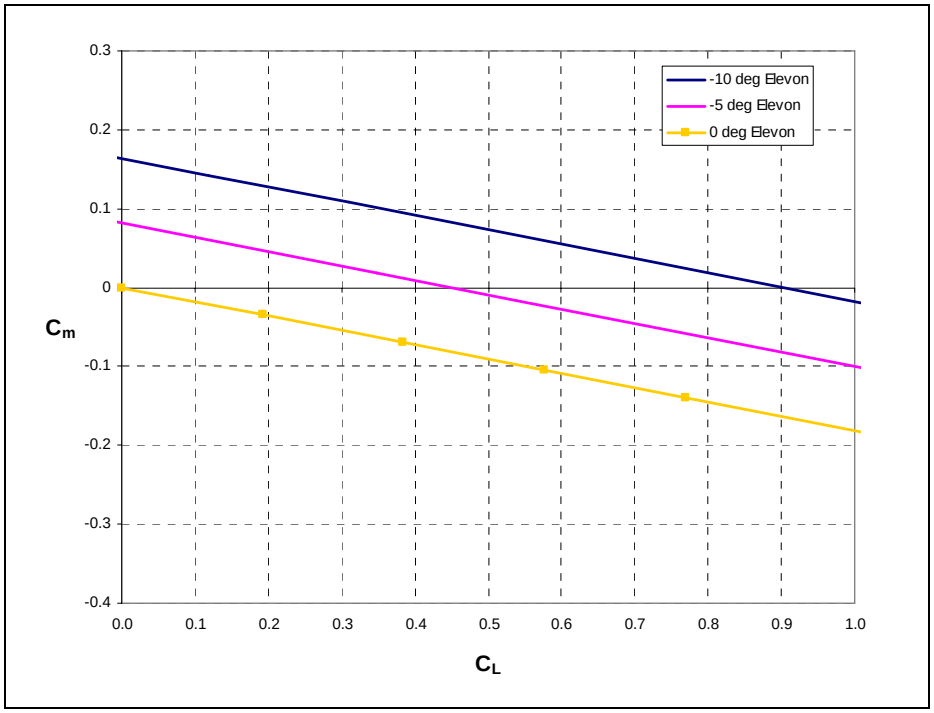

Figure 56: 25° Trim Cross Plot for C_m, Stability Axis

Figure 57 through Figure 58 show the case at 40,000 ft, Mach 0.8, and a 45° oblique slew.

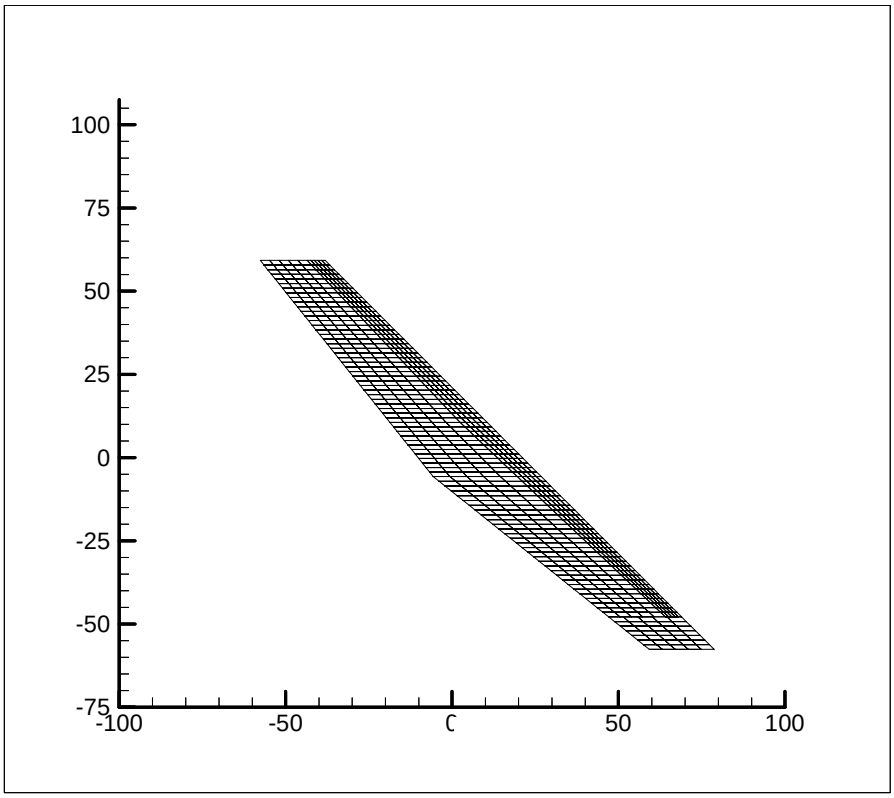

Figure 57: 45° HASC Vorlax Model Output

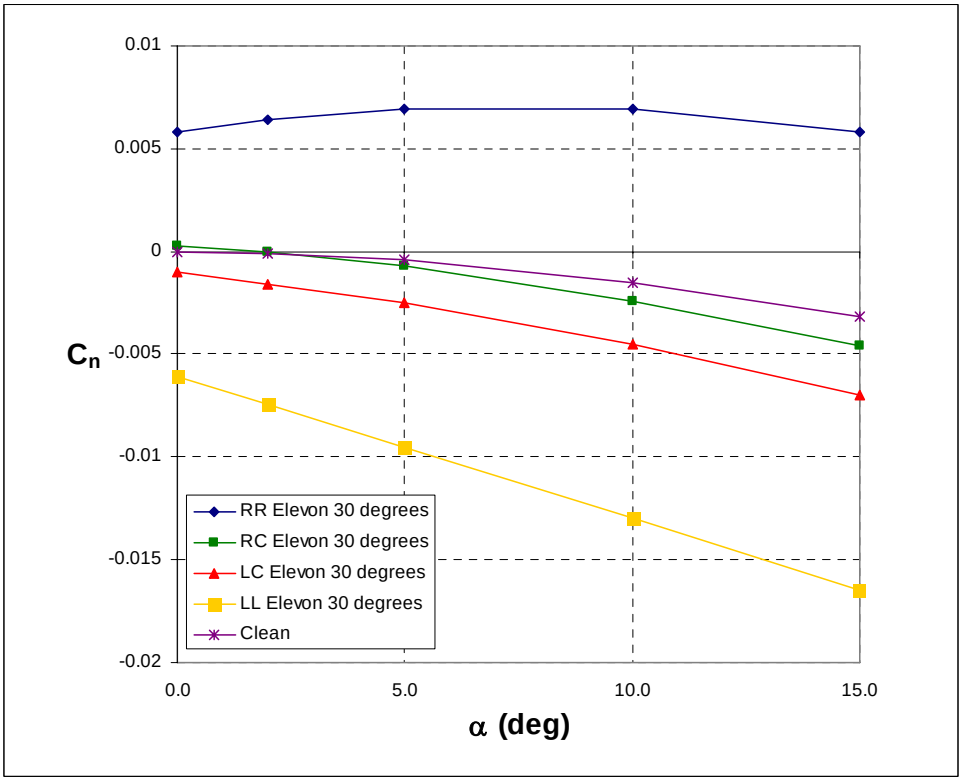

Figure 58: 45° Sweep Total C_n Due to Individual T.E. Elevons, Stability Axis

Table 9: 45° Sweep Coefficient Variations

Case	C_{L_α}	C_{m_α}	C_{l_α}
Due to Alpha	0.061	-0.011	0.00086
	$C_{L_{\delta\_selected}}$	$C_{m_{\delta\_selected}}$	$C_{l_{\delta\_selected}}$
Due to Combined Elevon	0.023	-0.022	0.0013
Due to LL Elevon	0.0094	-0.014	0.0012
Due to LC Elevon	0.0049	-0.0053	0.00059
Due to RC Elevon	0.0034	-0.0038	0.00023
Due to RR Elevon	0.0054	0.0021	-0.00058

Figure 59 through Figure 60 show the case at 40,000 ft, Mach 0.8, and a 60° oblique slew.

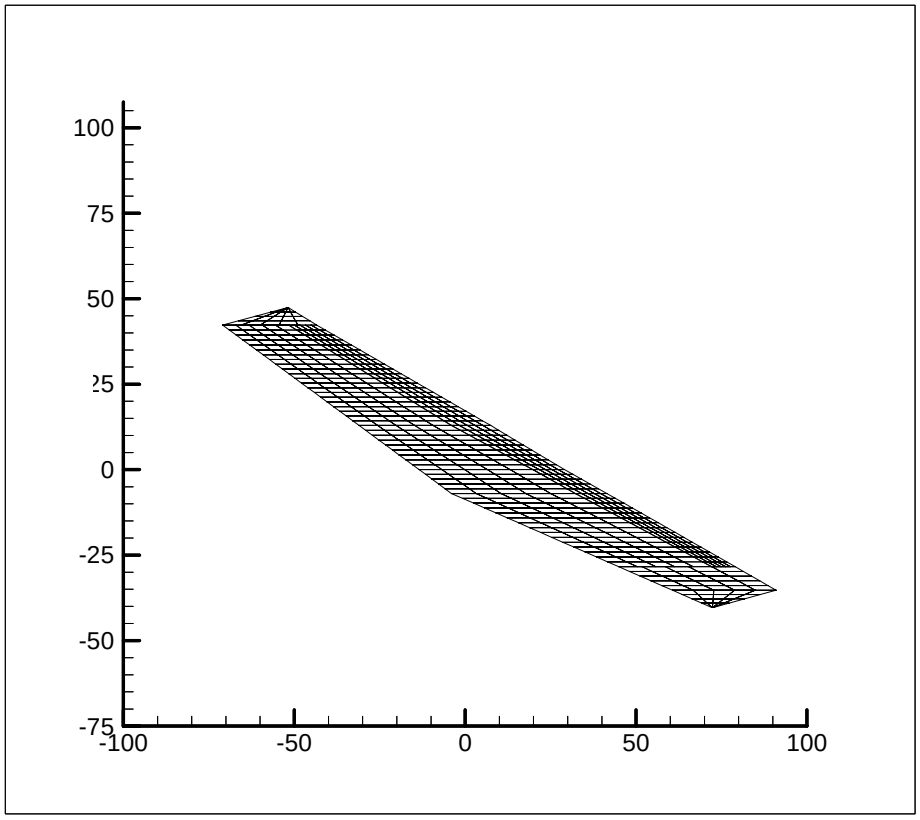

Figure 59: 60° HASC Vorlax Model Output

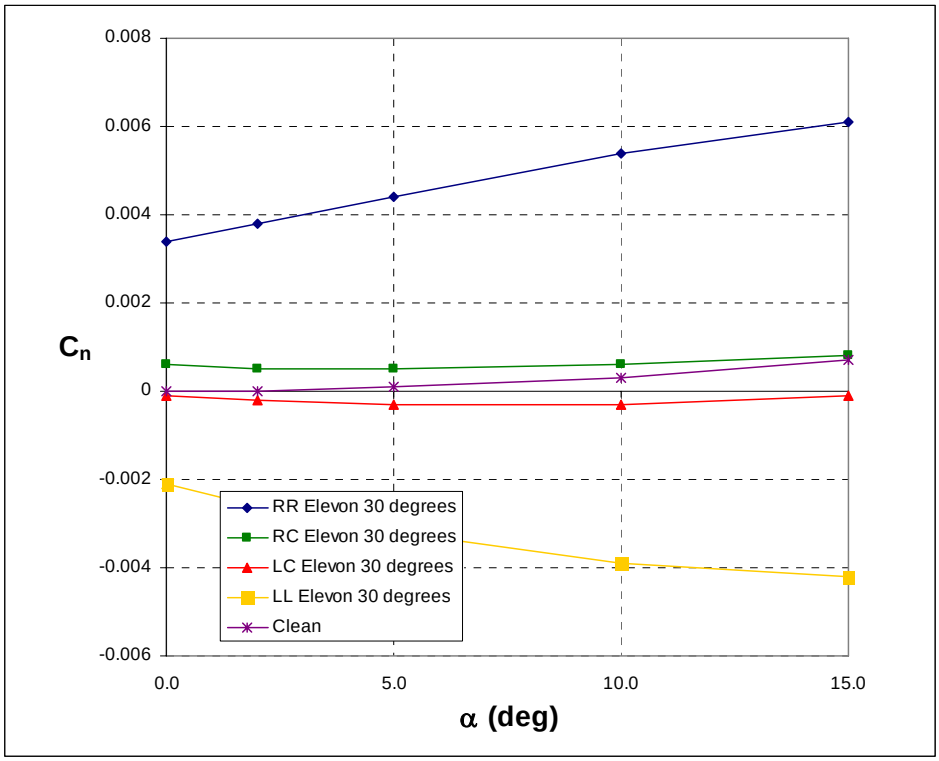

Figure 60: 60° Sweep Total C_n Due to Individual T.E. Elevons, Stability Axis

Table 10: 60° Sweep Coefficient Variations

Case	C_{L_α}	C_{m_α}	C_{l_α}
Due to Alpha	0.039	-0.00039	-0.00019
	$C_{L_{\delta\_selected}}$	$C_{m_{\delta\_selected}}$	$C_{l_{\delta\_selected}}$
Due to Combined Elevon	0.014	-0.013	0.00053
Due to LL Elevon	0.0058	-0.010	0.00065
Due to LC Elevon	0.0033	-0.0025	0.00011
Due to RC Elevon	0.0015	-0.0025	0.00019
Due to RR Elevon	0.0035	0.0026	-0.00043

Lateral Response in Sideslip

Using the same models shown previously, change in rolling moment with sideslip is found by adding a sideslip angle case for each oblique sweep. Figure 61 shows the results to be proportional to angle of attack. For the 25° swept case there is more rolling moment due to sideslip than the unswept case because of the increased lift on the +Y side of the wing at this angle. As sweep further increases there is less rolling moment. This is due to the rolling moment arm decreasing as the wing obliquely sweeps.

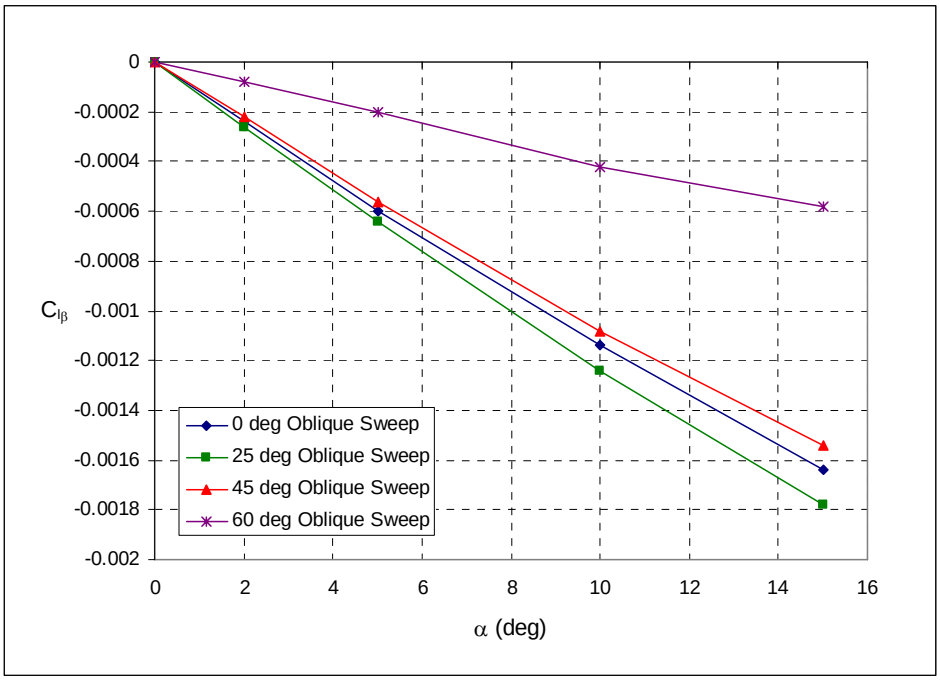

Figure 61: Change in $C_{l\beta}$ with Oblique Sweep, Stability Axis

Since the results are reasonably linear, the rolling moment due to sideslip per degree angle of attack was found. Table 11 shows the resulting linearized coefficients. Below 45 degrees sweep the results are similar, but wings with higher oblique sweep create less rolling moment at sideslip.

Table 11: Lateral Stability Coefficient

Oblique Sweep	**0°**	**25°**	**45°**	**60°**
$C_{l\beta}$ (per deg AoA)	-0.00012	-0.00013	-0.00011	-0.000040

3.3.3 Trim Analysis

A study was conducted for the wing using classical trim analysis in pitch and adjusting for lateral affects due to asymmetry in cruise. Equation 19 shows the lift coefficient required for 1-g flight. Equation 20 shows the combined elevon deflection required for zero pitch at the given lift.

$$C_{L_{trim}} = \frac{W}{qS} \tag{19}$$

$$\delta_{flap}(Long\ trim) = \frac{C_{m_0} + \frac{\partial C_m}{\partial C_L}\left(C_{L_{trim}} - C_{L_0}\right)}{-C_{m_{\delta flap}} + \frac{\partial C_m}{\partial C_L} C_{L_{\delta flap}}} \tag{20}$$

The angle of attack at the trimmed flight condition is given by equation 21.

$$\alpha_{trim} = \frac{\left(C_{m_0} + C_{m_{\delta flap}} \delta_{flap}\left(Long\ trim\right)\right)}{C_{m_\alpha}} \tag{21}$$

For an asymmetric oblique wing there is a remaining rolling moment created by the wings and control surface deflections that needs to be trimmed. In this case, the left and right most elevons are used. An opposing, additional deflection is added to the two elevons.

$$\Delta\delta_{flap}(Lat\ trim) = \frac{\delta_{LL} C_{l\delta LL} + \delta_{LC} C_{l\delta LC} + \delta_{RC} C_{l\delta RC} + \delta_{RR} C_{l\delta RR} + \alpha C_{l\alpha}}{C_{l\delta LL} - C_{l\delta RR}} \tag{22}$$

There is some pitching moment created by moving the flaps. This can also be accounted for with additional combined flap deflection, shown in equation 23. Since that may also create a small lateral trim issue the process can be iterated until the wing is trimmed in both longitudinal and lateral axes.

$$\Delta\delta_{flap}(Long\ trim) = \frac{C_{m\alpha}\alpha + C_{m\delta flap}\delta_{flap}(Long\ trim) + (-C_{l\delta LL} + C_{l\delta RR})\Delta\delta_{flap}\left(Lat\ trim\right)}{C_{m\delta all}} \tag{23}$$

Takeoff

Takeoff is assumed to be at a Mach number of 0.25 at sea level. There is no oblique angle used, but there are still asymmetries in the planform to be trimmed out in roll. A height above ground of 0.15b was selected. Table 12 shows the resulting aerodynamics used for trim.

Table 12: Unswept Takeoff Coefficient Variations

Case	C_{L_α}	C_{m_α}	C_{l_α}
Due to Alpha	0.102	-0.00597	0.00349
	$C_{L_{\delta\_selected}}$	$C_{m_{\delta\_selected}}$	$C_{l_{\delta\_selected}}$
Due to Combined Elevon	0.045	-0.011	0.0018
Due to LL Elevon	0.0066	-0.0032	0.0041
Due to LC Elevon	0.014	-0.0028	0.0023
Due to RC Elevon	0.014	-0.0027	-0.0014
Due to RR Elevon	0.010	-0.0019	-0.0019

A set of control deflections necessary for null pitching and rolling moments was found using equations 16 and 17 and shown in Figure 62. All elevons are giving a negative deflection in this case. The far left elevon gives a higher negative deflection, and the two close to the center are used solely for pitch. There is likely some yaw that again will need to be trimmed out, but isn't quite as linear as the other coefficients. For lift, the angle of attack associated with take-off gross weight is 7.23° angle of attack. The deflection angles going from left to right surfaces are -5.90°, -3.75°,-3.75°, and -1.70°. Additional roll is created by left tip than the right tip that must be trimmed out even though the vehicle is unswept. High deflections to trim out the roll are due to the longer moment arm to the asymmetric tip that is causing the issue.

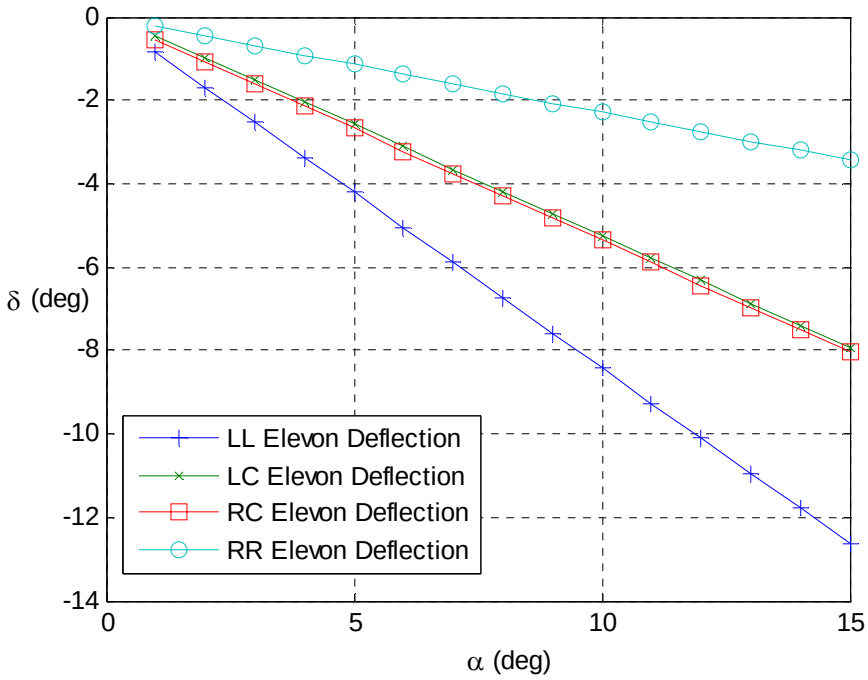

Figure 62: Takeoff Longitudinal, Lateral Trim Control Surface Deflections

Subsonic Cruise

Subsonic cruise is assumed to be at a Mach number of 0.8 at 40,000 ft. and an oblique angle of 45°. Weight is assumed to be half of the fuel load at 135,000 lbs. This equates to a lift coefficient of 0.25. The coefficients used in this case are shown in Table 9. In order to achieve trimmed 1-g flight an angle of attack of 4.96° is necessary using equation 15.

A set of control deflections necessary for zero pitching and rolling moments was found using equations 16 and 17 and shown in Figure 63. In opposition with the takeoff case, the only elevon that gives a positive deflection is on the far left to control roll. The far right elevon gives a higher negative deflection as well, and the two close to the center are used solely for pitch. For trimmed 1-g flight, the deflection angles going from left to right surfaces are 2.18°, -2.5°,-2.5°, and -7.18°. Less effort in trim is required in pitch due to the wing being skewed such that the moment arm is longer. The opposite is true for rolling moment, but there is less to trim out due to asymmetries in level flight. This also works with respect to the body axis because the large oblique sweep angle creates more

lift on the right side of the vehicle that needs to be trimmed out in roll with a positive deflection on the left side.

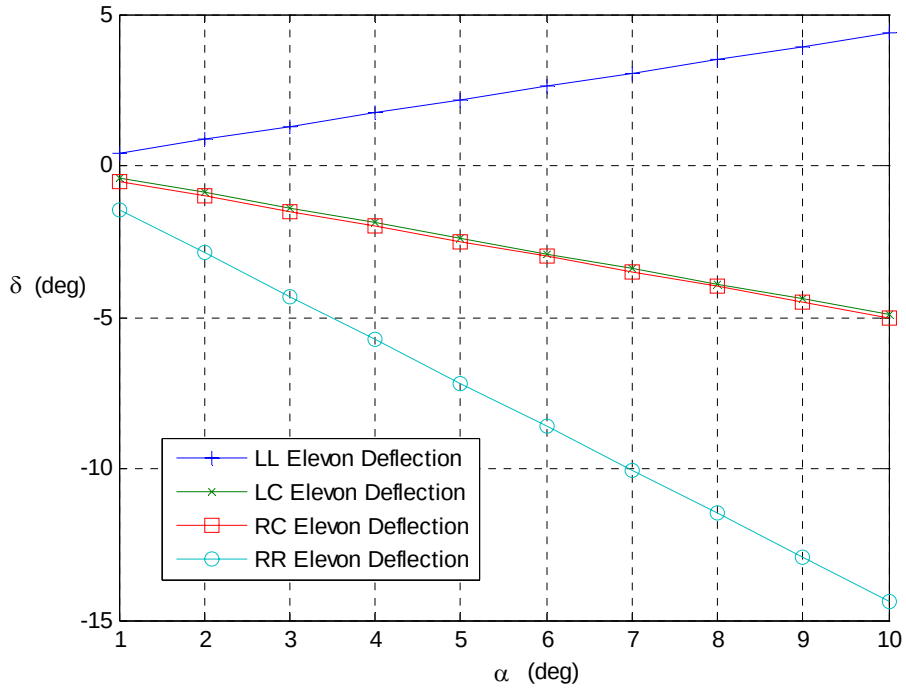

Figure 63: Subsonic Cruise Longitudinal, Lateral Trim Control Surface Deflections

4. Conclusions

The problem of controlling an oblique flying wing is more complex than other aircraft because this type of vehicle is considered to have multiple configurations based on the operation speed. This doesn't fit together with many analysis tools used for early investigation of such a concept. Conceptual design tools are sometimes simplified with assumptions like X-Z plane symmetry that are incompatible. Programs that were found to be most useful tended to be more general and could be applied to any type of aircraft. The need exists for tools that are applicable to a wide variety of concepts, but still have the ability to perform the necessary analysis without unnecessary complication.

It was shown that an asymmetric oblique wing can be trimmed in pitch and roll using control surfaces on the wing at nominal flight conditions. The control system doesn't need to be to fully maneuverable at every possible situation such as 0° oblique sweep at Mach 2.0, but it should be able to recover back to the optimal orientation if there is a departure. Takeoff and landing with some oblique sweep is also possible, but high sweeps should be avoided due to some possibility of lateral moment reversal due to ground effect. A swept takeoff should be a design consideration due to the potential benefit to simplify the pivot mechanism.

Adding an aeroelastic analysis to couple aerodynamics, structures, and controls is a logical step to a more realistic evaluation. This will likely require a more narrow design space to simplify the structural layout. T. A. Weisshaar has written several papers on aeroelastic tailoring of oblique wing aircraft[32]. These results, integrated with the aerodynamic results in this report can be used for a six-degree-of-freedom simulation. This combination would allow for an accurate prediction of maneuvers for the different oblique orientations and show how dynamics are affected in each case.

References

1. "Switchblade Oblique Flying Wing Phase I: Proposer Information Pamphlet (PIP) for Broad Agency Announcement (BAA) Solicitation", Defense Advanced Research Projects Agency, 2005.
2. Seebass, R., "Oblique Flying Wing Studies," *CISM Courses and Lectures: New Design Concepts for High Speed Transport*, H. Sobieczky, Editor, Springer-Verlag, Vienna/New York, 1997, pp. 317-336.
3. Hirschberg, M., D. Hart, and T. Beutner, "A Summary of a Half-Century of Oblique Wing Research," 45th AIAA Aerospace Sciences Meeting and Exhibit, AIAA Paper 2007-150, Jan. 2007.
4. Curry, R.E. and A.G. Sims, "Unique Flight Characteristics of the AD-1 Oblique-Wing Research Airplane," *Journal of Aircraft*, Vol. 20 No. 6, Jun. 1983.
5. NASA Dryden Research Aircraft Photo Collection, http://www.dfrc.nasa.gov/Gallery/photo/index.html [retrieved 7 Jan 2008]
6. Morris, S. and B. Tigner, "Flight Tests of an Oblique Flying Wing Small Scale Demonstrator," AIAA, Paper 95-3327-CP, Aug. 1995.
7. Raymer, D.P., *Aircraft Design: A Conceptual Approach*, 3rd ed, AIAA, Reston, VA, 1999.
8. Van der Velden, A., "Aerodynamic Design and Synthesis of the Oblique Flying Wing Supersonic Transport," Ph.D. Dissertation, Stanford University, May 1992.
9. Tejtel, D., et al., "Breathing New Life into Old Processes: An Updated Approach to Vehicle Analysis and Technology Assessment," AIAA, Paper 2005-7304, Sep. 2005.
10. "Bihrle Applied Research, Inc.: Products_Simgen," Bihrle Applied Research, http://www.bihrle.com/site/products_simgen.html [retrieved 7 Jan 2008]
11. Albright, A.E., C.J. Dixon, and M.C. Hegedus, "Modification and Validation of Conceptual Design Aerodynamic Prediction Method HASC95 With VTXCHN," NASA CR-4712, Mar. 1996.
12. Miranda, L.R., R.D. Elliott, and W.M. Baker, "A Generalized Vortex Lattice Method for Subsonic and Supersonic Flow Applications," NASA, CR-2865, Dec. 1977.
13. Downen, T., et al., "Design of an Oblique All-Wing Supersonic Transport Aircraft," University of Kansas, Dec. 1992.
14. McCullers, L.A., "User's Guide for the Revised Wave Drag Analysis Program (AWAVE)," NASA Langley Research Center, Apr. 1992.
15. Davis, P.C., Gelhausen, P.A., Gloudemans, J.R., "A Rapid Geometry Modeler for Conceptual Aircraft," AIAA, Paper 1996-52, Jan. 1996.
16. Craidon, C.B., "User's Guide for a Computer Program for Calculating the Zero-Lift Wave Drag of Complex Aircraft Configurations," NASA TM-85670, 1983.
17. Aftosmis, M. and M. Berger, "CART3D v1.3," http://people.nas.nasa.gov/~aftosmis/cart3d/ [retrieved 9 Oct 2007]

18. Mason, W.H., "FRICTION," Computer Program, Virginia Polytechnic Institute and State University: Blacksburg, VA, 2006.
19. White, F.M., *Viscous Fluid Flow*, McGraw-Hill, New York, NY, 2006, 589-590.
20. Hopkins, E.J., "Charts for Predicting Turbulent Skin Friction From the Van Driest Method (II)," NASA, TN D-6945, Oct. 1972.
21. "Oblique Flying Wings: An Introduction and White Paper," Desktop Aeronautics, Inc., 2005.
22. Wintzer, M., P. Sturdza, and I. Kroo, "Conceptual Design of Conventional and Oblique Wing Configurations for Small Supersonic Aircraft," AIAA Paper 2006-930, Jan. 2006.
23. Lanham, C., "Inertia Calculation Procedure for Preliminary Design," Aeronautical Systems Div, TR-79-5004, Apr. 1979.
24. "The Oblique Flying Wing Page," http://www.obliqueflyingwing.com/ [retrieved 9 Oct 2007]
25. Smith, J.H., "Lift/Drag Ratios of Optimized Slewed Elliptic Wings at Supersonic Speeds," *The Aeronautical Quarterly*, Aug. 1961.
26. Jones, R.T. and D. Cohen, *High Speed Wing Theory*, Princeton University Press, Princeton, NJ, 1960.
27. Torenbeek, E., *Synthesis of Subsonic Airplane Design*, The Netherlands, Delft University Press, 1976.
28. Roskam, J., *Airplane Design Part VI: Preliminary Calculation of Aerodynamic Thrust and Power Characteristics*, Lawrence, Kansas, Design, Analysis and Research Corporation, 1997.
29. Jones, B.L., M.E. Franke, and E.J. Stephen, "Aerodynamic Ground Effects of a Tailless Chevron-Shaped UCAV," AIAA, Paper 2006-2832, Jun. 2006.
30. Drezner, J.A. and R.S. Leonard, "INNOVATIVE DEVELOPMENT: Global Hawk and DarkStar - Flight Test in the HAE UAV ACTD Program," RAND: Project AIR FORCE, 2002.
31. Tirpak, John A. "The Robotic Air Force," Journal of the Air Force Association, Vol. 80, No. 9, Sep. 1997. http://www.afa.org/magazine/sept1997/0997robot.asp [retrieved 9 Oct 2007]
32. Weisshaar, T.A., "Integrated Structure/Control Concepts for Oblique Wing Roll Control and Trim," *Journal of Aircraft*, Vol. 31 No. 1: pp. 117- 124, Jan.-Feb. 1994.

Appendices

A. Annotated Bibliography and Extended Reference List

While this annotated bibliography best supports this study, the Stanford maintained "Oblique Wing Bibliography" represents a more exhaustive listing than what is found here. It can be located at: http://aero.stanford.edu/Reports/OWReferences.html

Classification of Reports:

Reports in this bibliography are broken up into the following topics:

Oblique Wing Aircraft
1. Wave Drag Theory
2. Aircraft Design
3. Stability and Controllability
4. AD-1 Demonstration Vehicle

Oblique Wing Aircraft

- Hirschberg, M., D. Hart, and T. Beutner, "A Summary of a Half-Century of Oblique Wing Research," AIAA Paper 2007-150, Jan 2007.
  A recent survey paper of oblique wing aircraft. Discusses a wide range of oblique flying wing and wing-body aircraft designs and demonstration vehicles.

- "Switchblade Oblique Flying Wing Phase I: Proposer Information Pamphlet (PIP) for Broad Agency Announcement (BAA) Solicitation," Defense Advanced Research Projects Agency, Aug 2005.
  Describes Phase I of Switchblade program which has a goal of developing technologies for a military OFW vehicle including a supersonic demonstrator. Design objectives for an operational vehicle are discussed.

- Seebass, R., "Oblique Flying Wing Studies," *CISM Courses and Lectures - New Design Concepts for High Speed Transport*, H. Sobieczky, Editor, Springer-Verlag, Vienna/New York, 1997, pp. 317-336.
  Develops drag calculation for an oblique flying wing transport. Discusses designs for a passenger aircraft. An example method for shape optimization of one such design is given.

- Van der Velden, A., "Aerodynamic Design and Synthesis of the Oblique Flying Wing Supersonic Transport," Stanford University, May 1992.
  A complete design and investigation of an oblique flying wing used for a civil transport. This includes a look at the theory, weights, sizing, and environmental impacts of such a vehicle.

1. Wave Drag Theory

- Graham, A., R.T. Jones, and F. Boltz, "An Experimental Investigation of an Oblique Wing and Body Combination at Mach Numbers Between .6 and 1.4," NASA, TM X-62207, Dec. 1972.

- Graham, A., R.T. Jones, and F. Boltz, "An Experimental Investigation of Three Oblique Wing and Body Combinations at Mach Numbers Between .6 and 1.4," NASA, TM X-62256, Apr. 1973.

- Jones, R.T., "The Minimum Drag of Thin Wings in Frictionless Flow," *Journal of the Aeronautical Sciences*, Feb. 1951.

- Jones, R.T., "Theoretical Determination of the Minimum Drag of Airfoils at Supersonic Speeds," *Journal of the Aeronautical Sciences*, Dec. 1952.

- Jones, R.T. and D. Cohen, *High Speed Wing Theory*, Princeton University Press, Princeton, NJ, 1960.

- Kennelly, R., et al., "Transonic Wind Tunnel Test of a 14% Thick Oblique Wing," *NASA* TM 102230, Aug. 1990.

- Kulfan, J., "Study of the Single-Body Yawed Wing Aircraft Concept," in NASA, CR-137483, 1974.

- Lee, G.H., "Slewed Wing Supersonics," *The Aeroplane*, Mar. 1961.

- Li, P., H. Sobieczky, and R. Seebass, "Oblique Flying Wing Aerodynamics," AIAA, Paper 96-2120, Jun. 1996.

- Mehta, U., "The Computation of Flow Past an Oblique Wing Using the Thin-Layer Navier-Stokes Equations," NASA, TM 88317, Jun. 1986.

- Smith, J.H., "Lift/Drag Ratios of Optimized Slewed Elliptic Wings at Supersonic Speeds," *The Aeronautical Quarterly*, Aug. 1961.
  Detailed method for finding volumetric wave drag of elliptical wings at different slew angles. This is cited by multiple authors as a method used in designing an oblique wing vehicle. This is used to find a minimum L/D value for these shapes.

2. Aircraft Design

- Barber, M., M. DeAngelis, and R. Traskos, "F-8 Oblique Wing Research Aircraft - A Progress Report," Society of Flight Test Engineers 17th Annual Symposium, Aug. 1986.
  Paper is not part of the symposium proceedings, but labeled as an addendum. SFTE database of papers does not list this paper.

- BCAC Preliminary Design Dept., "Oblique Wing Transonic Transport Configuration Development – Final Report," NASA, CR 151928, 1977.

- Bradley, E., et al., "An Analytical Study for Subsonic Oblique Wing Transport Concept – Final Report," NASA, CR 137896, 1976.

- Downen, T., et al., "Design of an Oblique All-Wing Supersonic Transport Aircraft," University of Kansas, Dec. 1992.
  Design report presented to NASA. Does not seem to be available from NASA. Extensive assessment of a specific OFW transport. Describes issues with prior multi-disciplinary designs. Vertical tail sizing issue for one engine out.

- Galloway, T., P. Gelhausen, and M. Moore, "Oblique Wing Supersonic Transport Concepts," AIAA, Paper 92-4230, Aug. 1993.
  Models two oblique wing configurations, one oblique wing body concept and the other an oblique all wing concept, in ACSYNT for a supersonic transport. This paper is a companion to the paper by M. Waters, AIAA Paper 92-4220.

- Kroo, I., "The Aerodynamic Design of Oblique Wing Aircraft," AIAA 86-2624, Oct. 1986.

- Kroo, I., "Tailless Aircraft Design – Recent Experiences (White Paper)"

- Jones, R.T., "Aerodynamic Design for Supersonic Speed," *Advances in Aeronautical Sciences*, Pergammon Press, 1959.

- Jones, R.T., "Possibilities of Efficient High Speed Transport Airplanes," *Proceedings of the Conference on High-Speed Aeronautics*, Jan. 1955.

- Jones, R.T., "New Design Goals and a New Shape for the SST," *Astronautics and Aeronautics*, Dec. 1972.

- Jones, R.T. and J.W. Nisbet, "Transonic Transport Wings-Oblique or Swept?," Astronautics and Aeronautics: pp. 40-47, Jan. 1974.
  Discusses supersonic transport design.

- Jones, R.T., "The Flying Wing Supersonic Transport," Aeronautical Journal, Mar. 1991.

- Jones, R.T., "The Oblique Wing – Aircraft Design for Transonic and Low Supersonic Speeds," *Acta Astronautica*, Vol. 4, 1977.

- Jones, R.T. "Trans-Pacific Supersonic Transport (White Paper)"

- Kurkchubasche, R. and I. Kroo, "A Preliminary Study of Lift to Drag Ratios For the Oblique Flying Wing Supersonic Transport," Stanford University, Aug. 1990.

- Li, P., H. Sobieczky, and R. Seebass, "Manual Aerodynamic Optimization of an Oblique Wing Supersonic Transport," Journal of Aircraft, Vol. 36 No. 6: pp. 907- 913, Dec. 1999.

- Nelms, W., "Applications of Oblique Wing Technology & An Overview," AIAA, 76-943, Sep. 1976.

- "Oblique Wing Research Aircraft Preliminary Design (RFP)," NASA Ames Research Center, Nov. 1984.

- Van der Velden, A., "The Oblique Flying Wing Transport," *CISM Courses and Lectures: New Design Concepts for High Speed Transport*, H. Sobieczky, Editor, Springer-Verlag, Vienna/New York, 1997, pp. 291-315.
  Presents a brief history of oblique wing and demonstration aircraft as it pertains to design of an oblique flying wing and wing-body aircraft. Examines the issues in developing such a design for an oblique flying wing passenger transport.

- Van der Velden, A. and E. Torenbeek, "Design of a Small Supersonic Oblique-Wing Transport Aircraft," Vol. 26 No. 3: pp. 193-197, Mar. 1989.

- Van der Velden, A. and I. Kroo, "Sonic Boom of the Oblique Flying Wing," *Journal of Aircraft*, Vol. 31 No. 1: pp. 19-25, Jan.-Feb. 1994.

- Van der Velden, A. and I. Kroo, "The Aerodynamic Design of the Oblique Flying Wing Supersonic Transport," NASA CR 177552, Jun. 1990.

- Waters, M., et al., "Structural and Aerodynamic Considerations for an Oblique All-Wing Aircraft," AIAA Paper 92-4220, Aug. 1992.
  Discusses layout of an oblique flying wing supersonic transport. Includes a parametric sizing of such a vehicle. This paper is a companion to a paper from T. Galloway, AIAA 92-4230.

- White, S. and E. Beeman, "Future Oblique Wing Designs," SAE, 861643, Oct. 1986.

- Wiler, C. and S. White, "Projected Advantage of an Oblique Wing Design on a Fighter Mission," AIAA Paper 84-2474, Nov. 1984.

3. Stability and Controllability

- Alag, G., R. Kempel, and J. Pahle, "Decoupling Control Synthesis for an Oblique-Wing Aircraft," NASA, TM 86801, Jun. 1986.

- Burken, J., G. Alag, and G. Gilyard, "Aeroelastic Control of Oblique-Wing Aircraft," NASA, TM 86808, Jun. 1986.

- Campbell, J. and H. Drake, "Investigation of Stability and Control Characteristics of an Airplane Model with a Skewed Wing in the Langley Free Flight Tunnel," NACA, TN 1208, May 1947.

- Coleman, G., B. Chudoba, and T. The University of Texas at Arlington - Arlington, "A Generic Stability and Control Tool for Conceptual Design: Prototype System Overview," AIAA, Paper 2007-659, Jan. 2007.

- Crittenden, J. and e. al., "Aeroelastic Stability Characteristics of an Oblique-Wing Aircraft," *Journal of Aircraft*, Vol. 15 No. 7, Jul. 1978.

- Graham, A., R.T. Jones, and J. Summers, "Wind Tunnel Test of an F-8 Airplane Model Equipped with an Oblique Wing," NASA, TM X-62273, Jun. 1973.

- Hopkins, E. and E. Nelson, "Effect of Wing Bend on the Experimental Force and Moment Characteristics of an Oblique Wing," NASA, TM X-3343, Mar. 1976.

- Jones, R.T. and J. Nisbet, "Aeroelastic Stability and Control of an Oblique Wing," *The Aeronautical Journal of the Royal Aeronautical Society*, Aug. 1986.

- Jones, R. T. "Stability and Control of an Oblique Flying Wing (White Paper)." Discussing stability issues for flying wings and relates them to issues for an oblique flying wing. Shows a simple simulation of oblique flying wing dynamics. Good discussion of yaw and roll coupling due to asymmetries.

- Kempel, R., et al., "A Piloted Evaluation of an Oblique Wing Research Aircraft Motion Simulation with Decoupling Control Laws," NASA, TP 2874, Nov. 1988.

- Luckring, J.M., "Theoretical and Experimental Analysis of Longitudinal and Lateral Aerodynamic Characteristics of Skewed Wings at Subsonic Speeds to High Angles of Attack," NASA, TN D-8512, Dec. 1977.

- Morris, S. and B. Tigner, "Flight Tests of an Oblique Flying Wing Small Scale Demonstrator," AIAA, Paper 95-3327-CP, Aug. 1995.

Discusses two RPV's designed to explore stability and control issues associated with an oblique flying wing. The second design was unstable and was effectively flown using a flight control system.

- Morris, S.J., "Integrated Aerodynamics and Control System Design for Oblique Wing Aircraft," Ph.D. Thesis, Stanford University, Jun. 1990.

- "Oblique Flying Wings: An Introduction and White Paper ", Desktop Aeronautics, Inc., Jun. 2005.
  A general assessment of an oblique flying wing. Develops an example case including a stability and control assessment.

- Phillips, J., "Modal Control of an Oblique Wing Aircraft," NASA, TP 2898, Jan. 1989.

- Smith, R., R.T. Jones, and J. Summers, "Transonic Wind Tunnel Tests of an F-8 Airplane Model Equipped with 12 and 14-percent Thick Oblique Wings," NASA TM X-62478, Oct. 1975.

- Smith, R., R.T. Jones, and J. Summers, "Transonic Longitudinal and Lateral Control Characteristics of an F-8 Airplane Model Equipped with an Oblique Wing," NASA TM X-73103, Mar. 1976.

- Tigner, B., et al., "Test Techniques for Small-Scale Research Aircraft," AIAA 98-2726, Jun. 1998.

- Weisshaar, T.A., "Integrated Structure/Control Concepts for Oblique Wing Roll Control and Trim," *Journal of Aircraft*, Vol. 31 No. 1: pp. 117- 124, Jan.-Feb. 1994.
  Investigates aero-elastic issues coupling with roll trim of the aircraft and effect on sizing of aileron control surfaces.

- Weisshaar, T. and J. Crittenden, "Flutter of Asymmetrically Swept Wings," *AIAA Journal*, Aug. 1976.

- Weisshaar, T. and T. Zeiler, "Dynamic Stability of Flexible Forward Swept Wing Aircraft," *J. Aircraft*, Vol. 20 No. 12, Dec. 1983.

- Wintzer, M., P. Sturdza, and I. Kroo, "Conceptual Design of Conventional and Oblique Wing Configurations for Small Supersonic Aircraft," AIAA, Paper 2006-930, Jan 2006.
  Describes an aerodynamic optimization of high speed transports. Makes use of Kriging-based response surfaces from high-fidelity methods in optimization. An oblique wing body (OWB) concept is presented which is in part optimized using this approach using the CART3D Euler CFD code.

The result is an analysis capability of unique configurations which doesn't rely on methods developed for other concepts.

4. AD-1 Demonstration Vehicle

- Andrews, W. and et. al., "AD-1 Oblique Wing Aircraft Program," SAE 801180, Oct. 1980.

- Curry, R.E. and A.G. Sims, "Unique Flight Characteristics of the AD-1 Oblique-Wing Research Airplane," *Journal of Aircraft*, Vol. 20 No. 6, Jun. 1983.

- Curry, R.E. and A.G. Sim, "In-Flight Total Forces, Moments, and Static Aeroelastic Characteristics of an Oblique-Wing Research Airplane," NASA TP-2224, 1984.

- Curry, R.E. and A.G. Sim, "Flight Characteristics of the AD-1 Oblique-Wing Research Airplane," NASA, TP-2223, 1984.

- Curry, R.E. and A.G. Sim, "Flight-Determined Aerodynamic Derivatives of the AD-1 Oblique Wing Research Airplane," *NASA*, TP-2222 Oct. 1984.

- Painter, W.D., NASA Dryden Flight Research Facility, Edwards, CA, "AD-1 Oblique Wing Research Aircraft Pilot Evaluation Program," AIAA, Paper 83-2509, Oct 1983.
  Describes the AD-1 program from the prospective of its goal to demonstrate a controllable vehicle at high asymmetric wing sweep angles. This includes a description of the vehicle flying qualities, data from the tests, and pilot evaluations.